The Development of Fluorescent Sensors for Specific RNA Using Chemistry and Combinatorial Biology

by

Brian A. Sparano

BS, Baldwin Wallace College, 2000

Submitted to the Graduate Faculty of

The College of Arts and Sciences in partial fulfillment

of the requirements for the degree of

Doctor of Philosophy

University of Pittsburgh

2007

UNIVERSITY OF PITTSBURGH

COLLEGE OF ARTS AND SCIENCES

This dissertation was presented

by

Brian A. Sparano

It was defended on

August 9, 2007

and approved by

Billy W. Day, Professor, Department of Pharmaceutical Sciences

Chris Schafmeister, Assistant Professor, Department of Chemistry

Stephen Weber, Professor, Department of Chemistry

Dissertation Advisor: Kazunori Koide, Assistant Professor, Department of Chemistry

Copyright © by Brian A. Sparano

2007

The Development of Fluorescent Sensors for Specific RNA using Chemistry and Combinatorial Biology

Brian A. Sparano

University of Pittsburgh, 2007

Here we describe the development of small molecule-based fluorescent sensors for RNA. The sensors described here and the new paradigm they represent are a convergence of chemical and biological methods. The resulting sensor system consists of two components: a rationally designed small-molecule fluorescent sensor and a reporter RNA sequence that binds to and enhances its fluorescence, isolated with combinatorial biology. First, we rationally designed and synthesized a series of modular fluorescent chemosensors which would be quenched in solution and fluorescent only when bound to their target. These sensors consist of a fluorophore (2',7'-dichlorofluorescein, DCF) conjugated to a pair of quencher units (aniline derivatives in this case) which quench the fluorescence of DCF by the PET (photoinduced electron transfer) mechanism. NMR and fluorescent spectroscopic analyses of these DCF derivatives revealed important correlations between their conformations, the PET, and fluorescent intensity in addition to insight on their solvatochromism and pH dependence. These studies allowed us to choose a candidate sensor for the next step: using combinatorial biology to isolate a reporter sequence. In order to isolate RNA that would enhance the fluorescence of our sensor, RNA that bound to the aniline-based quencher was isolated via *in vitro* selection (a.k.a. SELEX or systematic evolution of ligands by exponential enrichment). These RNA sequences (aptamers) were then screened for their ability to switch on the fluorescence of the sensor. One of these aptamers was found to enhance the fluorescence intensity of the DCF-aniline conjugate in a concentration-dependent

manner, leading to further study of that aptamer with mutation studies and additional *in vitro* selection experiments. To demonstrate the power and generality of this approach, a parallel *in vitro* selection was performed with aptamers from this selection having similar activities. These results show that one can develop fluorescence-inducing reporter RNA and morph it into remotely related sequences without prior structural insight into RNA-ligand binding through the rational design of fluorescent chemosensors and subsequent isolation of RNA from combinatorial libraries.

TABLE OF CONTENTS

LIST OF TABLES

LIST OF FIGURES

LIST OF ABBREVIATIONS

ATP…….….adenosine 5’-triphosphate

Boc……...……..*tert*-butoxycarbonyl

CCD…..……..charge coupled device

CD…….....cyclodextrin

CE…….……..capillary electrophoresis

COSY……..……..…..correlation spectroscopy

CRT……...……..cathode ray tube

CTP…….….cytidine-5'-triphosphate

DCF…….....….2’,7’-dichlorofluorescein

DIPEA……..……..... *N*-diisopropylethylamine

DMF.....dimethylformamide

DMSO.....dimethyl sulfoxide

DNA.....deoxyrobonucleic acid

dNTP.....deoxynucleotide triphosphate

dsDNA.....double stranded DNA

EDTA.....ethylenediaminetetraacetic acid

EMSA.....electrophoretic mobility shift assay

ES.....electrospray

FAB-MS.....fast atom bombardment mass spectrometry

FAM..... 6-carboxyfluorescein

FISH.....fluorescence *in situ* hybridization

FIVH.....fluorescence *in vitro* hybridization

FRET.....fluorescence resonance energy transfer

GFP.....green fluorescent protein

GTP.....guanosine triphosphate

HEPES..... 4-(2-hydroxyethyl)-1-piperazineethanesulfonic acid

HOMO.....highest occupied molecular orbital

HRMS.....high resolution mass spectrometry

IR.....infrared spectroscopy

LUMO.....lowest unoccupied molecular orbital

MPP..... 1-(4-methoxyphenyl)piperazine

mRNA.....messenger RNA

NMR.....nuclear magnetic resonance spectroscopy

NOE..... nuclear Overhauser effect

NOESY..... nuclear Overhauser effect spectroscopy

NTP.....nucleotide triphosphate

PAGE.....polyacrylamide gel electrophoresis

PCR.....polymerase chain reaction

PDMA..... poly(*N*-*N*-dimethylacrylamide)

PET.....photoinduced electron transfer

PMT.....photomultiplier tube

RNA.....ribonucleic acid

ROESY..... rotating frame Overhauser effect spectroscopy

SELEX.....systematic evolution of ligands by exponential enrichment

TAMRA..... 6-carboxytetrametnylrhodamine

TBE.....tris-borate EDTA

TIBS-Cl..... triisopropylbenzenesulfonyl chloride

TLC.....thin layer chromatography

RT-PCR.....reverse transcription-PCR

UTP.....uridine triphosphate

ACKNOWLEDGEMENTS

I would like to thank the members of the Koide group, both past and present for their assistance on these projects and their patience with having a biochemist in their lab. I would also like to thank Dr. Ronald Breaker, Dr. Jack Szostak and Dr. Hiroaki Suga for their assistance with *in vitro* selection experiments. I would like to thank Dr. Soumitra Basu for his guidance in the realm of RNA and Dr. Simon Watkins for his help with biological imaging. I also appreciate the assistance of Drs. Fu-Tyan and Fu-Mei Lin with NMR experiments and Dr. Dave Waldeck for his knowledge of cyclodextrins. I would also like to thank Dr. Stephane Petoud for his assistance with fluorescence spectroscopy and Dr. James Schneider and his lab for their help with capillary electrophoresis. Finally, I would like to thank my advisor Dr. Kazunori Koide and my committee members, Dr. Steve Weber, Dr. Gilbert Walker, Dr. Chris Schafmeister for their guidance and endless support on this long road.

1.0 INTRODUCTION

Every characteristic of an organism, from the layout of its bodyplan to its susceptibility to disease, is controlled by the DNA contained in its cells. Organized into genes, DNA not only carries the blueprint for every protein in the organism, it also carries the instructions for when, where and in what quantity these proteins are produced. It has been long established that genes are expressed through the transcription of DNA into RNA, which is then translated into the corresponding protein. Although entire genomes have been sequenced,[1-3] the relationship between the DNA sequence and phenotype has yet to be fully understood. Pivotal to this understanding is not only determining which gene codes for which protein but how the physiological levels of these proteins are controlled by the DNA sequence and gene regulatory system.

To answer these questions, it is necessary to be able to monitor gene expression at the DNA, RNA, and protein levels. Much has been gained in the field of gene regulation through the study of proteins. However, the correlation between the production of an RNA and the amount of its corresponding protein is nonlinear in many cases,[4,5] leaving a gap in the understanding of RNA levels. The recent discovery of RNA interference adds another layer of complexity, adding complex regulation at the RNA level.[6] Thus, the ability to understand the role of the levels, localization and interactions of RNA in living biological systems is essential to the study of gene expression. Central to developing this understanding is the *in vivo* detection

and visualization of RNA molecules. It is then the focus of the research described in this document to develop fluorescent sensors capable of detecting RNA.

2.0 BACKGROUND

2.1 FLUORESCENT DETECTION AND IMAGING OF RNA

Due to the relative noninvasivity, high sensitivity and wide array of fluorescence imaging techniques, fluorescent bioimaging has become one of the most promising techniques for biomolecule visualization and detection.[7] The most common tool for fluorescent bioimaging is the microscope. Fluorescence microscopy is dominated by two major classes of instruments: conventional optical microscopes and confocal scanning optical microscopes.

A conventional optical microscope in an epi-fluorescence mode utilizes a filter set to limit the light used to illuminate the sample to a chromophore's excitation wavelength and an emission filter to limit the observed light from the sample to the chromophore's emission wavelength. Central to this filter set, is a dichroic mirror that reflects excitation light to the sample and allows the emission light to proceed to the CCD or eyepiece.[8] The result is an image composed only of light produced by the fluorescence of the sample. By viewing only the fluorescence of specific chromophores, the sensitivity of fluorescence microscopy is two orders of magnitude higher than bright-field microscopy.[9] Figure 1 shows a typical filter "cube".

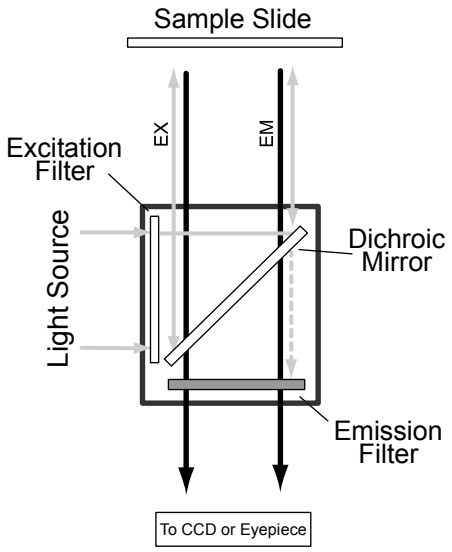

Figure 1 Typical filter cube

Excitatory light from the light source passes through the excitation filter, and is reflected by the dichroic mirror to the sample. The emitted fluorescence from the sample and any reflected excitatory light is passed back to the dichroic mirror, where excitatory light is reflected back to the light source and emissions are passed through the emission filter to the CCD or eyepiece (adapted from [8]). The use of modular filter cubes allows a single instrument to cycle through multiple excitation/emission wavelengths quickly, forming super-imposable images for multiple wavelength analysis. To increase sensitivity and allow for convenient documentation, the microscope is usually fitted with a CCD detector connected to a PC with image acquisition software.

Confocal microscopes, confocal laser scanning microscopes in particular, are based on optics that allow for scanning of the focal plane, rejecting out of plane, out of focus light. The result is the ability to create optical sections of intact, even living samples. This ability is utilized in the creation of three-dimensional images of thick transparent objects such as whole cells or tissues without the need for physical sectioning.[10] By illuminating only the focal plane

of the sample, the fluorescence emissions or reflections from above and below the focal plane, which contribute as out of focus blur to conventional epi-illumination microscopy, are eliminated, thereby increasing contrast and sharpness. The use of single point illumination by a laser allows for the scanning of a sample, much like a television CRT produces an image by scanning across the screen, the laser irradiates one voxtel (3d pixel) of the sample at a time, with the image being produced by software that pieces the voxtels into an image. This contrasts the conventional fluorescence microscope where the image is projected onto the CCD image plane and the CCD is scanning the already formed image. Scanning also has the benefit of reducing photobleaching of the chromophore. Since only the portion of the sample being scanned is illuminated, chromophores out of the voxtel do not get excited, preventing them from becoming bleached by extended exposure. The use of a high-sensitivity PMT instead of a CCD allows the confocal microscope to image samples with a lower fluorescent intensity than is possible with conventional epi-fluorescent microscopy.

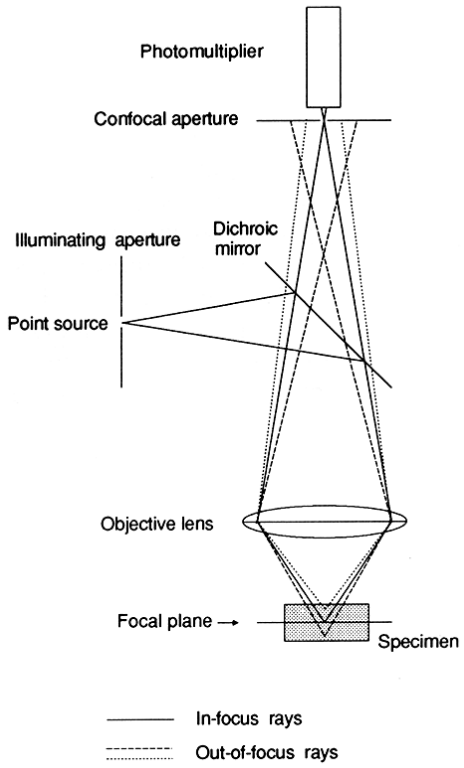

Figure 2 Confocal scanning microscope

Figure 2 shows the confocal principle of epi-fluorescence scanning optical microscopy. Monochromatic excitatory light emitted from a laser or other light source is reflected by the dichroic mirror, focused through the objective lens onto a diffraction-limited spot in the focal plane of the sample. Fluorescence emissions from the illuminated in-focus voxtel and from the out of focus cones above and below it are passed back through the objective lens and through the dichroic mirror and emission filter (not shown). Out of focal plane emissions (dotted lines) have drastically different image plane foci and are physically blocked from the PMT by the confocal aperture resulting in only in-focus rays being detected, and a virtually blur-free image.[10]

When more high-throughput fluorescence detection is necessary, fluorescent plate readers with the capability of reading up to 1536 well plates offer a commercially available solution.

Such plate readers have the benefit of being extremely sensitive: the Victor^2 V (Perkin Elmer) can detect <2 fmol/well of fluorescein and can be completely automated by integrating robotic technology.

2.2 FLUORESCENT IMAGING OF PROTEINS.

The ability to fluorescently label proteins has revolutionized protein imaging and enhanced our understanding of biology.[11] Proteins are fluorescently labeled through the production of genetically fused chimeras of the target protein with a fluorescent protein such as green fluorescent protein (GFP) (Figure 3B) or through covalent derivatization of specific residues with commercially available organic dyes. Although GFP approaches can be used to express fluorescently labeled chimeric protein in cells and have found many successful applications,[12,13] the bulk of GFP can be detrimental to the structure and function of the target protein.[14] Dyes are much smaller than fluorescent proteins, but dye-labeled proteins must be introduced into cells by microinjection.[12] To address both of these problems, Tsien and his colleagues developed the FlAsH method,[15] which allows proteins containing a tetracysteine motif to be expressed and covalently labeled in live cells with a cell permeable fluorogenic reagent. With this method, it is possible to rationally design a modular short peptide that can enhance fluorescence when bound to a fluorogenic small molecule.

2.3 FLUORESCENT IMAGING OF GENE EXPRESSION

The conjugation of a target protein with a fluorescent or fluorescence-inducing probe is a powerful method used to study the biology of proteins (Figure 3B). Of equal importance is the mechanism by which each gene expresses the corresponding protein. Since gene expression is controlled by a non-coding regulatory domain that acts independently of the coding region, a commonly used technique to monitor gene expression involves replacing the coding region of the gene with a reporter gene (e.g. GFP,[16] β-galactosidase Figure 3A). A gene encoding a fluorescent protein is inserted downstream of the target promoter to study promoter's activity. Expression of the gene results in production of the reporter gene product that then can be measured (fluorescent proteins in the case of GFP, or conversion of fluorogenic substrates in the case of β-galactosidase assays).

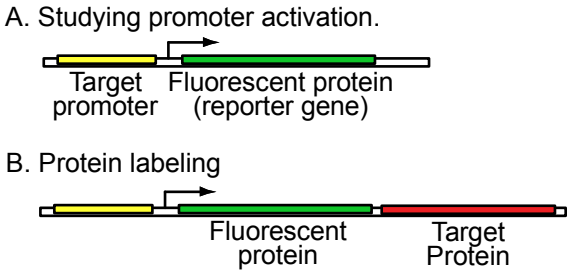

Figure 3 Methods of imaging proteins

2.4 FLUORESCENT DETECTION OF RNA

Traditionally, fluorescent detection of non-endogenously fluorescent biomolecules involves the introduction of a biomolecule covalently derivatized with a fluorophore, which will then interact

with the endogenous species of interest and subsequently be imaged or detected by virtue of the fluorescence.[17] Various manifestations of this general theme have met with much success in the fields of RNA detection and localization.

2.4.1 Non-Specific RNA Detection

Non-specific RNA detection involves the detection of RNA regardless of its sequence. Reverse transcription coupled to the polymerase chain reaction (RT-PCR) is one such strategy. In this biochemical technique, RNA is isolated from cells or produced via in vitro transcription reactions. First strand synthesis of complementary DNA (cDNA) is produced via the reverse transcriptase enzyme. This single-stranded DNA (ssDNA) is then amplified via polymerase chain reaction (PCR) and separated by length using gel electrophoresis. If quantitative information is desired, commercial instruments for real-time quantitative RT-PCR measurements are available. One such system, the ABI Prism 7700 sequence detector (TaqMan; Perkin Elmer/ Applied Biosystems), allows for real-time fluorescence spectra to be measured in a 96 well plate format for high-throughput analysis. Although the reverse transcription step is the same, real-time PCR differs from standard PCR in that a non-extendible fluorogenic probe is used to continuously monitor PCR product during the reaction. This probe consists of a fluorophore and a quencher covalently attached to the 5' and 3' ends, respectively, of an oligonucleotide sequence complementary to a portion of the ssDNA to be extended. A common fluorophore/quencher pair is 6-carboxyfluorescein (FAM) and 6-carboxytetrametnylrhodamine (TAMRA). When the probe is intact, the FAM fluorescence is quenched by the proximal TAMRA. During the extension phase of PCR, the 5' nuclease activity of Taq polymerase hydrolyses the probe. The subsequent increase in FAM emission is correlated to the initial

amount of template. Using this emission data, the system's software constructs amplification plots from which starting copy numbers can be determined.[18]

The most significant limitations of RT-PCR analysis are the lack of information regarding mRNA localization and the difficulty of quantitative extraction of mRNA from intact tissues.[19] RNA isolation involving the digestion of tissue slices with proteinase K and subsequent isolation of RNA with chloroform extraction[19] does not allow for anything more than tissue-specific information regarding mRNA localization. The isolation of RNA using such methods consistently results in contamination from genomic DNA (gDNA).[20] The purity of an RNA template is crucial to quantification of initial RNA since this gDNA is often amplifiable despite careful primer design. Pretreatment of the RNA with DNase is of limited utility as DNase has been shown to degrade RNA resulting in the reduction or even loss of low-copy RNA transcripts from small tissue samples.[20]

With the commercial availability of fluorescently-labeled nucleotides (NTPs) and deoxynucleotides (dNTPs) such as fluorescein-12-uridine-5'-triphosphate (FITC-UTP) (see Figure 4) the synthesis of fluorescently-labeled DNA and RNA has become common.

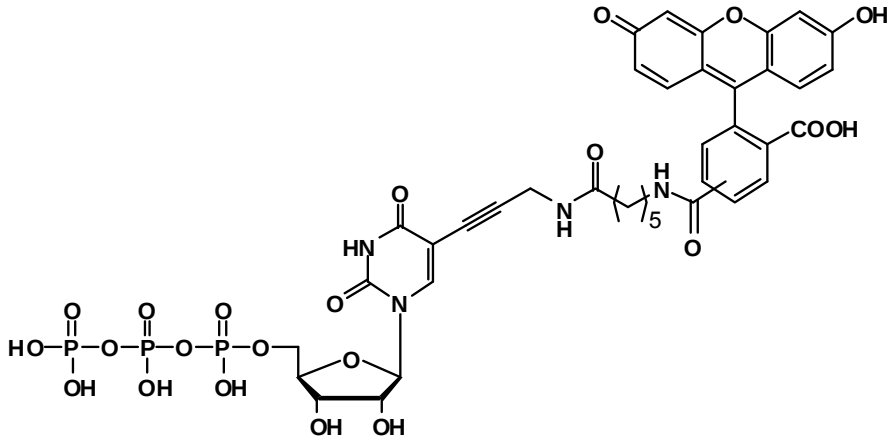

Figure 4 Fluorescein-12-uridine-5'-triphosphate (FITC-UTP)

These labeled NTP's and dNTP's are incorporated directly into DNA or RNA during standard chemical synthesis or can be enzymatically incorporated into RNA and DNA by their respective polymerases.[21] One such application of fluorescently-labeled nucleotides is the labeling of nascent RNA transcripts in living cells. After the microinjection of FITC-UTP into the cytoplasm and subsequent extraction of unincorporated label, the cells are visualized for RNA incorporation by confocal fluorescence microscopy.[22] This technique was used to detect and localize nascent RNA to PML (promyelocytic leukemia) gene product and coiled bodies in the nucleus. Labeling RNA i*n vivo* through incorporation of fluorescent nucleotides is relatively simple to perform and has the advantage that areas inaccessible to antibodies can be imaged, but no sequence specificity is afforded due to the universality of the labeled NTPs.

2.4.2 Sequence-Specific RNA Detection and Imaging

When the detection of specific RNA sequences is necessary, techniques involving fluorescent oligonucleotide probes are employed. Fluorescent oligonucleotide probes are short (15-50 bases) stretches of ssDNA or RNA with sequences complementary to the target RNA and containing one or more fluorescent labels. These antisense probes provide sequence specific detection through Watson-Crick base pairing with the RNA of interest. The probes can be chemically synthesized using commercially available DNA synthesizers or through enzymatic means by incorporation of labeled bases into PCR or *in vitro* transcription reactions. In addition, many commercial and private oligonucleotide synthesis facilities offer the synthesis of fluorescently-labeled probes with a wide range of excitation and emission wavelengths.

One of the earliest and probably the most popular method of sequence-specific RNA detection is the Northern blot. In a Northern blot, cells are lysed and the isolated RNAs are size-

fractionated on a gel and transferred to a nitrocellulose or nylon membrane by capillary or electrophoretic transfer. The nucleic acid is immobilized onto the membrane by UV cross-linking, by baking at 80°C, or by alkaline transfer. The membrane is then washed and hybridized with a biotin- or fluorescein-labeled probe. After hybridization, the unbound probe is removed with multiple post-hybridization washes. The membrane is then incubated with a protein block to reduce non-specific interactions, and the bound probe is detected by incubating the membrane with a series of antibodies against the probe label (biotin or fluorescein).[23] Although it allows for the sequence specific detection of target RNA, performing a northern blot analysis is time consuming, and like RT-PCR analysis, it supplies no information about location, origin or dynamics of RNA.

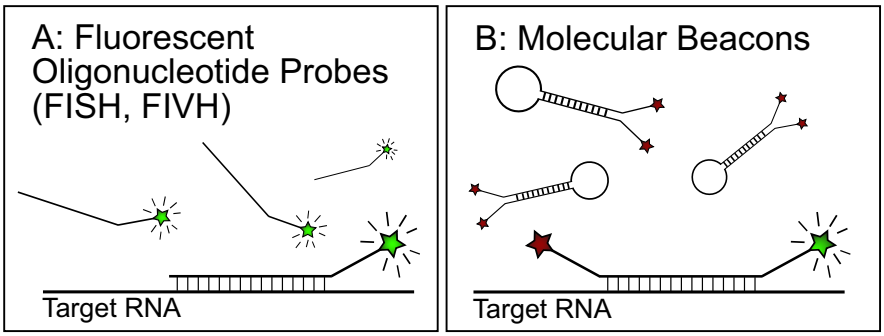

Figure 5 Methods of RNA imaging: FISH, FIVH and Molecular Beacons

For more cellularly relevant information, it is important to be able to image RNA in intact cells. Building on the use of antisense fluorescent probes, fluorescence *in situ* hybridization (FISH, Figure 5A) is conceptually similar to a northern blot except that the RNA is hybridized in intact cells instead of being isolated and electrophoretically separated.[24] Applicable to the detection of both DNA and RNA, FISH is probably the most popular method of RNA imaging

with applications ranging from localization of a specific RNA sequence within a particular cell organelle to monitoring the gene expression of an intact organism. In a typical FISH experiment, the cells to be viewed are first fixed and pre-treated with proteases or detergents to allow the non-cell permeable probes entry into the cell. Hybridization of the probe occurs easily through the permeabilized membranes of the fixed (killed) cells and the cells are stringently washed to remove unbound probe before visualization.[24] The sequence(s) of interest are then visualized with fluorescence microscopy by virtue of the fluorescent hybridized probe.

When using FISH to detect RNA, RNA probes synthesized from cDNAs of the RNA of interest are generally used due to the more stable nature of RNA-RNA hybrids compared with DNA-RNA hybrids.[24] Through the use of transcription vectors, large amounts of sense (negative control) and anti-sense (specific) RNA probes can be produced. It has also been shown that non-specific probe binding can be reduced by a post-hybridization RNase treatment and the fragment length can be controlled by alkaline hydrolysis treatment during the production of the probes.[24]

One of the greatest benefits of using fluorochromized probes in conjunction with fluorescence microscopy is the ability to study gene expression using combinations of spectrally distinct chromophores to visualize several RNA sequences in a single tissue or cell section. Dirks and Raap demonstrated this ability when they detected histone H3 mRNA simultaneously with, respectively, human cytomegalovirus immediate early (HCMV-IE) and luciferase mRNA in two different cell lines.[25] The use of tetramethylrhodamine-4-dUTP and digoxigenin-12-dUTP, the latter coupled to a series of fluorescein-labeled antibodies, facilitated visualization with a dual-pass filter.

Due to the harsh fixation and cell pretreatment procedures employed in FISH experiments, the deterioration of cell morphology and the disturbance of RNA localization

becomes likely.[20] Information about the dynamic behavior of RNA (namely synthesis, transport and processing) is gained more appropriately through the study of living cells in real-time fluorescent microscopy. It is for this reason that the field of fluorescence *in vivo* hybridization (FIVH) has grown in popularity.

Although the basic concepts of FIVH and FISH are the same (visualization of hybridized probes in intact cells) performing the hybridization in living cells poses some significant challenges. The most significant and first to be encountered is the efficient introduction of fluorescently-labeled probes into living cells without irreversibly altering their morphology and viability. The main obstacle is the cell membrane, and for nuclear RNA detection, the nuclear membrane.[26] Many techniques have been devised to pass the membranes. One of the least obtrusive makes use of pinocytosis, a naturally occurring uptake mechanism of cells.[27] Through pinocytosis, small amounts of probe can be taken up by a cell in pinocytotic vesicles and released into the cytoplasm after a hypertonic treatment of the cells. The major drawbacks of this approach are the large amounts of probes needed and the cell damage incurred by the hypertonic treatment that is needed to disrupt the pinocytotic vesicles before they fuse with lysosomes in the cytoplasm.

Although less effective, the mechanical methods of scrape and scratch loading have also been used to introduce exogenous molecules. Scrape loading, used with adherent cells, involves scraping the cells from their substratum into medium containing the probe to be introduced.[26] Scratch loading, a related technique utilizes mild injury through scratching of the cells with a sharp instrument while in probe containing medium. Upon recovery, the probe can be visualized in the effected cells.[7] More effective than scratch and scrape loading is the technique of bead

loading, where the probe solution, mixed with 75-150 μm glass beads is gently agitated with the cell culture, causing small legions in the membrane where the probes can enter.[26]

Due to its direct and quantitative nature, microinjection via micropipettes is a powerful technique for probe introduction.[28] After being delivered into the cytoplasm, small sized probes have been shown to freely diffuse into the nucleus within seconds. For larger probes, microinjection directly into the nucleus is possible.[26] Despite the popularity of this technique, it requires that each cell to be studied be individually injected, a technique that needs specialized equipment and is not trivial to master.

After the introduction of the probe, a problem plaguing FISH and FIVH is the removal of unbound probe. Since there is no means to distinguish bound from unbound probe, failure to completely remove unbound probe results in increased background fluorescence. Unlike FISH where stringent chemical washes are used, in FIVH techniques, cell viability is important, so high background due to unbound probe is a problem. For this reason, techniques developed to distinguish the hybridized signal from the omnipresent cell autofluorescence and unbound probe. The ideal probe for live cell studies is one that is non-fluorescent when introduced into a cell and fluoresces only upon hybridization with its target. Molecular beacons,[29] originally designed for real time PCR, are one approach to solving this problem (Figure 5B). They consist of a single stranded nucleic acid with a fluorescent chromophore at one end and a quencher at the other (see Figure 5C,D). The molecule forms a stem-loop structure with a 15-20 base loop sequence, complementary to the target nucleic acid, flanked by two sequences complementary to each other which anneal, forming the "stem". When in closed conformation, the proximity of the chromophore and quencher dictate that the molecule is quenched, during hybridization to the target sequence, the molecular beacon opens separating the quencher and chromophore, restoring

fluorescence. Although effective in concept and homogeneous solution, Dirks et al[26] has observed that when injected into the cytoplasm, molecular beacons open up immediately upon entering the nucleus. The authors speculate that the beacons' transient association with nuclear proteins is the cause for this instantaneous opening, but this relationship has yet to be proven.

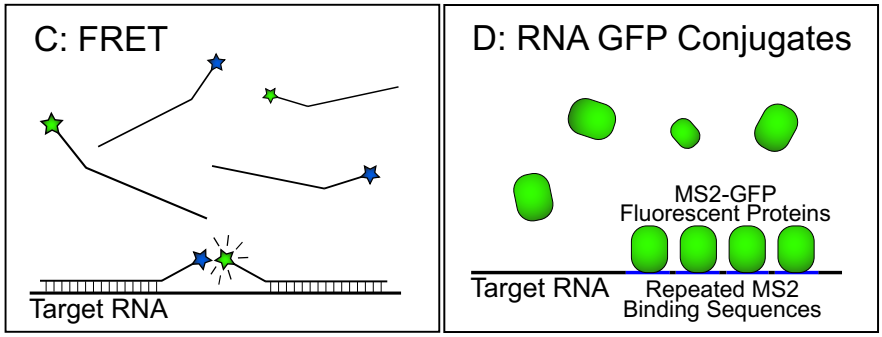

Figure 6 Methods of RNA imaging: FRET and RNA-GFP conjugates

An alternative approach is fluorescence resonance energy transfer (FRET, Figure 6A). With careful probe design, two probes labeled with donor and acceptor fluorophores, respectively, are hybridized to adjacent sequences on the target molecule. When the fluorophores are within 10 nm, the emission from the donor fluorophore will excite the acceptor, yielding a shift in fluorescent emission from the donor to the acceptor. The fluorophores must be chosen carefully, however because in order for FRET to occur, the emission spectrum of the donor chromophore needs to overlap with the excitation spectrum of the acceptor chromophore.[26] The FRET approach was used by Tsuji et al[30] for the detection of c-fos mRNA in the cytoplasm of transfected Cos7 cells. FRET has also been used to monitor nascent transcripts in the real-time monitoring of *in vitro* transcription by Tsuji's group.[31]

One method used to study RNA localization involves the introduction of fluorescently-labeled versions of target RNA into living cells monitoring their spatial and temporal distribution by live cell fluorescence microscopy. This RNA is typically labeled by the incorporation of fluorescent nucleotides during *in vitro* synthesis from full-length cDNA or by 3' end chemical labeling. In one of the earliest applications of this approach, Wang et al.[32] demonstrated that microinjected β-globin pre-mRNA localizes in speckle domains which are enriched for spliceosome components. From these early observations, they concluded that the intracellular movement of pre-mRNA to spliceosome regions is not necessarily coupled with transcription. With the microinjection of signal recognition particle (SRP) RNA, Thoru Pederson's group was able to track the movement of the SRP RNA in real time.[33] Within 5 minutes of nuclear microinjection, the SRP RNA was observed to localize in the nucleoli followed by a progressive decline in nucleolar fluorescence and an increase in signal at various cytoplasmic foci. With injection into the cytoplasm however, the RNA neither entered the nucleus nor concentrated in any specific locations in the cytoplasm. These data suggest that the SRP RNA was somehow processed in the nucleoli or assembled into a ribonucleoprotein particle for export into the cytoplasm. Microinjecting labeled RNA into living cells yields much information about localization and dynamic behavior, but it should be noted that due to the higher concentration of labeled RNA than would be present for the corresponding endogenous RNA, the existing cellular transport and processing routes may become saturated forcing the exogenous RNA molecules to follow different routes with different kinetics.[26]

An approach pioneered by the Singer group dispenses with organic chromophores altogether. Singer's system uses GFP fused to RNA binding protein MS2 to detect specific RNA in living cells (Figure 6B).[34-36] Used primarily to track RNA localization, the reporter sequence

that contains repeated MS2 protein binding motifs is inserted between the gene of interest and the RNA localization signal.[34] Although this technique has been used to study RNA localization,[34,37-39] RNA dynamics,[35,40,41] and transcriptional profiling,[36,42] it has several disadvantages. Most significantly, it has a low signal to noise ratio caused by presence of overexpressed, fluorescent MS2-GFP protein (the binding of RNA to the protein merely localizes the protein on the RNA, it does not elicit any change in the fluorescence). To combat the low signal to noise ratio, the authors employ a series of multiple repeats of the MS2 binding sequence, resulting in 24 to 96 individual MS2-GFP proteins bound to a single RNA,[35] likely causing the RNA to behave differently inside the cell. Lastly, in addition to the gene of interest, the expression of the MS2-GFP conjugate must be tightly regulated using a constitutive expression system, further complicating live cell experiments.[43]

2.5 PET-BASED SENSORS

Since our approach relied on the implementation of small molecule fluorescent sensors, and such molecules have seen limited application in the imaging of biomacromolecules, we turned to the widely successful field of fluorescent metal ion probes for inspiration.[44-51] An ideal probe for metal ions (or RNA) is non-fluorescent when free in solution and fluorescent only when bound to a specific target molecule. Such an off-on fluorescent sensor can rationally designed by implementing by the photoinduced electron transfer (PET) mechanism to modulate the fluorescence (Figure 7).[52] Fluorescence occurs when a fluorophore is excited with the appropriate wavelength of light, and an electron from the HOMO is promoted to the LUMO. The

decay of this electron back to the HOMO is accompanied by the release of energy in the form of a photon of light (Figure 7A).

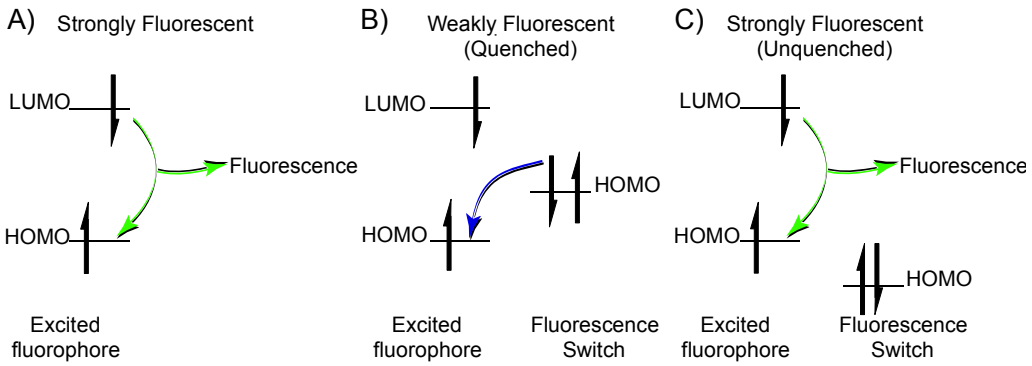

Figure 7 Fluorescence quenching as described using frontier molecular orbitals

When a quencher is present near a fluorophore and its HOMO energy level is between the HOMO and LUMO energy levels of the fluorophore (Figure 7B), PET occurs from the quencher to the excited fluorophore, forcing the excited electron to decay by non-radiative means, resulting in reduced fluorescence. The fluorescent intensity of such a sensor is correlated to the HOMO energy level of the quencher(s) as shown in the Rehm-Weller equation (Eq 1; E_{ox} = oxidation potential of a quencher, E_{red} = reduction potential of a fluorophore, ΔE_{00} = the singlet excited energy, w_p = the work term for the charge separation state).[53]

$$\Delta G_{PET} = E_{ox} - E_{red} - \Delta E_{00} - w_p \qquad \text{(Eq 1)}$$

As this equation indicates, increasing the HOMO level of the quencher (E_{ox}) *thermodynamically* and kinetically favors PET, thus reducing fluorescence signal. The binding of an analyte such as a metal ion can deactivate the quencher by lowering the HOMO level of the

quencher and restoring fluorescence (Figure 7C). This correlation between the HOMO-LUMO gap and fluorescent intensity is well established.[54]

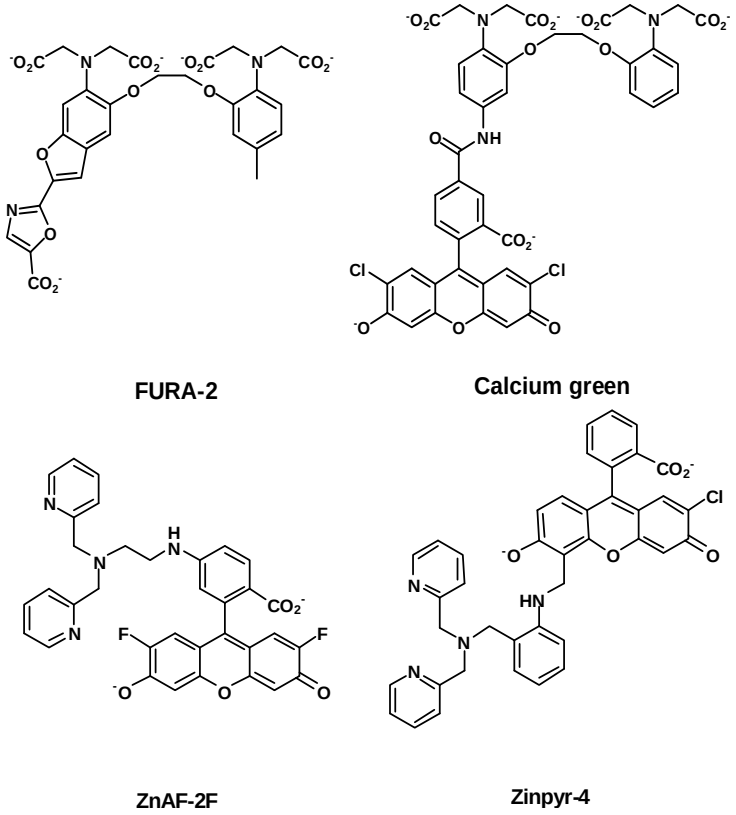

Figure 8 Intracellular calcium and zinc sensors

The modularity of PET-based ion sensors can be illustrated by comparing the Ca^{2+} and Zn^{2+} sensors shown in Figure 8. Although attached to different chromophores, the tetracarboxylate ligand binding groups are conserved between the Ca^{2+} sensors FURA-2[55] and calcium green-1[56] and have relatively similar K_d values of 24 nM and 190 nM, respectively. The intracellular Zn^{2+} sensors ZnAF-2F[57] and Zinpyr-4,[58] with K_d values of 5.5 nM and 0.65 nM, respectively, contain the same fluorescein scaffold and zinc chealator dipicolylamine acting as the ligand-binding switch, but differ in their point of attachment. For ZnAF-2F, with its quencher moiety on the benzoic acid, the enhancement of fluorescence was shown to be 60 fold

upon the addition of Zn^{2+} [57] whereas Zinpyr-4, with its quencher moieties on the xanthene ring, exhibited 5.7 fold enhancement.[58] The quenched quantum yield of the ZnAF-2F is only 0.006, but upon enhancement, becomes 0.24.[57] Zinpyr-4, with a higher background (quenched) quantum yield of 0.06, is enhanced to 0.34.[59] From these data, and that of the previous Zn^{2+} sensor Zinpyr1,[59] it becomes apparent that although substitution on the benzoic acid of fluorescein results in more efficient quenching and the enhanced fluorescence is not as intense, resulting in sensors capable of a lower background fluorescence. When quenching from the xanthene (as in Zinpyr-1), although the quenching of fluorescence may not be as efficient, the enhancement is more significant, with an enhanced quantum yield of 0.92 as compared to 0.95 of fluorescein (as a reference standard, in 0.1N NaOH[59]), indicating that the effect of the quencher is almost entirely deactivated through the binding of the ligand.

In principle, the deactivation of the quencher can also be accomplished by increasing the quencher-fluorophore distance, reducing PET efficiency (Figure 8C). The dependence of quenching efficiency on distance is known to be proportional to $e^{-\beta d}$, where d = the distance between the HOMO electrons of the quencher and the fluorophore. In other words, PET efficiency decreases as the quencher-fluorophore distance increases, allowing efficient radiative decay (i.e., stronger fluorescence) to occur from the LUMO to the HOMO of the fluorophore when the quencher is sufficiently distant. The use of this conformational switch is rare in sensor development, limited to only one example.[60,61]

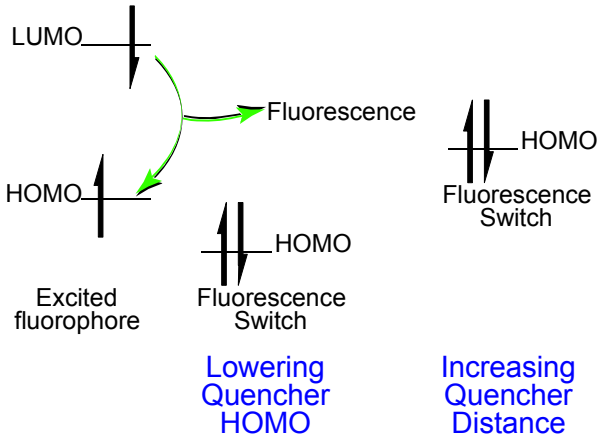

Figure 9 Unquenching of PET-dependent fluorescence

To summarize PET-dependent fluorescence, (Figure 9) *for a PET sensor to be switched on, an analyte must lower the HOMO energy level of the quencher and/or increase the distance between the quencher and the fluorophore*.

2.6 *IN VITRO* SELECTION

In vitro selection (AKA SELEX) is a combinatorial biology technique used to isolate RNAs with a rare activity (such as binding a small molecule) from a population of random sequences.[62-64] Briefly, in this technique (Figure 10), a chemically synthesized random library of 10^{13}-10^{15} DNA molecules is transcribed into RNA and incubated with an affinity column containing the desired ligand in binding buffer containing a high Mg^{2+} concentration (Mg^{2+} has been shown to be a necessary cofactor for RNA binding[62]). After several washings to remove unbound species, the bound RNA is eluted, reverse transcribed into cDNA and amplified by PCR (usually as one step RT-PCR). This PCR library becomes the template for the RNA of the next round of selection. The fraction retained by the column increases with each subsequent round until the population is

dominated by binding sequences (aptamers). Three to 15 rounds of selection is typically sufficient to "purify" away the non-binding RNA aptamers.[65] After the aptamers are sequenced, more detailed activity studies are conducted, such as determination of K_D or fluorescence enhancement (Figure 10).

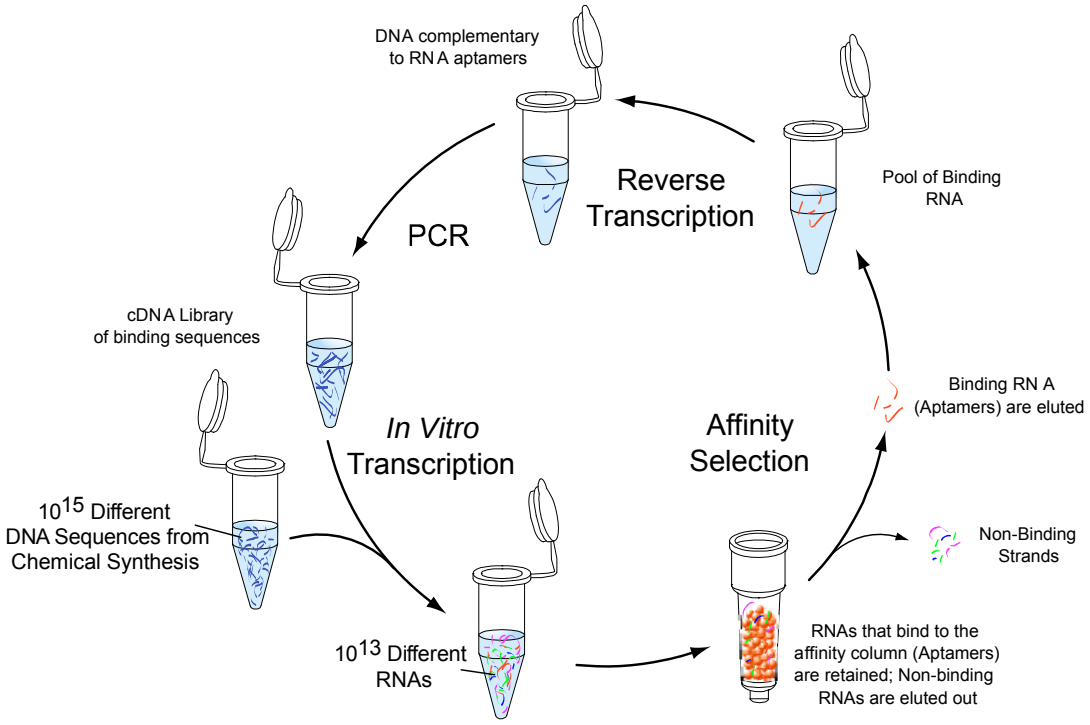

Figure 10 Systematic Evolution of Ligands by EXponential enrichment (SELEX)

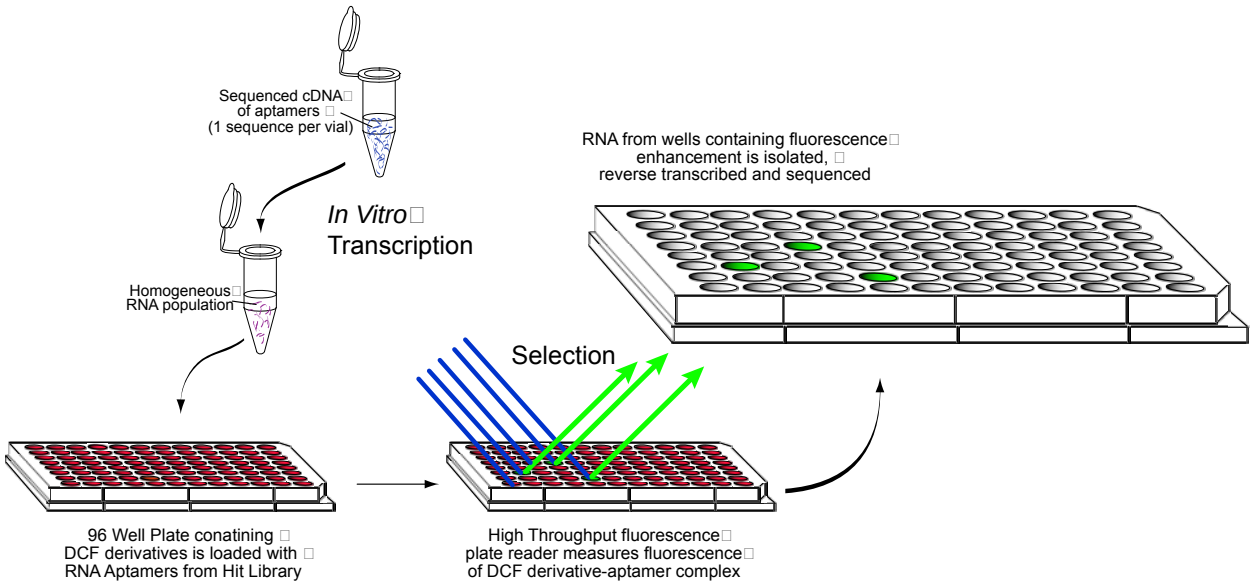

Figure 11 Screening of aptamers for fluorescence restoration ability

3.0 RESULTS AND DISCUSSION

3.1 GENERAL APPROACH FOR RNA CHEMOSENSORS

With the limitations of existing methods of RNA detection in mind, we set out to develop a new method of *in vivo* RNA detection based on the visualization of nascent RNA transcripts via membrane permeable sensor molecules whose fluorescence was controlled by specific RNA interaction. Since no generally applicable approach existed for the rational design of small molecule fluorescent sensors to detect RNA, we had the added challenge of devising the approach as well as developing the sensor system. To accomplish this, we needed two things. First, a cell-permeable fluorescent sensor was needed possessing both an affinity for RNA and some type of spectral change upon association with specific RNA sequences. Such a spectral change could be a significant increase in fluorescent intensity, a visible change in emission wavelength, or both. Second, we needed to identify a specific RNA sequence that would bind tightly to this molecule and elicit such a spectral change. The resulting system would consist of an expressible RNA reporter sequence that would function as a reporter gene, binding to the sensor forming a fluorescent complex detectible via fluorescence microscopy or high-throughput plate reader.

With this system, the sensor molecule would be fluorescent only when bound to the target RNA. Such a sensor is depicted in Figure 12. On the left, a conventional FISH or FIVH

experiment is shown where the excess fluorescent unhybridized probe is present in the cell leading to increased background signal. On the right, detection via RNA-specific sensor molecules is shown: the reporter (sensor-binding) sequence is appended to the target RNA, forming a fluorescent complex with the sensor while the unbound sensor molecule remains non-fluorescent in the cell. The implementation of this type of sensor system will result in low background due to unbound probe in addition to the generality of a reporter sequence able to be applied to virtually any gene of interest.

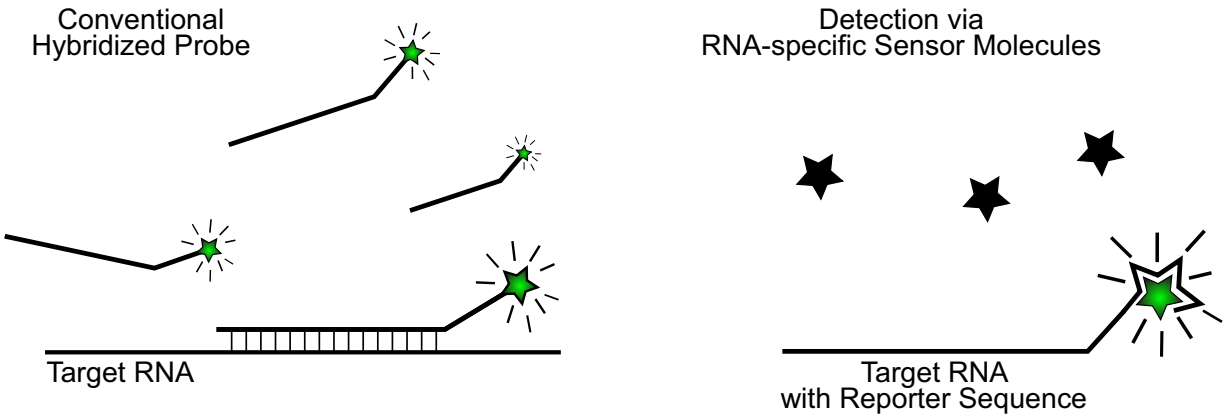

Figure 12 RNA-specific sensor molecules

3.2 NEOMYCIN DERIVITIZATION

To initiate our project into the development of fluorescent RNA sensors, we thought it apt to start by designing a modular sensor consisting of a known small molecule RNA ligand conjugated to a fluorophore. We surmised that such a molecule would be able to detect the small-molecule binding RNA by virtue of the attached fluorophore's fluorescence (or perturbation there of).

Due to its well studied interaction with the Rev-response element of HIV-1 virus[66-72], the aminoglycoside antibiotic neomycin B was chosen to serve as the RNA ligand. Neomycin has been shown to bind tightly to this RNA with an affinity of 82 nM[70] and also to affect the fluorescence of covalently attached fluorophores.[73] We then chose to conjugate neomycin to the fluorophore fluorescein through a scheme (see Scheme 1) developed to form neomycin-acridine conjugates.[73]

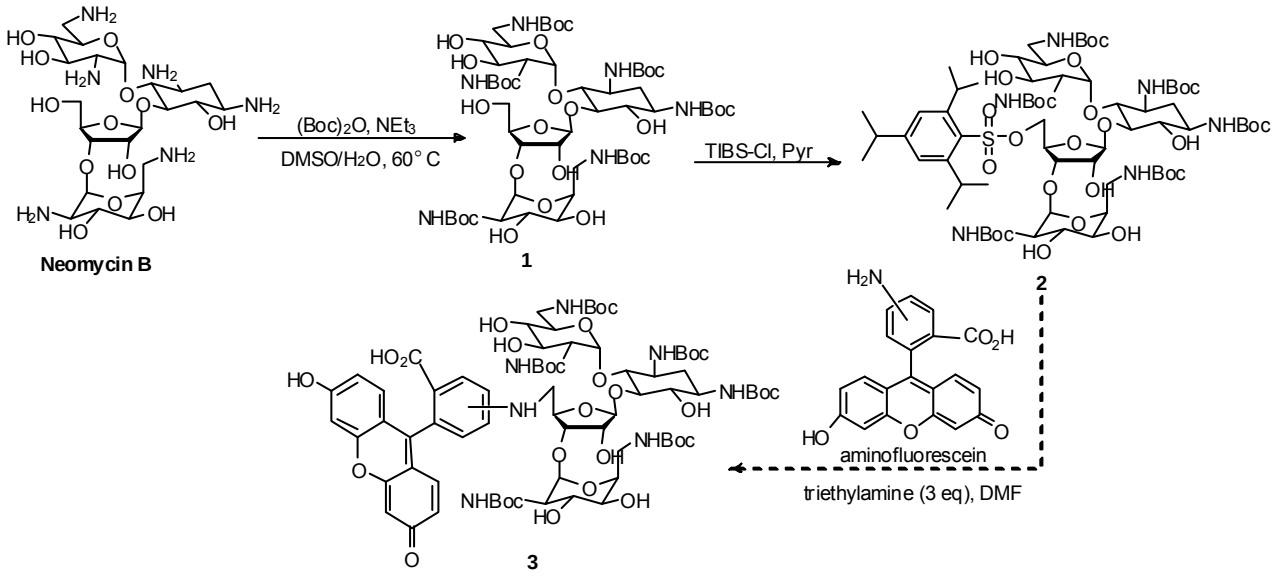

Scheme 1 Neomycin-fluorescein conjugate synthesis

Synthesis of Boc protected compound **1** and TIBS substituted compound **2** were achieved in 53% and 65% yields, respectively. Unfortunately, due to the complicated nature of the resulting NMR spectra and unreliable instrumentation used for fast atom bombardment mass spectrometry (FAB-MS) analysis, we were unable to fully characterize these neomycin derivatives, although the mass of **2** was verified by electrospray MS. The product from the subsequent conjugation with aminofluorescein was unable to be purified, although it was visible on TLC. This neomycin-based approach was abandoned due to slow progress caused by the

extreme length of the TIBS substitution reaction, the difficulty of structure verification and the difficulties encountered in the purification of the final product.

3.3 MODULAR SENSORS

3.3.1 Rational Design of Modular PET Sensors

In light of these difficulties, we decided to simplify the RNA ligand portion of the sensor and revise our approach. Instead of designing a known RNA-ligand interaction into the sensor, we would concentrate on designing fluorescence switching into the sensor and leave the RNA-ligand interaction to combinatorial biology. Through the implementation of a synthetic scheme amenable to creating a diverse library of sensors, we would be able to increase the possibility of finding a RNA-sensor interaction appropriate for use in living cells.

Using successful PET sensors such as those described above as a guide, we set out to rationally design a modular PET sensor to detect RNA. For the fluorophore portion of the sensor, we chose 2',7'-dichlorofluorescein (DCF). Known for their high quantum yields, fluorescein derivatives are commonly used in fluorescently-labeled nucleotide analogs as well as calcium green and the Zn^{2+} sensors described above, many of which are membrane permeable. A widely used fluorophore in bioimaging, DCF, was chosen because its fluorescence is pH-insensitive under physiological conditions unlike fluorescein (the pK_a of the hydroxy group of DCF and fluorescein are 5.2[74] and 6.5,[75] respectively), DCF is brightly fluorescent (Φ = 0.85), and the chloride groups block two of the possible four nucleophilic centers, enabling us to use DCF as a nucleophile without regioselectivity issues. Dichlorofluorescein's high quantum yield is

important to maximize the signal-to-noise ratio inside cells. Chromophores based on the fluorescein scaffold with excitation and emission wavelengths around 490 and 525 nm, respectively, facilitate use in confocal microscopes and plate readers since no quartz optics are needed (as with UV excitable chromophores). Their absorption at 490 nm allows them to be excited with the 488 nm line of the argon-ion laser utilized in most confocal laser scanning microscopes and also the standard filter sets of fluorescent plate readers and conventional epi-fluorescence microscopes.

The choice of a fluorescence switch was not as straightforward. In order to maximize sensitivity, it is important that the difference in fluorescence from bound to unbound sensor be as large as possible. The challenge was then to find a quencher moiety that would efficiently transfer electrons to the xanthene core of DCF yet be able to have that electron transfer reversibly interrupted by RNA binding. We chose aniline derivatives for this purpose due to their low pK_a values and high HOMO energy levels and diverse selection of commercially available analogs. Nitrogen containing groups have been incorporated into many sensors to control fluorescence via PET.[55,57,59] They are also vital to many RNA ligands such as the aminoglycoside antibiotics that owe their potency to tight complexes with RNA. This affinity is not reserved for naturally occurring RNA sequences, however. *In vitro* selected RNA for tobramycin has been found with a K_d of 6 nM.[76]

Based on these criteria we designed model compound **4** and sensor candidate **5** (scheme 2). We hypothesized that the lone pairs on the aniline nitrogens would effectively quench the fluorescence, yet still permit the molecule to be unquenched if the lone pairs were to become complexed with RNA. To verify that the aniline nitrogens were responsible for PET quenching, we designed analog **6**. Since the quenching ability is proportional to the electron density (the

higher the electron density the greater the quenching ability and lower the fluorescence), we mused that by tuning the electron density of the aniline ring, we could control the fluorescence of the resulting sensor. To test this, we designed analog **7** with chloride as an electron withdrawing group and analogs **8** and **9** with a methoxy group to increase electron density.

3.3.2 Synthesis of DCF Derivatives

Model compound **4** and its related DCF derivatives (Scheme 2) were prepared by means of Mannich reactions between DCF and the corresponding commercially available secondary amine according to the procedure of Burdette et al.[59] Silica gel chromatography and recrystallization afforded products **4**, **5**, **6** and **9** (DCF-2MPP) in yields of 85%, 73%, 77% and 39%, respectively. The synthesis of derivative **7** was unsuccessful due to the decomposition of the product before it could be isolated. Compound **8** was formed as an insoluble polymer and also was not isolated. Dr. Shahi in the Koide group prepared compound **10** to function as a control containing only one MPP quencher unit as described in *Org. Lett.* **2004**, *6*, 1947–1949. in detail.[77]

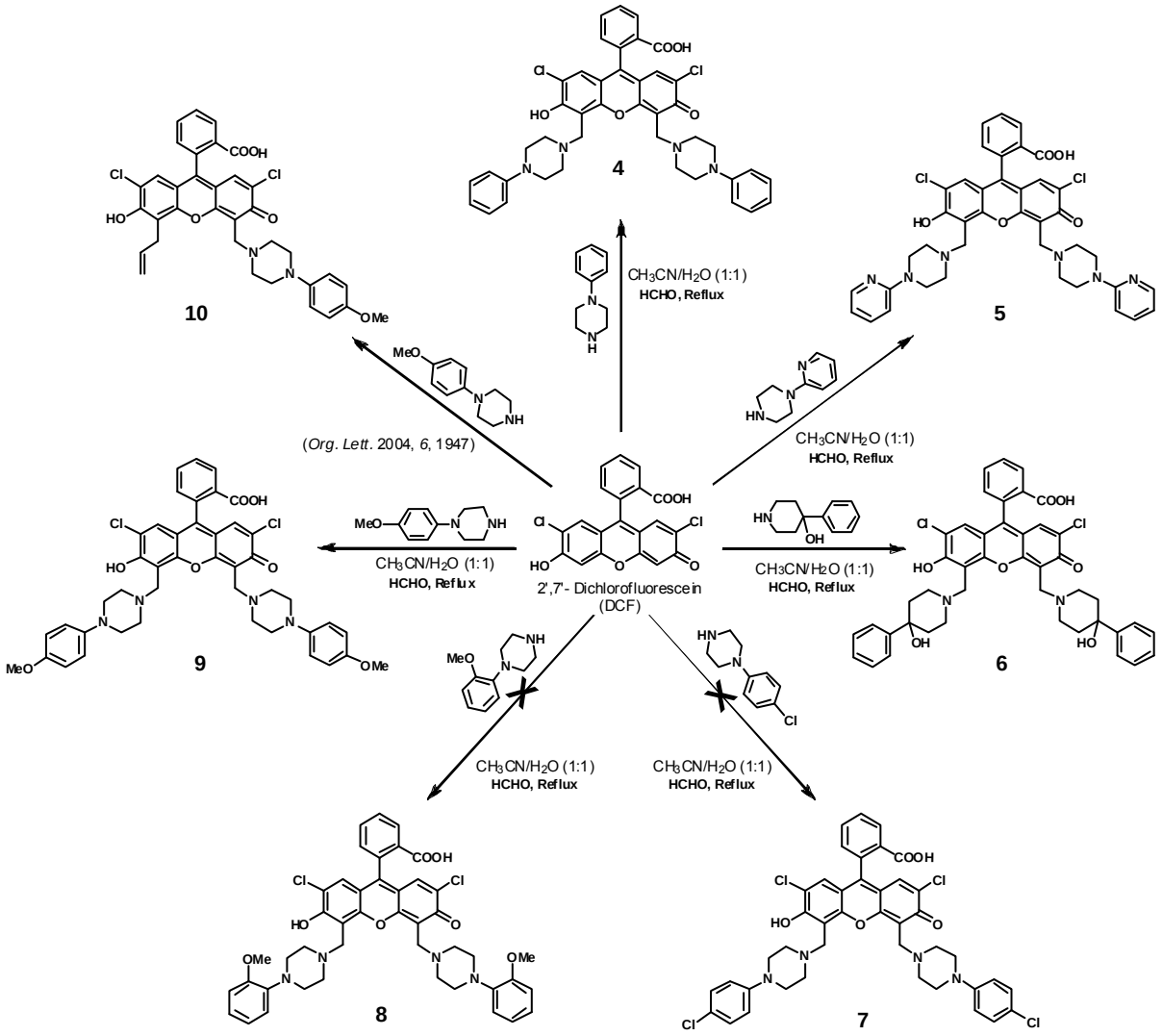

Scheme 2 Derivitization of DCF

3.3.3 Analysis of Candidate Sensors

3.3.3.1 Absorbance and Fluorescence Emission

We then gathered absorbance and fluorescence data on compounds **4**, **5**, **6**, DCF-2MPP and **10** in a pH 7 phosphate buffer (Table 1 and Figure 13). As expected, the model compound **4** displayed a low quantum yield (Φ) of 0.052, compared to its parent fluorophore DCF (Φ of 0.85), revealing that compound **4** or its related compounds would exhibit a large increase in

fluorescence if the PET can be suppressed. The significant role that the aniline nitrogens played in the PET quenching was revealed with the lack of aniline nitrogen atoms in compound **6** causing a high Φ of 0.710. This is consistent with the electrons of the aniline system being coupled to the relaxation of the excited chromophore. Although we were unable to synthesize the electron deficient **7**, we were still able to correlate the electron density of the quencher to its ability to quench the fluorescence. We hypothesized that based on the Rehm-Weller equation (Eq 1), the electron donating nature of the methoxy group of *para*-methoxyaniline derivative DCF-2MPP would cause it to be less fluorescent than aniline derivative **4**. This hypothesis was confirmed when we found the quantum yield of DCF-2MPP to be 0.025, significantly lower than that of compound **4**. Further support correlating the HOMO energy level to the fluorescence was found in compound **5**. The electron withdrawing nature of the pyridine ring of **5** compared to the phenyl ring of **4** gives the quenchers of **5** a lower HOMO level, rendering their quenching less favorable. This is evidenced in the higher quantum yield of compound **5** compared to that of compound **4** (Φ = 0.102 and 0.052, respectively). To illustrate the effect of the number of quencher units on the fluorescent intensity, we tested the mono-substituted analog of DCF-2MPP, finding the quantum yield of **10** to be 0.176, suggesting that the quenching of the di-substituted compounds is cooperative rather than additive. This cooperative quenching concept is currently being explored by others in the lab.

Table 1 Spectroscopic data in a pH 7 phosphate buffer.

Compound	$\lambda_{ab\text{-}max}$ (nm)	$\lambda_{em\text{-}max}$ (nm)	Φ
4	507	524	0.052
5	508	522	0.102
6	504	522	0.710
DCF-2MPP	508	528	0.025
10	512	533	0.176
DCF	502	522	0.850

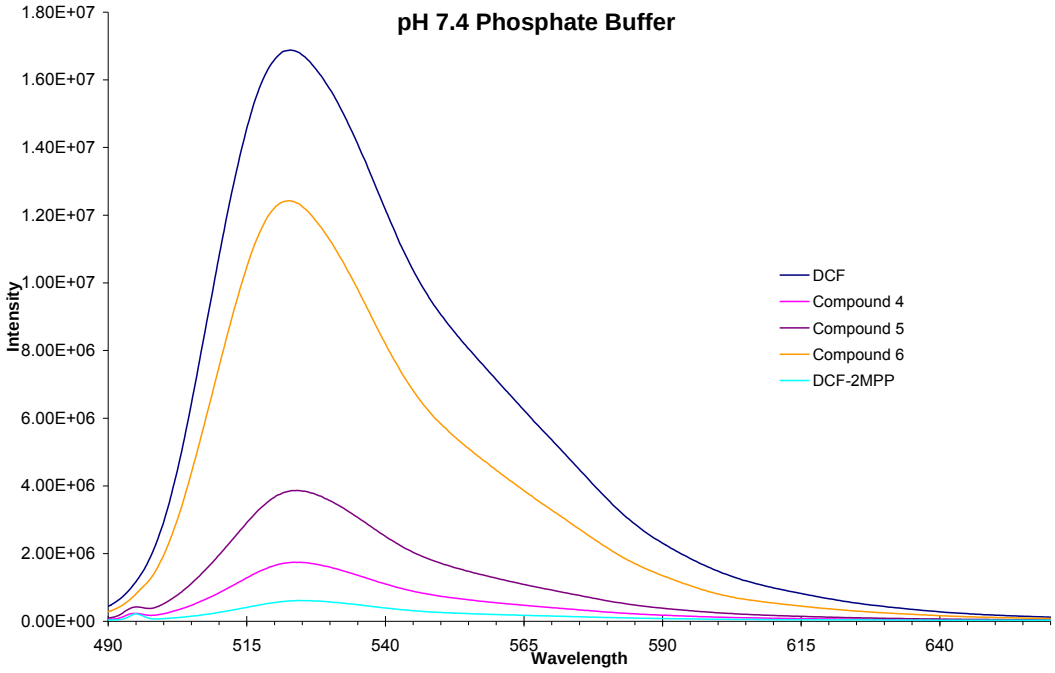

Figure 13 Relative intensities of DCF derivatives

3.3.3.2 Solvatochromism in UV Absorbance

While working up the first two compounds we synthesized (phenyl compound **4** and pyridinyl compound **5**), color shifts were observed when transferring the compound from one solvent to another. Although not essential to the overall goal of designing RNA sensors, this solvatochromism intrigued us and we decided to spend a brief period exploring it. The

solvatochromic properties of compounds **4** and **5** were investigated by acquiring absorbance and fluorescence emission spectra in 0.1N NaOH, MeOH, pH 7.4 phosphate buffer, MeCN, CH_2Cl_2, and $CHCl_3$. Figures 14 and 15 show the absorbance spectra of compounds **4** and **5**, respectively. In both spectra, two distinct groups of λ_{max} values emerge: NaOH, pH 7.5 buffer, and MeOH, clustered around 510 nm and DMSO, $CHCl_3$, MeCN and CH_2Cl_2, grouped around 535 nm. With the exception of DMSO, changes in absorbance intensity accompany the shifts, with $CHCl_3$, MeCN and CH_2Cl_2 having nearly an order of magnitude less absorbance than NaOH, pH 7.5 buffer, MeOH and DMSO. Although the reason for these shifts has not been ascertained, we hypothesize that it is due to a conformational change caused by solvent, by which the molecule assumes a different conformation in polar and non-polar solvents. Attempts to lend support to this hypothesis by means of NMR were unsuccessful, with compounds **4** and **5** lacking sufficient solubility to obtain useful spectra in solvents other than DMSO-d_6.

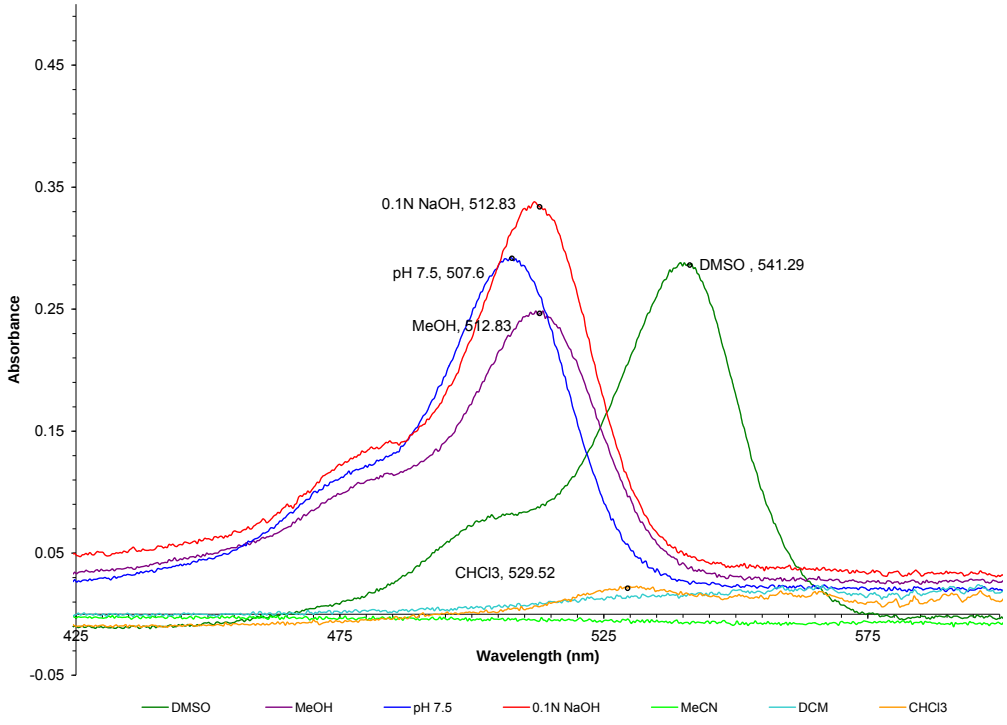

Figure 14 Absorbance spectrum of compound 4

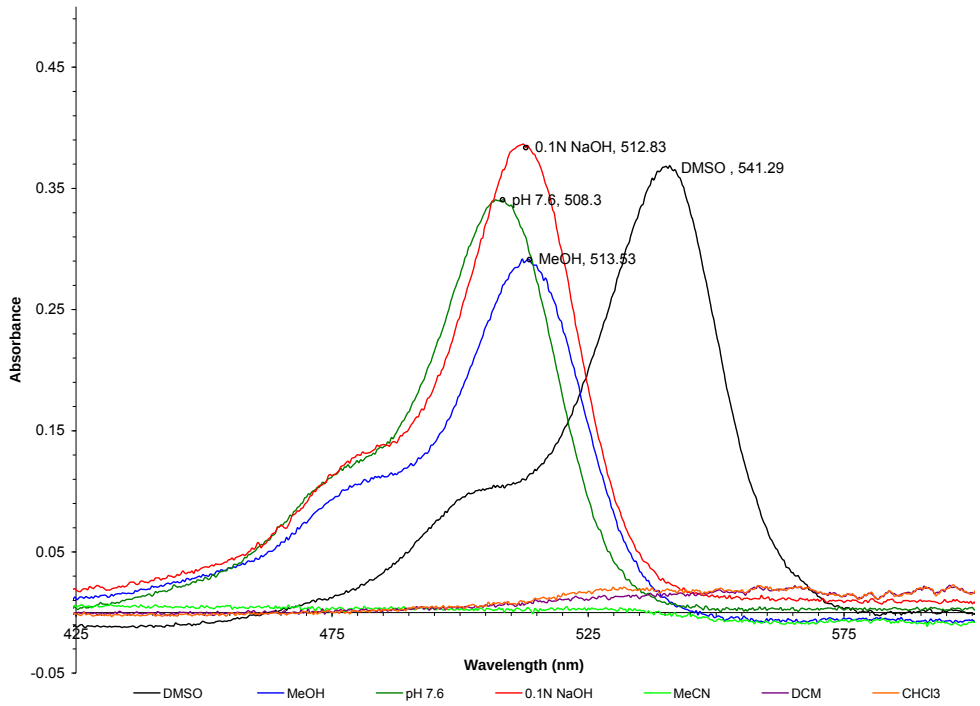

Figure 15 Absorbance spectrum of compound 5

3.3.3.3 Solvatochromism in Fluorescence Emission

Further evidence of solvatochromism can be found in the fluorescence emission spectra. Fluorescence samples were prepared as stated above for the absorbance experiment with the exceptions of $CHCl_3$ and CH_2Cl_2, which were omitted due to poor absorbance of compounds **4** and **5** and insolubility at higher concentrations. Figures 16 and 17 compare emission spectra for 0.1N NaOH, MeOH, pH 7.4 phosphate buffer and DMSO. The emission spectra show similar solvent-dependent effects; with DMSO and MeCN being red-shifted in relation to NaOH, pH 7.5 buffer, and MeOH. The fluorescent intensities of NaOH, pH 7.5 buffer, and MeOH are inversely related to their respective absorbances. In Figure 19, the intensity of compound **5** in pH 7.4 phosphate buffer is approximately 3.5 times that of 0.1 N NaOH, suggesting a pH dependence.

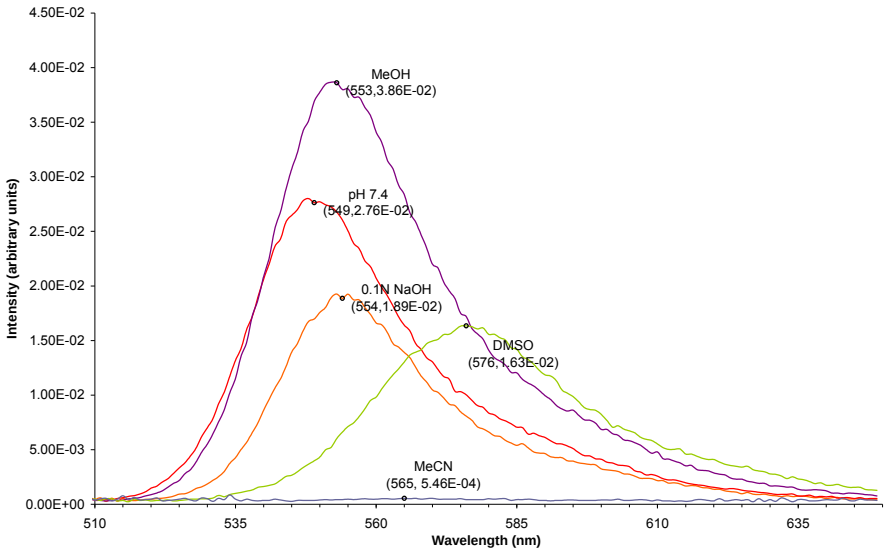

Figure 16 Emission spectra of compound 4 in various solvents

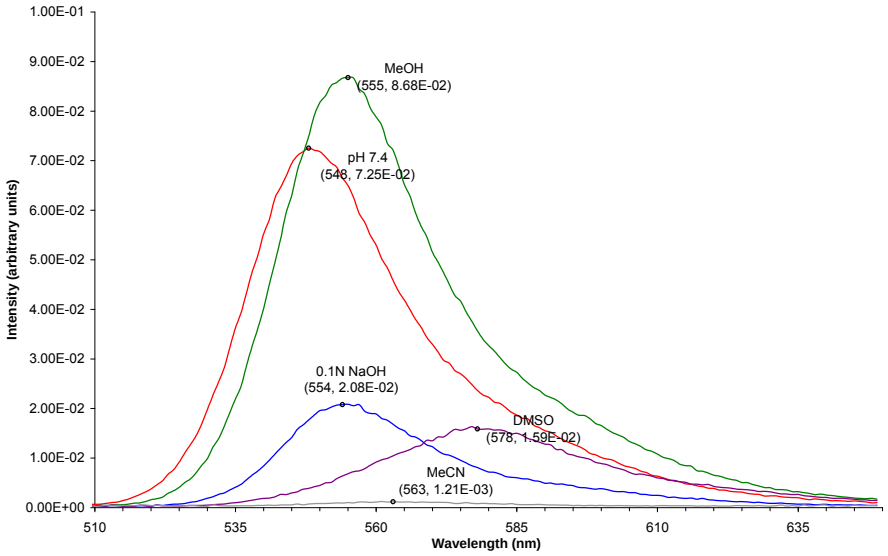

Figure 17 Emission spectra of compound 5 in various solvents

3.3.3.4 PH dependence of Fluorescence Emission

To further explore this pH dependence, we took a series of spectra in phosphate buffer solutions of varying pH from 2.5 to 12.5 (Figures 16-19). While compounds **4** and **5** are

quenched equally at basic pH (Figure 18), the intensity of compound **5** increases sharply below pH 4.5 by 8-fold, while compound **4** increases a modest 2-3 fold. Due to the fact that both aniline and pyridinyl nitrogens can have pKa values in this range, it is not obvious which nitrogen becomes protonated first. We had hoped to use these data to distinguish between the two, but due to the lack of a definite inflection point this was not possible. The wavelength of the emission maximum is also pH dependent, with a red shift of 5 and 6 nm observed for compounds **4** and **5**, respectively, as the pH increases from 2.5 to 12.5 (Figure 19). In Figures 20–21, the spectra are plotted as a function of pH. As the pH decreases, compounds **4** and **5** become unquenched; additionally, compound **5** shows a disproportionate increase in the intensity of a shoulder found around 560 nm that is not found in compound **4**. Although the origin of this shoulder remains yet undetermined, it can be speculated that it may be due to protonation of the second nitrogen. These experiments were repeated by other group members using similar techniques but the results were inconclusive.

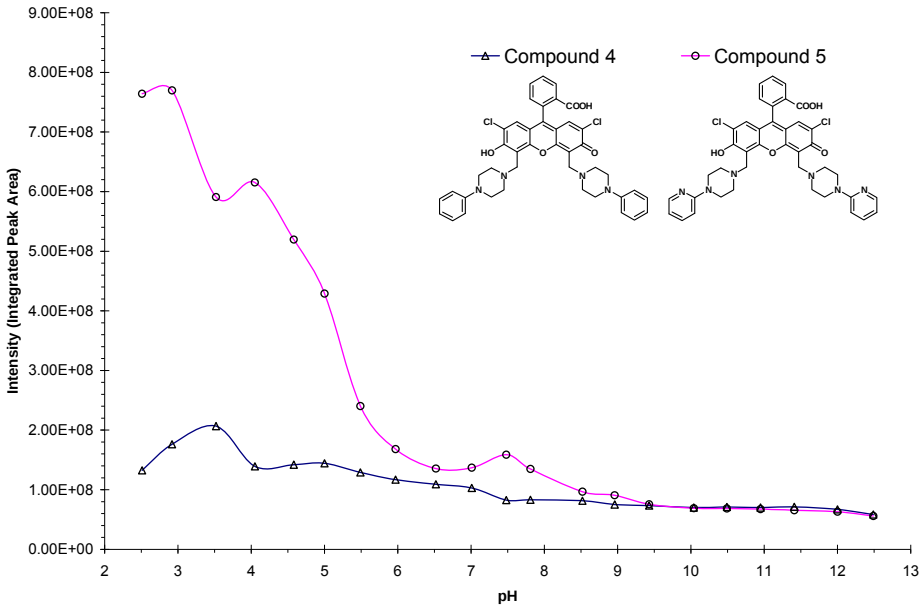

Figure 18 Intensity dependence on pH

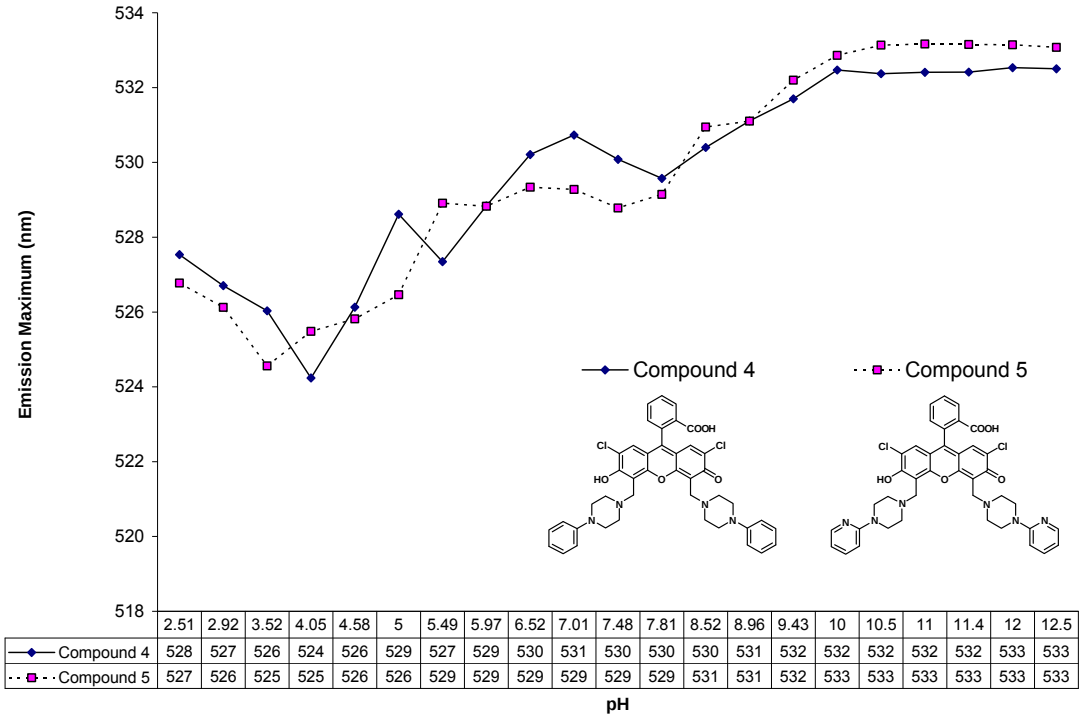

	2.51	2.92	3.52	4.05	4.58	5	5.49	5.97	6.52	7.01	7.48	7.81	8.52	8.96	9.43	10	10.5	11	11.4	12	12.5
Compound 4	528	527	526	524	526	529	527	529	530	531	530	530	530	531	532	532	532	532	532	533	533
Compound 5	527	526	525	525	526	526	529	529	529	529	529	529	531	531	532	533	533	533	533	533	533

pH

Figure 19 Emission maximum dependence on pH

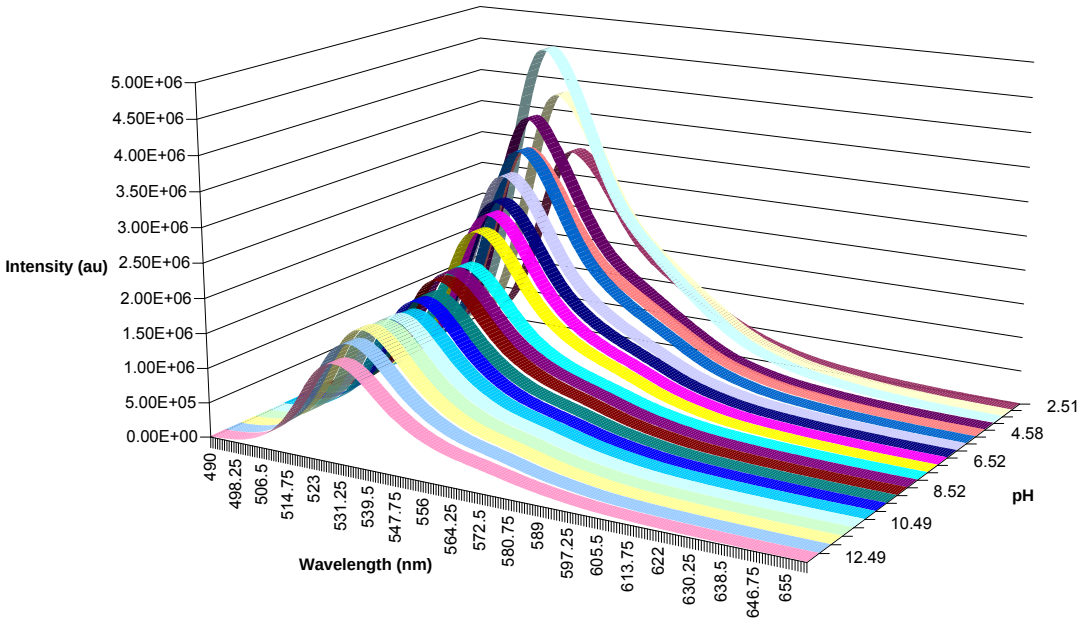

Figure 20 Fluorescence spectra of 4 as a function of pH

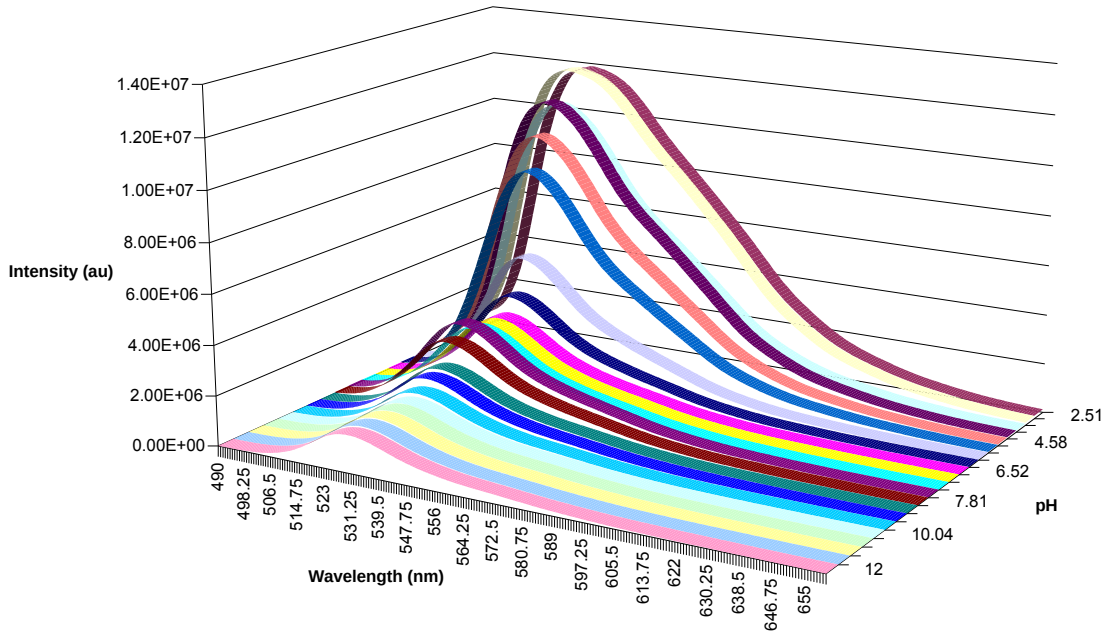

Figure 21 Fluorescence spectra of 5 as a function of pH

3.3.3.5 pH dependence of UV Absorption

Unable to determine the protonation states of DCF-2MPP from the inconclusive fluorescence emission results, we decided to attempt a pH titration while simultaneously acquiring absorbance and fluorescence spectra. The resulting absorbance data are shown in Figure 22. Due to the difference in sensitivity between fluorescence and UV-visible spectrometers, samples appropriate for absorbance were too concentrated for the more sensitive fluorometer, preventing the acquisition of both spectra on the same samples. Since no clear inflection points were present in the absorbance pH titration curve (not shown), the titration was not repeated using fluorescence, and the experiment as a whole was abandoned.

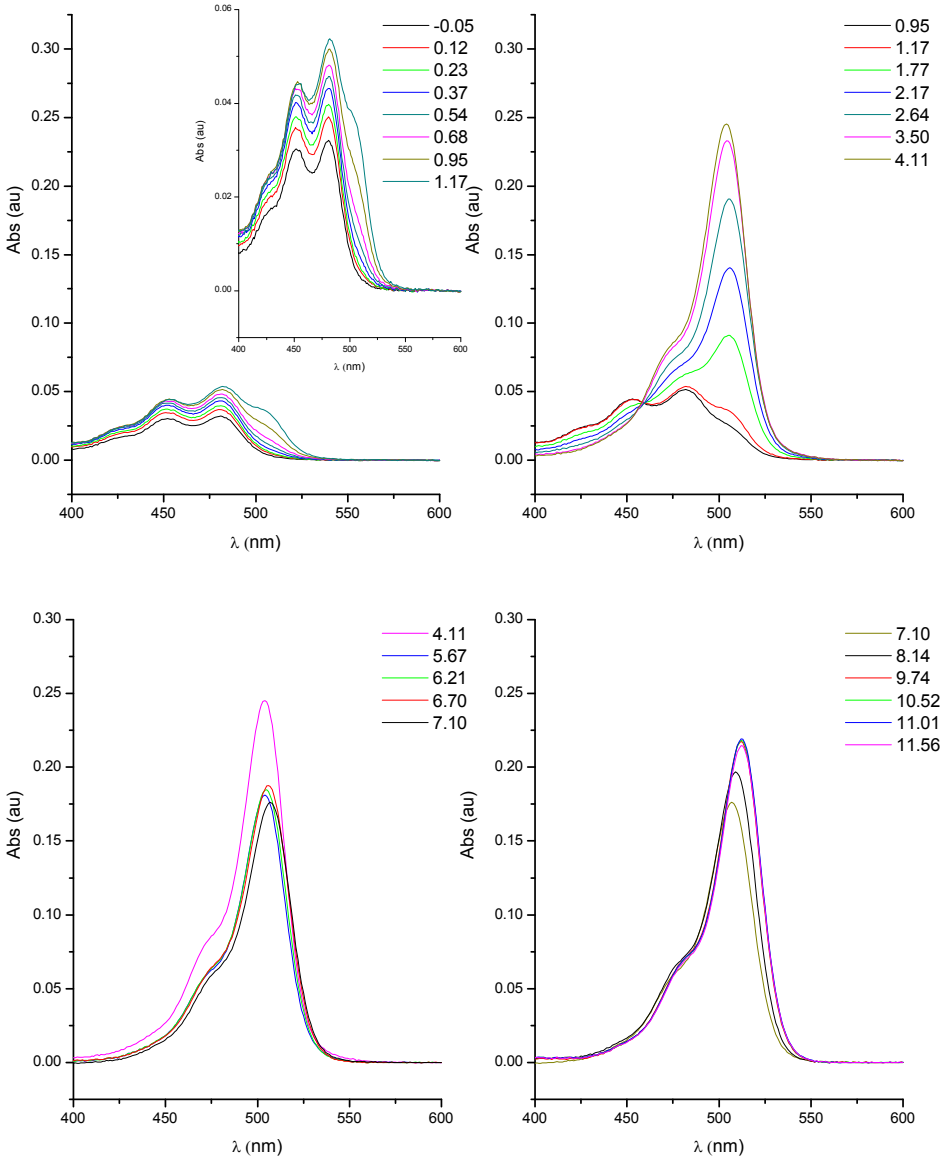

Figure 22 UV-visible absorbance of DCF-2MPP as a function of pH (data series is pH)

3.3.4 3D Structure and Conformational Analysis

Although we were satisfied by the correlation between the HOMO level of the quencher and the fluorescent intensity illustrated by the quantum yield values, upon closer inspection the

distance between the quenchers and the fluorophore appeared to be too great for efficient PET quenching. As shown in Figure 23 (left), we originally anticipated that compound **4** was in an open conformation where the piperazine rings were in chair conformations with the DCF-methylene unit in the equatorial position.

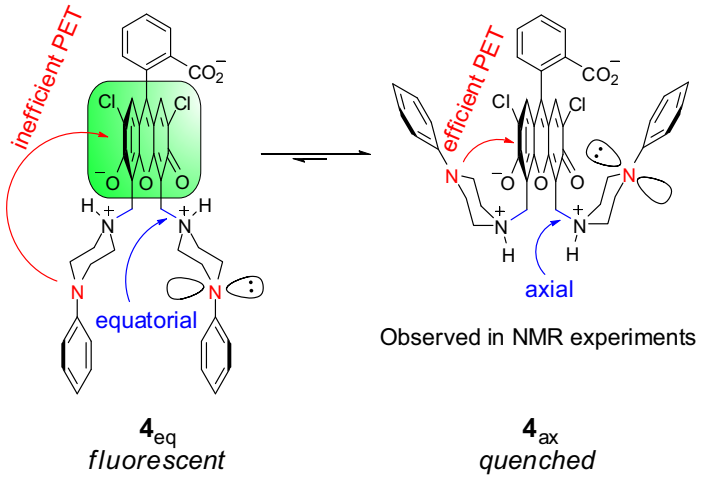

Figure 23 Dynamics of compound 4

To determine how such seemingly distant aniline nitrogen atoms are able to participate in PET quenching, we investigated the conformation of compounds **4** and DCF-2MPP using two dimensional NMR.[78] In Figure 24, the results of 500 MHz COSY, NOESY and ROESY experiments on compound **4** in DMSO-d_6 are shown.[79] It was immediately apparent from through-space enhancement between the phenyl ring of the quencher moiety and the benzoic acid of the fluorophore that the molecule assumed a closed conformation. This observation means that either the piperazine rings assume a boat conformation (not shown) or the DCF-methylene groups occupy axial instead of equatorial positions. In either case, the aniline nitrogen atoms would be proximal to the xanthene ring of the fluorophore, explaining why the

phenylpiperazine moieties are able to effectively quench the fluorescence through space by the PET mechanism. Figure 24A shows a 3D representation of the anchor-like conformation suggested by the NOESY and ROESY data (for clarity, only one of the phenylpiperazine moieties is shown). Key NOE enhancements are shown in Figure 24B followed by a full list of assigned enhancements in Figure 24C. The strongest evidence for this anchor-shaped conformation is the enhancement of protons 6 and 4 of the xanthene and benzoic acid moieties, respectively, by protons 8, 9, and 10 of the phenylpiperazine. This enhancement was present in both NOESY and ROESY spectra. Although we believe that the phenylpiperazine moieties are on alternate sides of the xanthene ring, the symmetry of this molecule prevents their differentiation in these experiments. The proximity of the phenyl ring and the aniline nitrogen of the phenylpiperazine to the xanthene ring supports the hypothesis of PET quenching. When NOESY spectra were acquired of methoxyphenyl compound DCF-2MPP, it was also found to share this anchor-shaped conformation, consistent with its similarly low quantum yield. One explanation for the non-entropically favored conformation observed in these molecules is that the π stacking interactions between the xanthene and aniline moieties which participate in PET quenching also provide sufficient stabilization[80] to sustain this conformation in DMSO. Attempts to support this conformation via computational methods[81] were inconclusive.

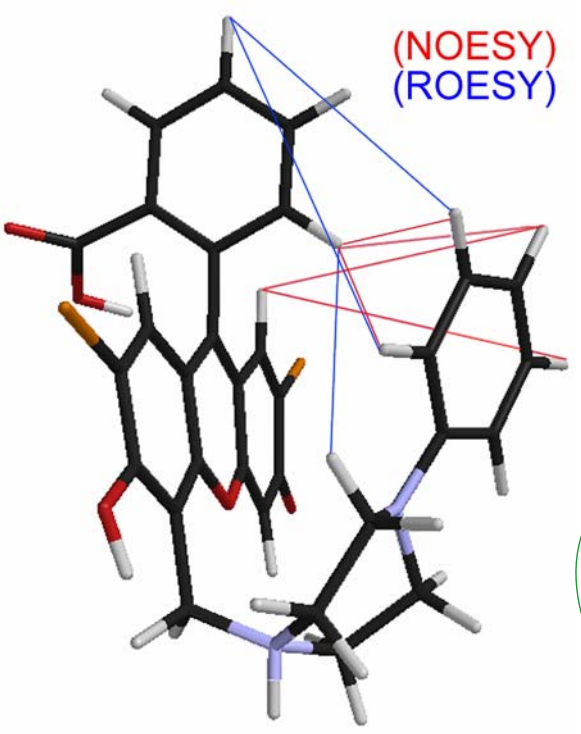

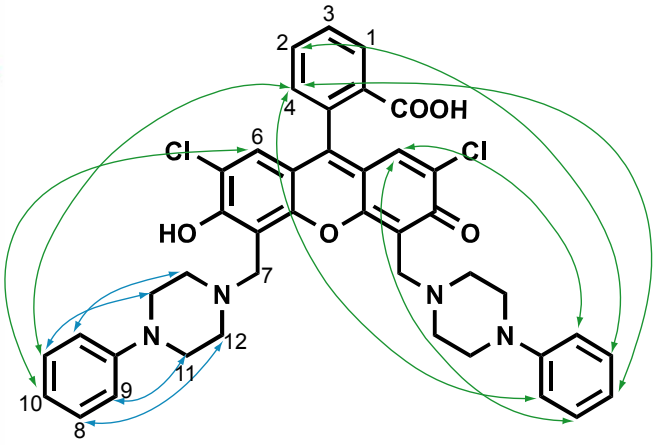

A **B**

COSY	
1	3
2	3,4
3	1
4	2
6	None
8	9,10
9	8,10
10	8,9

NOESY	
1	2,3
2	1,3,4
3	1,2,4
4	2,3,8,9,10
6	8,9,10
8	3,4,6,9,10
9	4,6,8,9,10, 11,12
10	4,6,8,9,10

ROESY	
1	3
2	1,3,4
3	2,3,8,9
4	4,6,9,10,11
6	8,9,10
8	4,6,9,10,11
9	4,6,8,10,11,12
10	6,8,9
11	8,9,12
12	8,9,11

C

Figure 24 2D NMR enhancements of compound 4, see text for details.

3.3.5 Correlation of Conformation to Fluorescence

With a picture of the dynamic nature of these sensors emerging, we wanted to understand the effect of conformation of the quencher moieties on the fluorescence. To demonstrate this, we needed a way to reversibly "open" the molecule while causing as little perturbation to it as possible. The solution to this problem came to us from another group that had been studying inclusion complexes with various cyclodextrins (CD). We reasoned that α- and β-CD, possessing millimolar affinities for benzene and substituted aromatic systems,[82,83] would bind to the phenyl groups of 4 and the anisole groups of DCF-2MPP. This would force the molecule to assume an open conformation, reducing the PET rate as described above and enhancing the fluorescence.

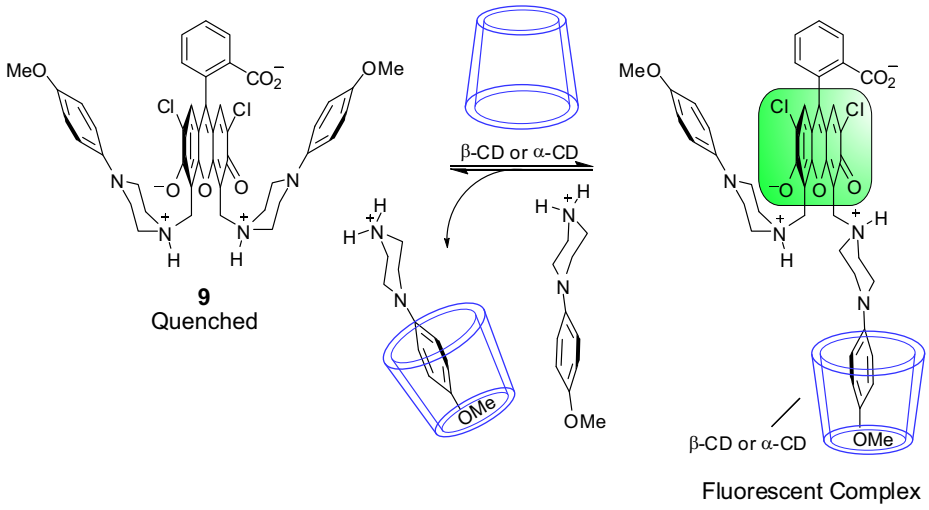

Figure 25 Fluorescence induction by cyclodextrin

Titration of α-CD (final concentration 100 mM) into a 5 μM solution of DCF-2MPP yielded a modest 1.7 fold increase in fluorescence. However, with titration of β-CD (final concentration 5 mM), we witnessed a 4.6-fold increase in fluorescent intensity.[84] The resulting

intensity (Φ ~ 0.14) is similar to that of mono-substituted compound 10 (Φ = 0.176). This correlation, coupled to the steric bulk of *β*-CD, leads us to speculate that β-CD and DCF-2MPP form a 1:1 complex in which one of the two *p*-methoxyphenyl groups is bound to β-CD (Figure 25). This interaction and resulting conformational change suggests that the unquenching of DCF-2MPP occurred because the aniline nitrogens of the complexed MPP moiety are now too distant from the xanthene ring for efficient PET quenching. To test this hypothesis, we added 1-(4-methoxyphenyl)-piperazine (MPP) to the mixture of DCF-2MPP and β-CD as a competitor for β-CD binding. This resulted in a 38% decrease in fluorescence, further supporting our hypothesis (Figure 26). Titration data was also acquired for compound **10** but was inconclusive. Due to the complicated nature of the cyclodextrin interactions, we were unable to construct titration curves sufficient to determine binding data. A possible explanation for this may be in additional interactions between the core DCF and cyclodextrins. Cyclodextrins have been shown to decrease the fluorescence of fluorescein and related dyes when complexed,[85] a phenomena running opposite to and possibly interfering with the fluorescence enhancement shown by DCF-2MPP.

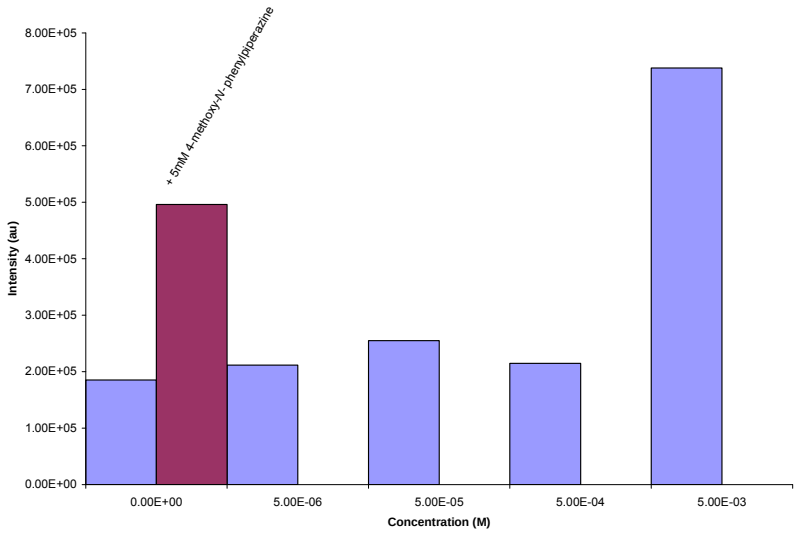

Figure 26 DCF-2MPP cyclodextrin titration

3.3.6 Effect of Metals on Fluorescence

Since our RNA chelating moieties are structurally similar to intracellular zinc sensors, we tested the fluorescence restoration ability of our compounds with various metals. Figure 27 shows the results from compounds **4** and **5**. As a control, each metal was tested with DCF. No metals were found to enhance fluorescent intensity, indicating that there will likely not be false positives due to inter or intra-cellular metal ions if this molecule were to be used in an intracellular environment.

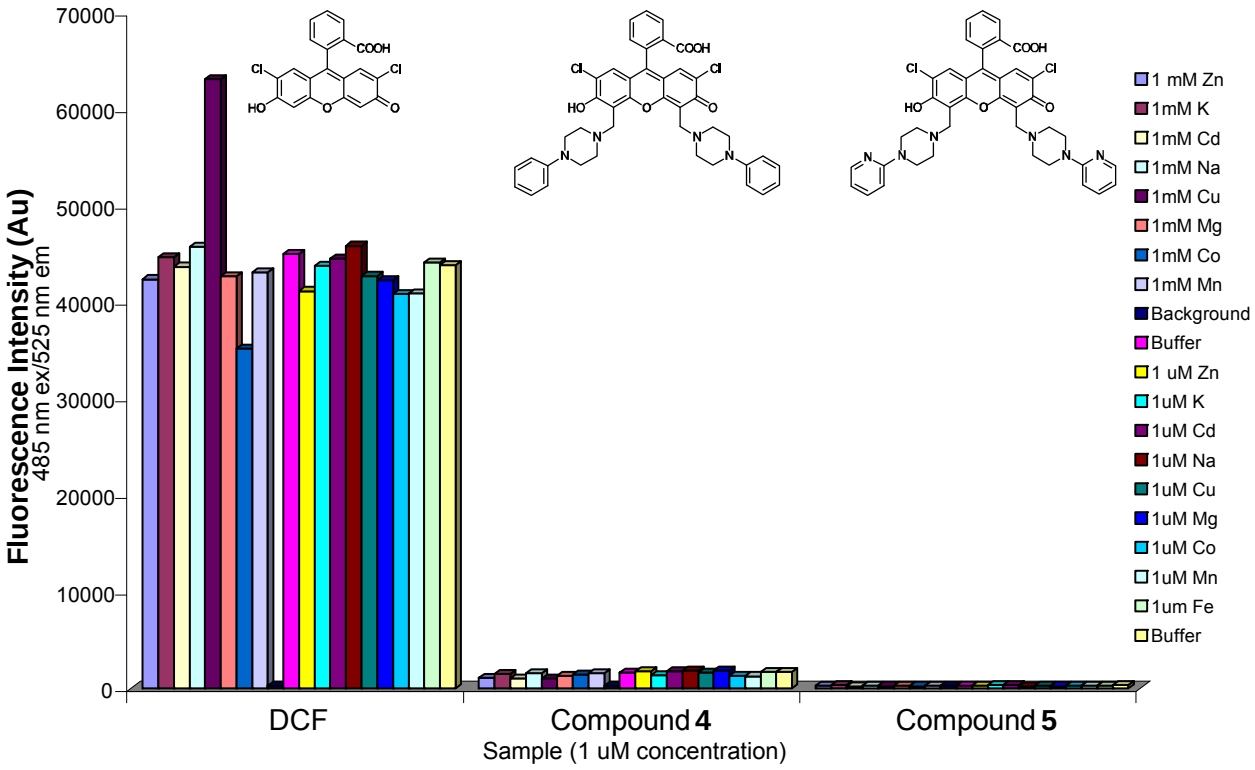

Figure 27 Effect of metal ions on fluorescence

3.3.7 Implications for RNA Detection: A New Approach for RNA Sensors

Having established that the fluorescence of our DCF derivatives is modulated by PET quenching (specifically by the HOMO level of the quenchers and the overall conformation of the molecule), we sought to rationally translate this into the development of RNA sensors. DCF-2MPP is presumably in equilibrium between open (fluorescent) and closed (quenched) conformers (Figure 23). If a specific RNA can be found with the ability to bind only to the open conformer, this interaction will shift the equilibrium toward the fluorescent conformer, resulting in fluorescence enhancement that can be used to visualize the bound RNA. In addition to this conformational change, RNA is likely to bind to the aniline nitrogen atom of the quencher moiety via hydrogen bonding or chelation, something not possible in our cyclodextrin

experiments, thereby lowering the HOMO energy level of the quencher and potentially resulting in further fluorescence enhancement. The challenge is then to find RNA that only binds to the open conformation despite the fact that DCF-2MPP prefers the closed conformation. In other words, it is crucial to find RNA that does not bind to DCF-2MPP in such a way as to lock the closed conformation (i.e., weakly fluorescent conformer). Since the binding of cyclodextrins to the MPP moieties of DCF-2MPP was able to elicit fluorescence enhancement, we reasoned that if RNA that binds to the MPP moieties could be isolated, the resulting conformational change should also elicit a fluorescence increase (Figure 28).

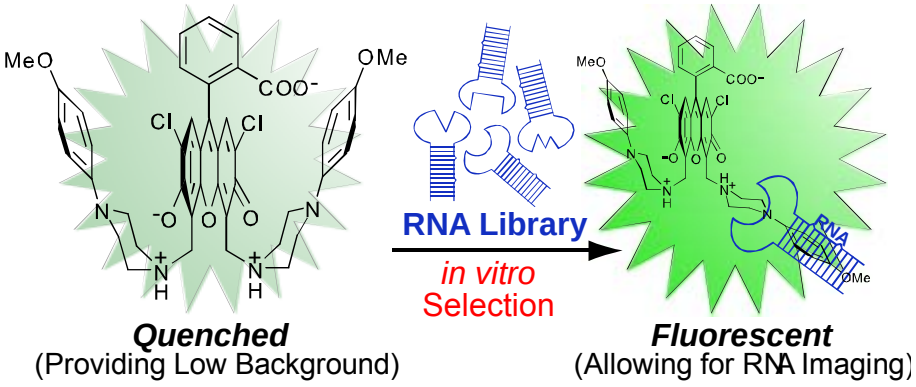

Figure 28 A new approach for RNA sensors

3.4 SYNTHESIS OF AFFINITY MEDIA FOR *IN VITRO* SELECTION

3.4.1 Tentagel Resin-bound DCF derivatives

Before we conducted the spectroscopic analysis necessary to develop the approach described above, we planned to isolate RNA for the PET sensors by synthesizing tentagel resin bound analogs of the sensor molecules. Solid phase synthesis of the derivatives was achieved

via amide bond formation of the amine substituted tentagel resin with carboxydichlorofluorescein directly (Scheme 3). The resulting DCF substituted resin, **11,** was further derivatized via Mannich reaction in the same manner as the solution phase reactions in Scheme 2. Compounds **11**, **12**, **13**, and **14** have been verified by 600MHz magic angle spin NMR. Compound **15** was synthesized to serve as a pre-column in the affinity selection, removing RNA molecules that bind strongly to the resin and linker from the selection pool.

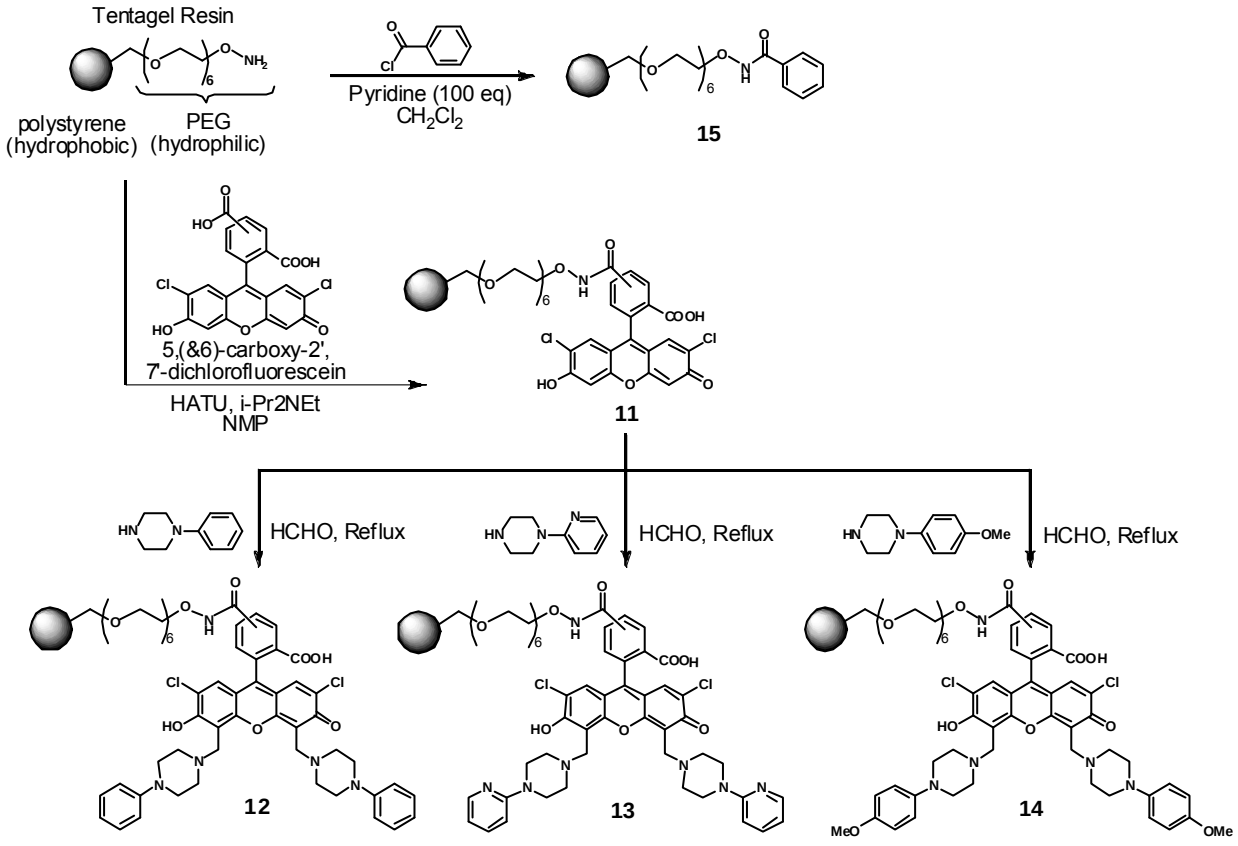

Scheme 3 Solid phase derivitization via amide bond formation

3.4.1.1 Fluorescence spectra of derivatized solid phase resin

With the assistance of Professor Simon Watkins of the Center for Biologic Imaging, University of Pittsburgh, fluorescence emission spectra were taken of compounds **12-14**. Our literature searches indicate no record of such spectra ever being taken of solid phase resin.

Figure 29 shows a scanning laser confocal microscope image of compound **14**. Figure 30 shows spectra taken during the validation of this new method. Of particular interest, is the dramatic red shift exhibited by all of the spectra. We speculate that this is due to perturbations in the solvation environment by immobilization on the solid support. Although interesting, this resin was abandoned due to change in approach.

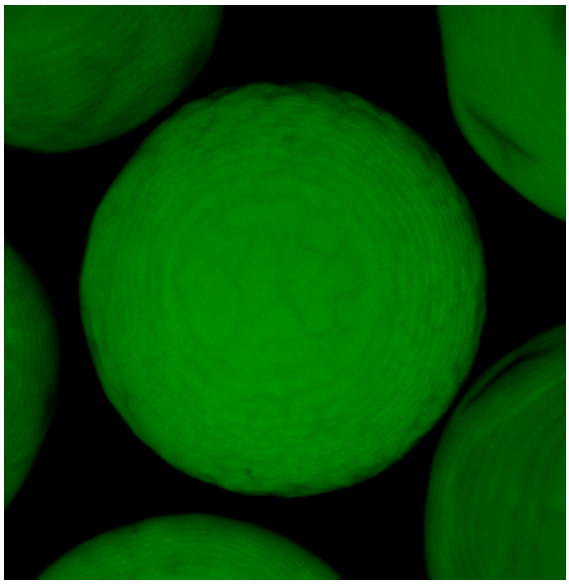

Figure 29 Scanning laser confocal microscope 3D composite image of compound 14

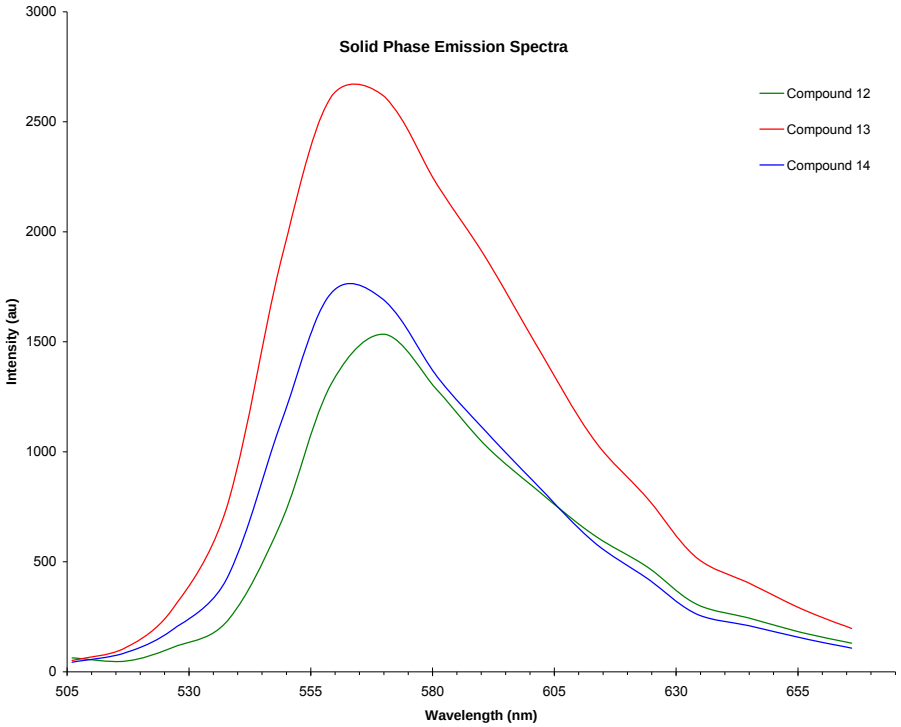

Figure 30 Emission spectra of solid phase resins 12-14

3.4.2 MPP Agarose Resin

Although we originally intended to use agarose resin for its ability to swell in aqueous buffers and its demonstrated success at *in vitro* selection in the literature,[86-89] it is not stable at the high temperatures necessary for the Mannich reaction, requiring us to use the more temperature stable Tentagel resin. After the change in approach resulting from the cyclodextrin experiments, we needed only to have MPP immobilized on a resin. This allowed us to switch back to the original plan to use agarose resin for the affinity media. MPP agarose resin 16 (Scheme 4) would allow us to isolate RNA that binds only to the quencher, increasing the odds of discovering an RNA that would enhance the fluorescence of 9 through the mechanism described above.

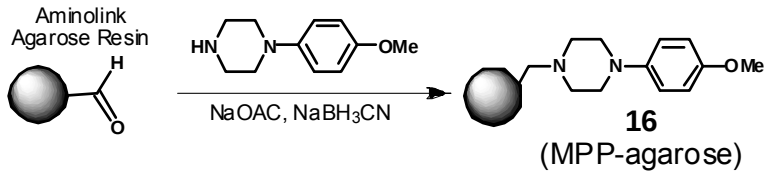

Scheme 4 Synthesis of MPP agarose

3.5 ISOLATION OF APTAMERS FOR MPP

3.5.1 Initial *in vitro* Selection

How does one develop RNA that is able to modulate the fluorescence of a PET sensor? Well aware that it would be a daunting task to rationally design small molecules that both participate in the PET process *and* bind to specific RNA, we chose to only rationally design the PET sensors and to look into alternative approaches to allow us to rapidly develop ligand-RNA binding systems without the need for prior insight into the specific RNA-small molecule interactions. Since we wished to develop reporter RNAs with universal applicability and minimal interactions with endogenous cellular components (similar to the use of tetracysteine moieties in the FlAsH method), we decided to concentrate on the use of artificial RNA sequences. The answer came in the combinatorial biology method *in vitro* selection.

In vitro RNA selection allows for isolating RNAs that possess a rare activity (RNA aptamers) from a large pool of random RNA (typically 10^{13}–10^{15} molecules).[90-92] To isolate aptamers that bind to a specific ligand, that ligand is typically immobilized on a solid support to be used as an affinity column. The RNA pool is incubated on the column, and the non-binding RNA is "purified" away. The binding RNA is then eluted and enzymatically amplified to

produce a new RNA pool (Figure 31). The process is repeated for several rounds until the pool is dominated by binding RNA.

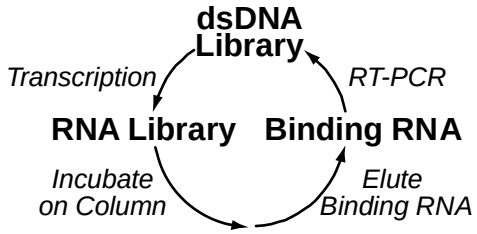

Figure 31 *In vitro* selection

To isolate aptamers for MPP, we synthesized a random RNA library containing a 70 base random region flanked by 20 base constant regions on the 5' and 3' ends for enzymatic manipulation. The layout of the RNA library is depicted in Figure 32 and was based on a library received as a gift from the Szostak lab.

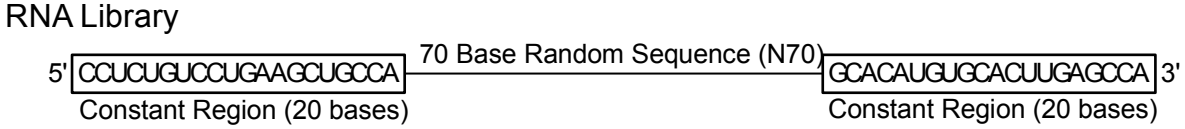

Figure 32 Schematic of RNA library used in *in vitro* selection experiments

The initial aptamers were isolated from a pool of approximately 10^{13} different RNA sequences (as working with 10^{15} molecule library was deemed too expensive). In order to isolate aptamers that only bind to MPP and not the resin itself, it is important to remove the vast majority of RNA that only binds to the agarose portion of the affinity column. This is achieved by employing negative selection for the first 6 rounds, where the RNA library was first passed over the unsubstituted agarose resin before being incubated with the MPP-agarose resin. To further increase the specificity of the aptamers, after the non-binding RNA was washed from the affinity column, the binding RNA was then eluted with elution buffer containing 3 mM MPP,

preferentially eluting aptamers with affinity for MPP. After RT-PCR and *in vitro* transcription to generate a new library, the process was repeated for 8 rounds. After the selection was complete, the aptamers were isolated, amplified by RT-PCR, cloned and sequenced. Of the 24 clones sequenced, 18 unique RNA sequences were identified and 3 sequences stood out due to their presence as multiple copies (indicating dominance in the final pool). The best represented was ***Apt07*** with 5 copies, then ***Apt01*** with 4 copies and finally ***Apt21*** with 3 copies. The lowest energy secondary structure of these aptamers, as predicted by Mfold,[93] is depicted in Figure 33.

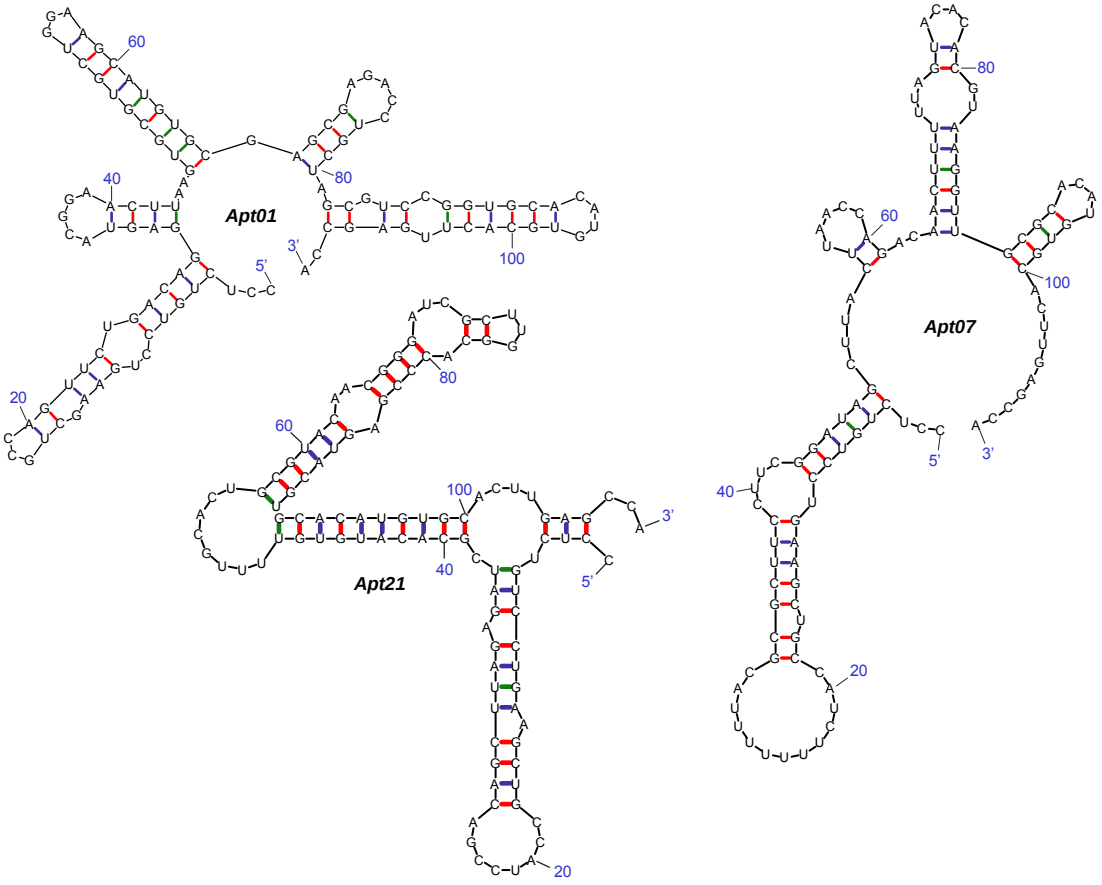

Figure 33 Secondary structures of aptamers from initial selection

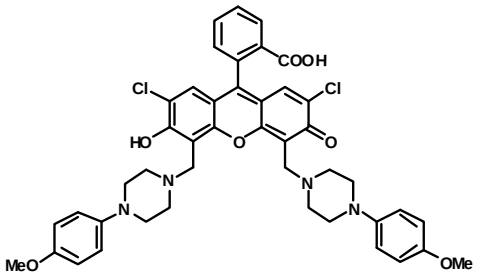

Figure 34 Structure of DCF-2MPP

3.5.1.1 Analysis of Hit Aptamers

To function as reporter sequences, not only did the aptamers need to bind to MPP, they also had to bind to the MPP moieties of DCF-2MPP in such a way to enhance its fluorescence. In order to screen these aptamers for their fluorescence enhancement ability, it was necessary to produce the aptamer RNA on a large scale. Initially, we attempted to use the restriction enzyme EcoR1 to extract the DNA corresponding to the aptamers from the plasmids we used to prepare DNA for sequencing. The aptamer encoding DNA would then be transcribed *in vitro* using the same methods we had used to prepare the library RNA. Due to the small size of the aptamer (110 bases) compared to the pCR4-TOPO plasmid (4k bp) combined with the low yields from the plasmid preparations, simply isolating the aptamer DNA from the plasmids would not produce sufficient DNA to produce RNA on the scale we needed, even after PCR. We determined that the best method to obtain reproducibly pure aptamer DNA was to have it commercially synthesized and use a high-yield commercial transcription kit such as the Promega Ribomax®.

With sufficient amounts of the three aptamers, we screened them for their ability to enhance the fluorescence of **9** and **10** by fluorescence titration. Although our original intention was to screen the aptamers on a 96 well plate format in a fluorescence plate reader, the Cary Eclipse fluorometer to which we had access lacked sufficient sensitivity and dynamic range to

directly compare the quenched and unquenched fluorophores on the same plate. Knowing that the Spex fluorometer we used for the fluorescence characterization experiments had this capability, we decided to use this instrument with 1 mm x 10 mm quartz cuvettes for the fluorescence enhancement studies. The fluorescent intensity of the sensor was monitored at RNA concentrations up to 100 μM for each aptamer. Although two of the three aptamers did not demonstrate significant fluorescence enhancement (one showing only 2-fold enhancement and another showing no enhancement), one RNA proved to be different; this aptamer, ***Apt01*** (Figure 35) was found to enhance the fluorescence of DCF-2MPP by 13-fold at the 100 μM concentration in a concentration dependent manner. None of the aptamers exhibited any enhancement of compound **10**, however. As with the cyclodextrin experiment, the addition of MPP was found to antagonize the fluorescence induction effect, suggesting that ***Apt01*** binds to the MPP quencher moiety, (Figure 36) presumably eliciting a conformational change and lowering the HOMO level of the quencher thereby enhancing fluorescence. The titration curve implies that the stoichiometry may be 1:1 (Figure 35, inset). Substituting the random N70 RNA library for ***Apt01*** did not result in fluorescence enhancement, thus ruling out the possibility of non-specific interactions between RNA and DCF-2MPP.

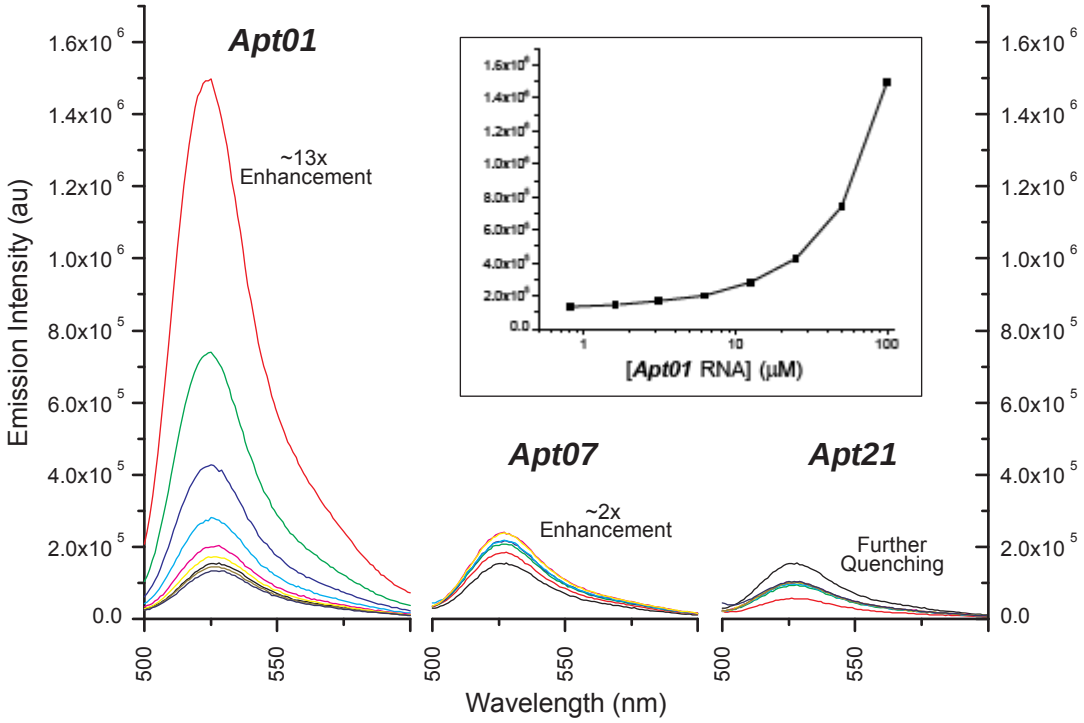

Figure 35 Fluorescence induction of compound DCF-2MPP by aptamers. Inset: Plot of peak intensity vs [Apt01 RNA]

It is noteworthy that the fluorescence intensity of the DCF-2MPP - ***Apt01*** complex exceeds that of compound **10**. If ***Apt01*** only binds to and deactivates one of the two MPP quencher moieties of DCF-2MPP, the maximum fluorescence enhancement should be 7-fold (quantum yield: 0.025 to 0.176). As we were hoping throughout these studies, it is possible that the DCF-2MPP - ***Apt01*** binding induces the conformational change of the second MPP due to favorable electrostatic interaction between the positively charged piperazine ring and negatively charged RNA. This conformational change should result in an increase in the distance between the second MPP moiety and the fluorophore, leading to further fluorescence enhancement.

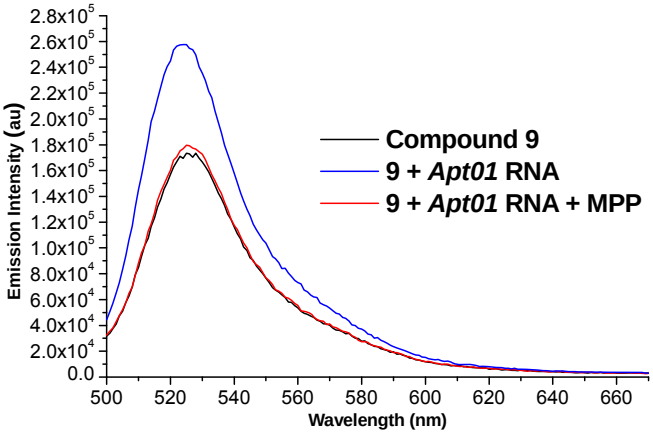

Figure 36 Reversal of fluorescence induction by MPP

3.5.1.2 Mutation Studies

Once the original stock of the ***Apt01*** dsDNA used to prepare the RNA used in the above experiments was consumed and subsequent batches of preparations of template dsDNA did not produce RNA capable of producing the same results, it became apparent that some type of mutation had occurred somewhere in the preparation of the ***Apt01*** dsDNA. Attempts to amplify remaining dsDNA from the original stock yielded DNA incapable of producing fluorescence enhancing RNA. We attempted to determine the sequence by RT-PCR of the ***Apt01*** RNA followed by standard sequencing, but the results were inconclusive. Attempts to determine the RNA sequence by cleavage of ***Apt01*** using RNAse were mostly inconclusive except for the observation that the sequence of the ***Apt01*** RNA was nearly indistinguishable from the intended sequence, meaning that any mutations were small point mutations or short deletions. In light of this result, (and to improve binding) we performed mutation studies based on the initial secondary structure of ***Apt01***, as predicted by Mfold (depicted in Figure 37). We tested four mutants containing the various deletions and point mutations shown in Figure 37

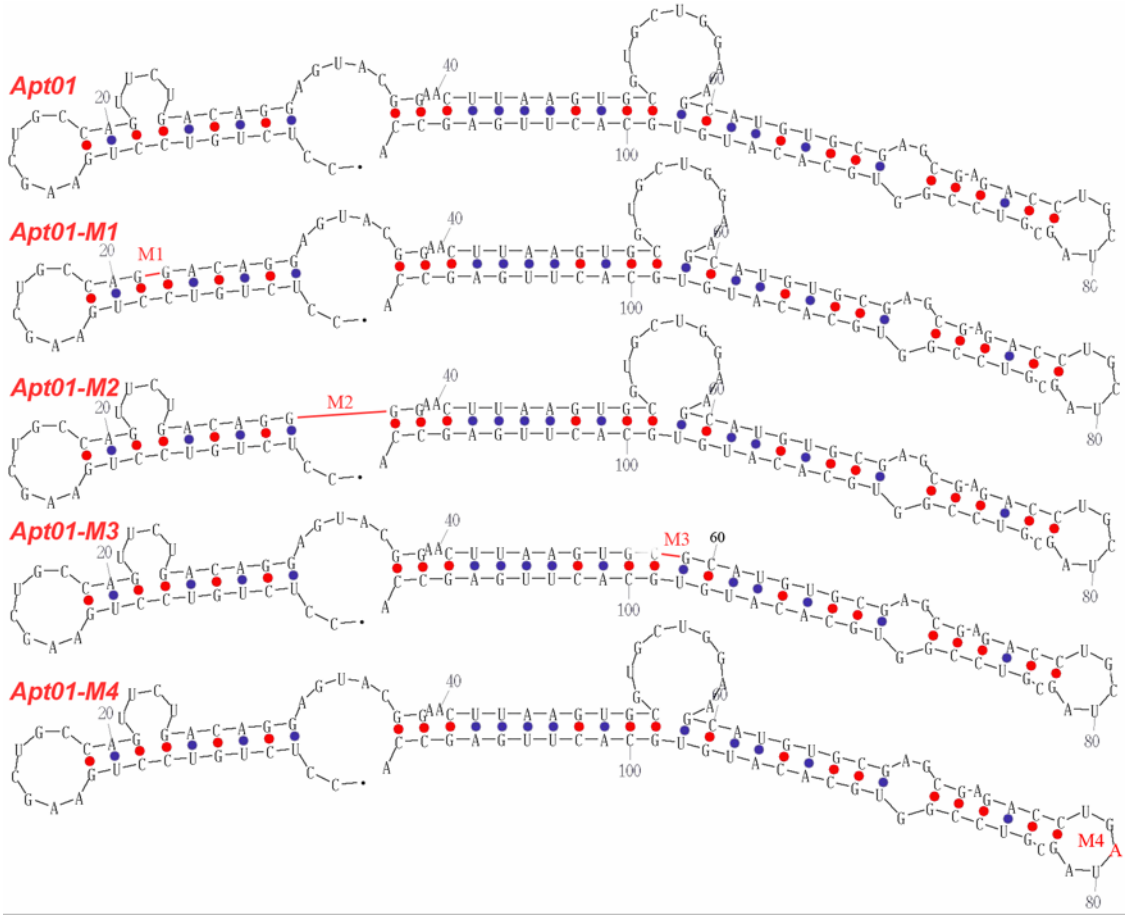

Figure 37 Mutations of Apt01

The mutant aptamers were prepared and tested using the same experimental conditions as the RNA titrations with an RNA concentration of 50 µM. None of the four mutants showed fluorescence enhancement. One possible explanation for these results is incorrect secondary structure. Although initial Mfold results indicate the secondary structure of ***Apt01*** as shown in Figure 37, subsequent predictions show a completely different structure as depicted in Figure 33. If the secondary structure that we based the mutations on was not correct, the changes that we made to the RNA structure may have not resulted in stable conformations similar enough to the ***Apt01*** to perform the conformational change necessary to enhance fluorescence. Future work will have to be done to determine which of the possible secondary structures is correct.

3.5.2 First Biased Library

With the lack of success using mutation studies to construct a tighter binding version of ***Apt01***, we needed a less rational approach not requiring detailed knowledge of the structure of the DCF-2MPP - ***Apt01*** complex. One such approach was to reisolate aptamers for MPP using a library biased toward the sequence of ***Apt01***. A biased library is based on a desired sequence but partially randomized at each nucleotide position during chemical synthesis. The use of a biased library enables the introduction of a controlled number of random point mutations, permitting the screening of many mutations simultaneously. We designed this first biased library to have an 82% bias toward the ***Apt01*** sequence, meaning that at each nucleotide position, there would be an 82% possibility that that base would be the same as the original sequence (wild type) and a 6% chance that it would be any of the other three bases. The actual *in vitro* selection procedure was similar to the initial selection, but with two minor changes. First, we did not do the negative selection, rationalizing that since we were starting with a sequence already "purified" of the resin binding RNA that it was not necessary. Second, we introduced a pre-elution step to increase the stringency of the selection. We hypothesized that if we washed the aptamer-bound column with a 3 μM MPP solution to elute the weak binding RNA before washing with the 3 mM MPP solution to elute the more strongly binding RNA that we could increase the efficiency and stringency of the selection by preferentially eluting more tightly binding aptamers. As before, the selection was run for eight rounds, at which point the sequences of the hit aptamers were determined.

Much to our surprise, after the sequencing of 24 clones, we found little or no homology between the sequences. The addition of 10 more clones did little to improve the situation, although we were able to find one group of eight closely related sequences, containing a pair of

identical sequences (***AptB17***, Figure 38) in addition to a group of three identical sequences (***AptB25***, Figure 38) and three more pairs of identical sequences, of which we arbitrarily chose one to test further (***AptB6***, Figure 38).

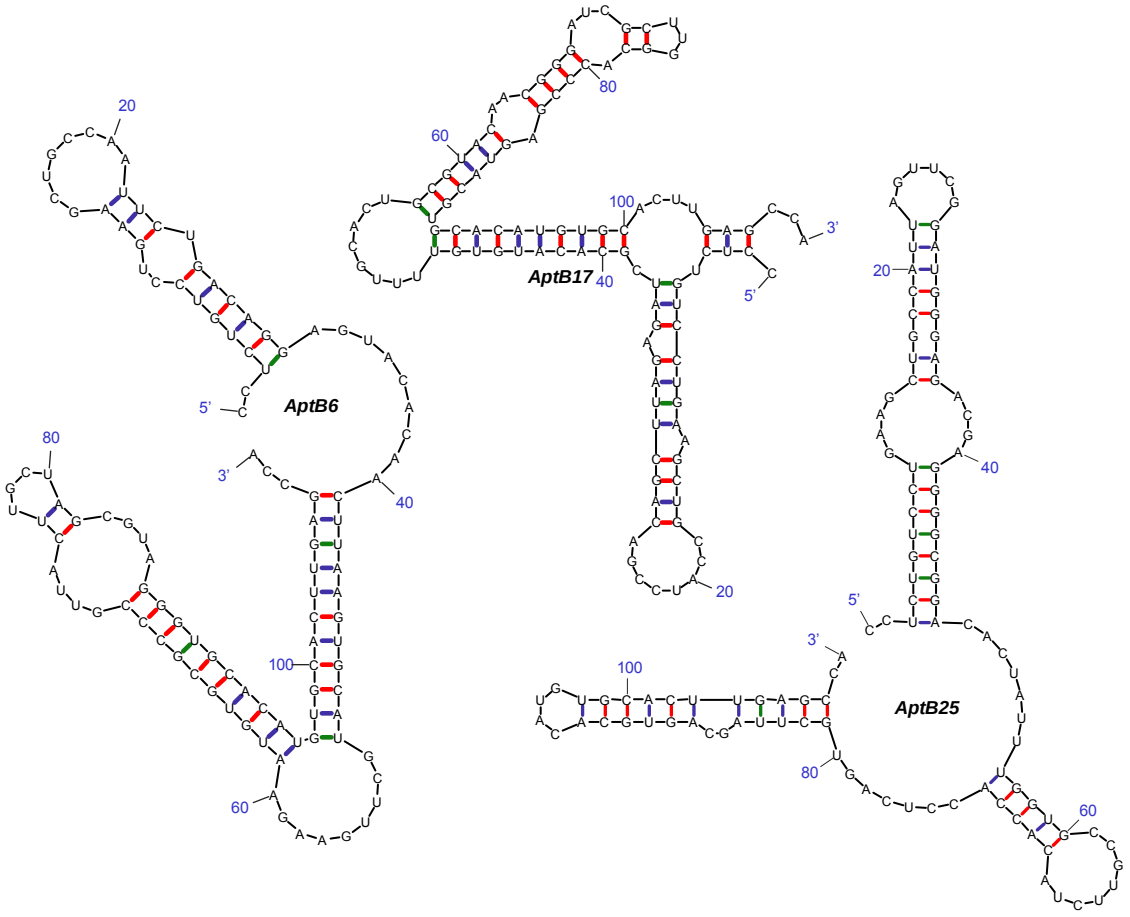

Figure 38 Mfold predicted secondary structures of aptamers from the first biased library selection

The biased library aptamers were then produced on a large scale and tested for their ability to enhance the fluorescence of DCF-2MPP as described above. When considering the lack of homology in the sequenced hits, it was little surprise when the three aptamers produced inconclusive results, without any of them showing fluorescence enhancement. Upon closer inspection of the secondary structures, it occurred to us that the sequences of ***AptB17*** and ***Apt21***

were identical. Despite the fact that this sequence does not enhance the fluorescence of DCF-2MPP, it is interesting that it was isolated twice using two independent libraries. One possible explanation is that it binds to MPP in such a way that is incompatible with binding to the entire DCF-2MPP molecule or binds in such a way so as to not enhance the fluorescence. Further investigation into this hypothesis is necessary once a reliable method is found to study aptamer-DCF-2MPP and aptamer-MPP binding without the need to monitor fluorescence enhancement.

3.5.3 Second Biased Library

These negative results prompted us to revisit the design of the biased library. The fact that none of the biased library hits showed any homology to each other or, most importantly, the ***Apt01*** (wild type) sequence on which the library was based, indicated that the library was not biased enough toward the wild type. Based on literature guidelines,[94] in order for a 70 random base library to have ~85% of the molecules with 3–8 mutations per molecule, it should have a degeneracy of ~7%. Our first biased library had a degeneracy of 18%, meaning that ~85% of the library contained between 8 and 17 mutations per molecule. Although this level of degeneracy is sufficient for mutation of short segments, it is too randomized for a large span of 70 bases. With this new information, we resynthesized the biased library to have 7% degeneracy and repeated the selection experiment with the new library.

The selection was performed in a similar fashion to the initial selection, except that it was conducted for 10 rounds with the negative selection not being performed in rounds 3-5. Of the 12 unique sequences isolated, three sequences most intrigued us (Figure 39); the first, ***AptB221*** was well represented in the library (with five copies in our sampling), the second, ***AptB213*** was also well represented with four copies and the third, ***AptB212*** was the most similar to the wild

type, with 87% homology.[95] To test the aptamers for their ability to enhance the fluorescence of DCF-2MPP, the aptamers were again produced on a large scale and titrated to a maximum RNA concentration of 50 μM while monitoring the fluorescent intensity.[96] In a departure from previous titration experiments, an initial screening step was performed where each aptamer was first tested at 50 μM on the Spex fluorometer (Figure 39) for its ability to enhance fluorescence before a full titration was performed. Titrations of the aptamers that showed fluorescence enhancement were performed in a 96 well plate format on a Molecular Devices M2 plate reader. ***AptB212*** did not significantly enhance the fluorescence of DCF-2MPP, which is not surprising due to its lack of wide representation in the collection of sequences determined. However, the more represented ***AptB213*** (Figure 41) and ***AptB221*** (Figure 42) aptamers showed 3.8 and 4.1 times enhancement, respectively. This enhancement is comparable to the 4.7 times enhancement exhibited by ***Apt01*** at 50 μM.

This experiment demonstrates the power of a biased library to improve hit rates in the search for signaling aptamers. In the initial selection, only one of three well represented aptamers was capable of enhancing the fluorescence of DCF-2MPP. After the biased library selection, both of the well represented aptamers were capable of fluorescence enhancement, displaying rates comparable to the original aptamer the library was based on.

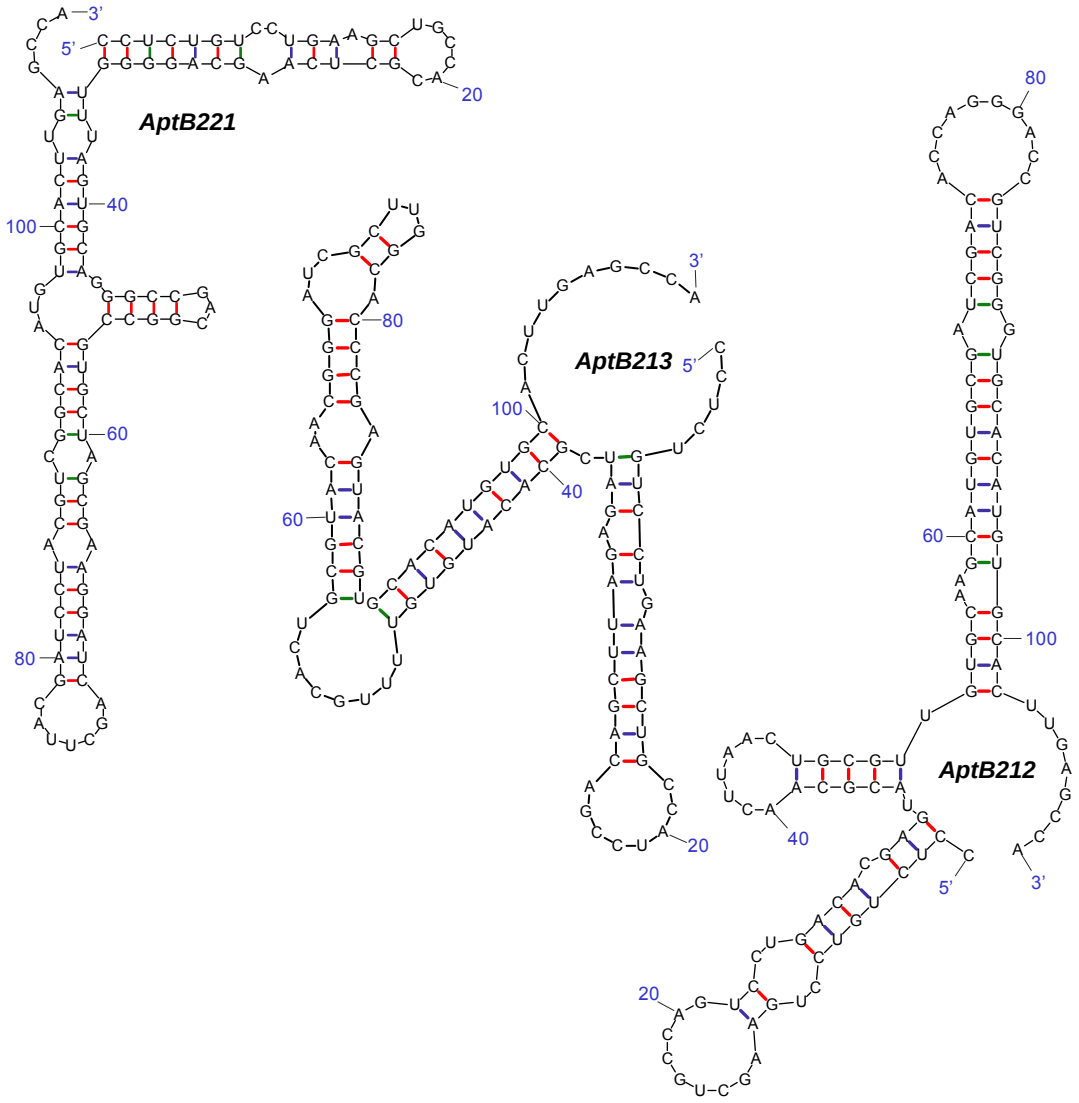

Figure 39 Mfold predicted secondary structures of aptamers from the second biased library selection

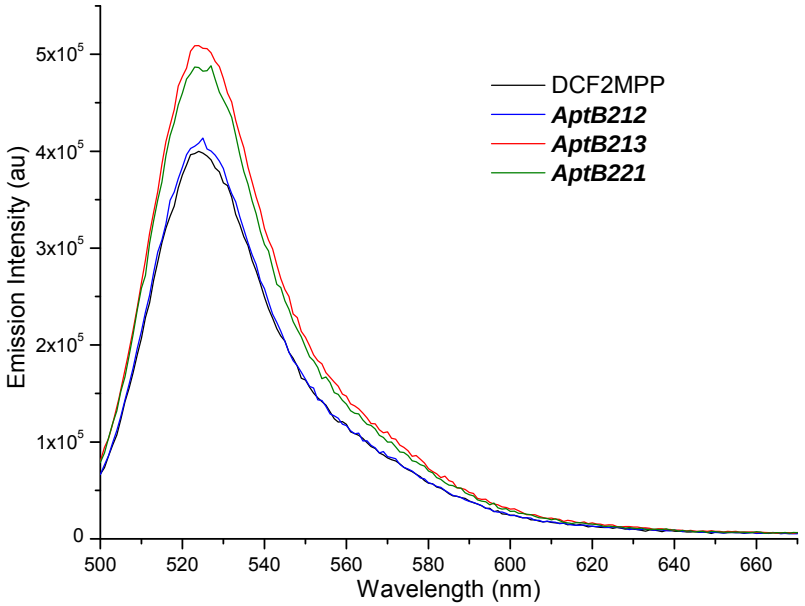

Figure 40 Preliminary screening of second biased library aptamers. [RNA] = 50 µM

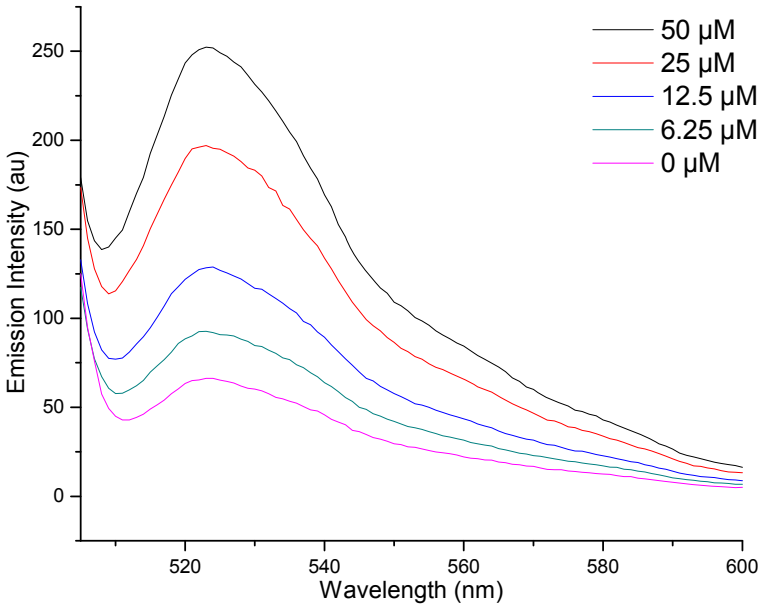

Figure 41 Titration of Aptb213 with 1 µM DCF-2MPP

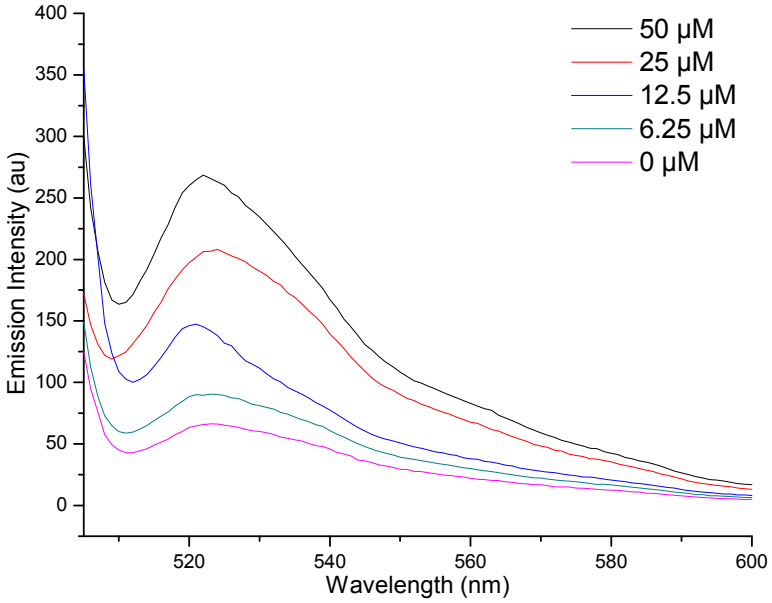

Figure 42 Titration of AptB221 with 1 µM DCF-2MPP

3.5.4 "Less G" Library

To investigate the effect of fluorescence quenching by guanosine residues suggested by Knemeyer, et al[97] and Rupcich, et a,l[98] we synthesized a new library biased *against* guanosine. Our thinking was that if we were able to isolate aptamers for MPP that contained fewer guanosine residues, their ability to enhance the fluorescence would be greater due to the resulting decrease in guanosine quenching. To achieve this, we biased the library to contain 12% G instead of the standard 25%. This selection was conducted simultaneously with the second biased library to save time. Procedurally, nothing was changed from the initial selection, except that the negative selection was delayed to the 6th round of to increase initial hit rates with the selection being carried through 10 rounds. Of the 24 sequenced hits, we found one group of seven closely related sequences represented by ***AptG17***, one group of three identical sequences

(***AptG24***) and a few sets of two identical sequences. Interestingly, neither of these aptamers shows any bias away from the 25% G composition we would have expected (Figure 43).

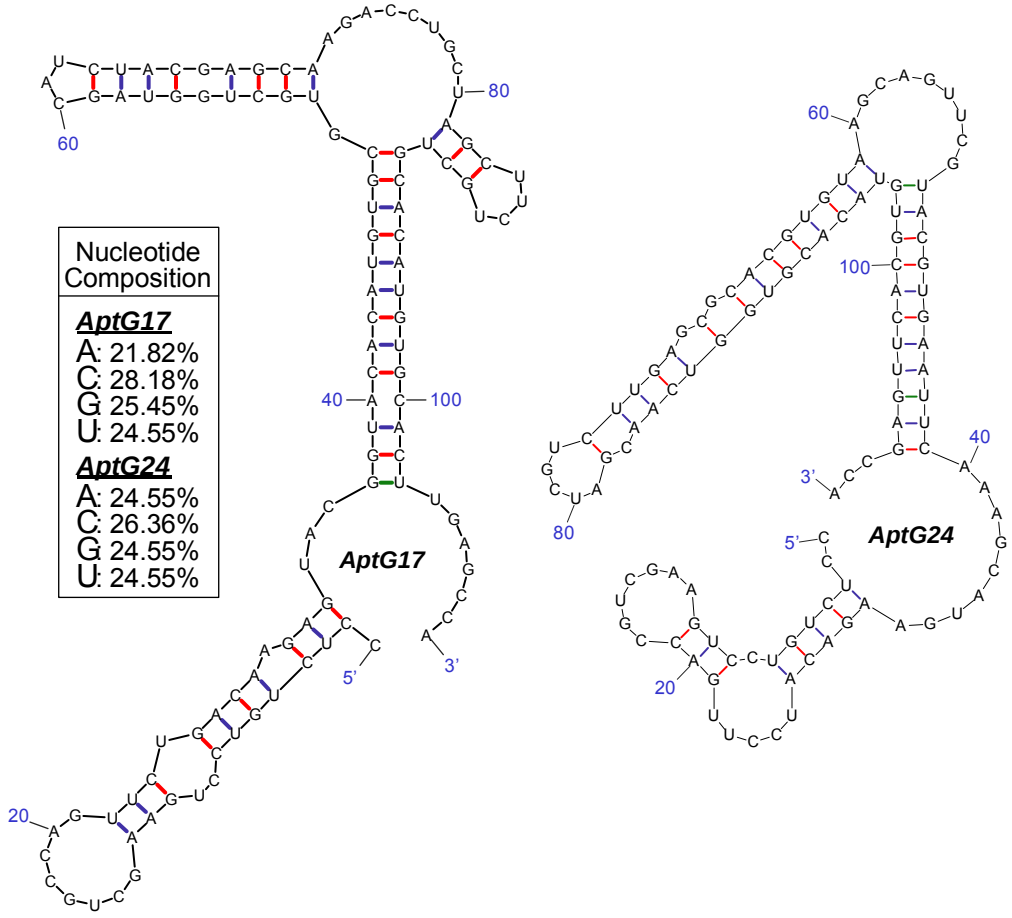

Figure 43 Mfold predicted secondary structures of "Less G" library aptamers. Nucleotide compositions are shown in inset

As with the second biased library, the aptamers were produced on a large scale and screened at 50 µM on the Spex fluorometer for the enhancement of 1 µM DCF-2MPP (Figure 44). Of the two aptamers tested in this way, ***AptG24*** showed enhancement and was subsequently titrated using the plate reader method described above (Figure 44, inset). With this method, ***AptG24*** was found to enhance the fluorescence of DCF-2MPP by 4.0 fold. Despite the fact that we were unable to isolate an RNA aptamer with a lower percentage of guanosine with this

selection, the isolation of ***AptG24*** is good support for the generality of the approach, as we have demonstrated that aptamers capable of fluorescence enhancement can be isolated from each of two completely independent libraries. It is intriguing that ***AptG24*** has 86% homology to ***Apt01***, despite the fact that the two libraries were unrelated in sequence.

It is worthwhile to note that all of the aptamers studied here proved to be quite stable, allowing us to recycle and re-purify the RNA many times with no degradation visible by polyacrylamide gel electrophoresis.

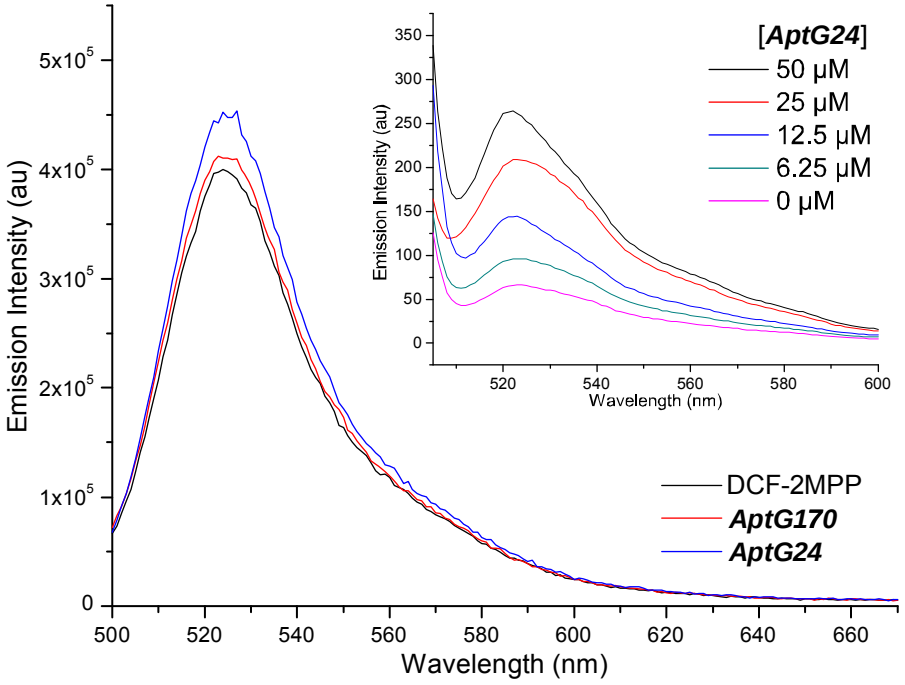

Figure 44 Fluorescence enhancement of "less G" library aptamers. Inset is titration of AptG24 with 1 µM DCF-2MPP

3.6 STUDY OF RNA-SMALL MOLECULE INTERACTIONS

3.6.1 Electrophoretic Mobility Shift Asays

After the inability of the first biased library to produce aptamers that would enhance the fluorescence of DCF-2MPP, we realized that it would be useful to have an alternate method to evaluate the binding between the RNA aptamers and various small molecules (namely MPP and DCF-2MPP). Through personal communication with Dr. Adam Roth of Yale University, we decided that by adapting electrophoretic mobility shift assays[99,100] (EMSA) commonly used to study protein interactions, we should be able to observe RNA-small molecule interactions. The theory behind mobility shift assays is simple: since non-denaturing electrophoresis separates species based on their size/diameter as well as their charge, a DNA-protein (or in our case RNA-small molecule) complex will have substantially different mobility that that of the DNA (or RNA) alone. Provided the complex is stable over the time course of the separation, it is possible to evaluate the binding of a pair of species by comparing the bands of the RNA and RNA-small molecule complex. In such a case, K_D = [Ligand] x R (R= Ratio of the unbound RNA to bound complex). Therefore, when the bands corresponding to the free RNA and RNA-small molecule complex are of equal intensity, the K_D is equal to the ligand concentration (small molecule in our case). A typical EMSA gel is depicted in Figure 45. In this figure, the RNA is denoted by the black band and the RNA-small molecule complex is denoted by the blue band. As the complex travels slower than the free RNA, it can be separated and the two bands can be visualized by using radioactively labeled RNA or an RNA-specific dye such as Sybr Green II (Molecular Probes. Eugene, OR).

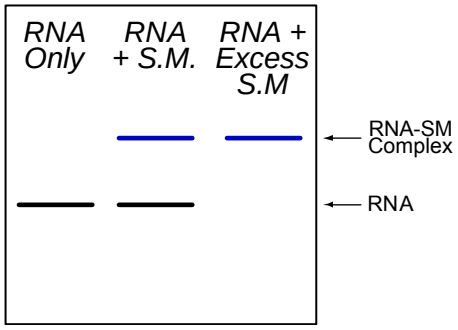

Figure 45 EMSA assay

DNA-protein interactions have the advantage that they are easy to study using EMSA due to the large difference in mobility from the free DNA to the complex. This comes from the significant size and charge change upon binding and stable interactions in the low ionic strength buffer used in EMSA. One of the challenges in studying RNA-small molecule interactions using such techniques is that, unlike RNA-protein interactions, there is not a significant difference in size when adding a small molecule to an RNA. Therefore, the majority of the separation will be based on the charge difference between the free RNA and the complex with the small molecule (typically positively charged). We felt that through careful optimization of the gel composition we would be able to perform such a separation.

Initially, we used standard 10% acrylamide gels with tris-borate EDTA (TBE) buffer to test the ability of the biased library aptamers to bind to MPP. To accomplish this, we incubated aptamer RNA from the first biased library (25 nM) with varying concentrations of MPP and loaded the mixtures on the gel. The gel was run and the RNA was detected with Sybr Green II dye to compare the bands to see if any shifts occurred (Figure 46). We did not observe any shifts, which is not entirely surprising given that the aptamers from the first biased library showed no fluorescence enhancement. In an attempt to validate this method, we reran the gel

using the aptamers from the first selection (two of which having displayed fluorescence enhancement). Again, no shifts were observed (Figure 46).

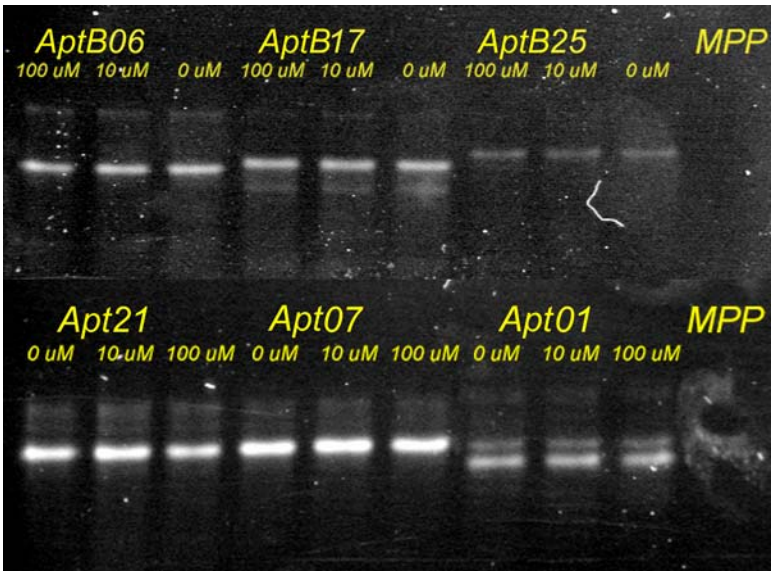

Figure 46 Actual EMSA assay

We then decided to rerun the ***Apt01*** RNA with MPP and also with neomycin, to function as a control and verify that RNA can bind to small molecules under these conditions (Figure 47).

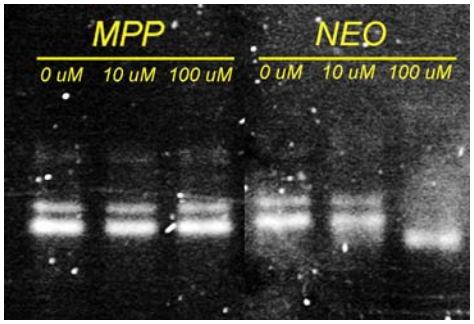

Figure 47 EMSA of Apt01 with MPP and neomycin

Much to our delight, we found that ***Apt01*** bound to neomycin at the 100 μM concentration. Why did ***Apt01*** not bind to MPP under these conditions? We speculated that

either the addition of the 5% glycerol necessary to load the solution into the wells or more likely the buffer composition preventing binding. The electrophoresis buffer used in these experiments was drastically different from the buffer we used for the *in vitro* selection experiments. The electrophoresis buffer also contained EDTA, which would have chealated the Mg^{2+} ions necessary for RNA to form proper secondary structures. Subsequent attempts were made with various buffers and gel concentrations, but no combination possessed sufficient resolution to conclusively replicate the binding observed in solution.

3.6.2 Capillary Electrophoresis (CE)

Once we determined that the likely problem plaguing the EMSA experiments was the inability to resolve the bound from unbound bands, we envisioned repeating these experiments using capillary electrophoresis (CE). Following the same basic principles as gel electrophoresis, CE has the benefit of significantly higher resolution, built-in UV or fluorescence detection, and the ability to automate experiments for better reproducibility.

Initial experiments involved running ***Apt07*** RNA and attempting to determine its affinity for MPP (which was previously demonstrated by fluorescence titration). This was soon deemed not possible due to the high ionic strength of the buffer causing Joule heating in the capillary, resulting in decreased resolution and broadening of the peak below the detection limit. Since there were no literature guidelines for studying RNA-small molecule interactions with CE, we decided to first develop and test a method on a well studied RNA-small molecule system (preferably one with low ionic strength binding buffer).

For such a model system, we turned to the neomycin:Rev-RRE interaction that we had used to initiate our project on sensor development. Neomycin has been demonstrated to bind to

the 67 base *R*EV *r*esponse *e*lement of HIV-1 virus with 82 nM affinity *in vitro*[70] in a relatively low ionic strength buffer (10 mM Tris, pH 7.6, 10 mM $MgCl_2$, 50 mM NH_4Cl). In addition, we hypothesized that the +6 charge of neomycin at pH 7.6 would produce a noticeable change in the mobility of the RNA upon binding. Once the conditions were optimized, we were able to detect the free RNA, but the RNA:neomycin complex could not be observed. Neomycin could be associating with the coating on the capillary wall, thus preventing it from forming a complex with the RNA. Another possible explanation is that, due to the positive charge on the neomycin and the extreme difference in mobility between free neomycin (+ charge) and free RNA (- charge), the complex will not migrate to the detector in a reasonable amount of time (greater than the 120 minute run time of the experiments), thus preventing its detection.

After the failures with neomycin, with the help and guidance of the Schneider lab at Carnegie Mellon University, we decided to move to another test system that was related to another project currently being conducted in the Koide group. The ferritin iron responsive element (f-IRE) has been shown to have 3.9 μM affinity for yohimbine[101] (Figure 48). In addition to this tested affinity, the f-IRE binding buffer used in the literature experiments has a low ionic strength (10 mM HEPES, pH 7.2, 40 mM KCl, 3 mM $MgCl_2$), reducing problems caused by Joule heating. The short length of the f-IRE RNA (50 bases) allows it to be commercially synthesized, providing a fast route to very pure RNA.

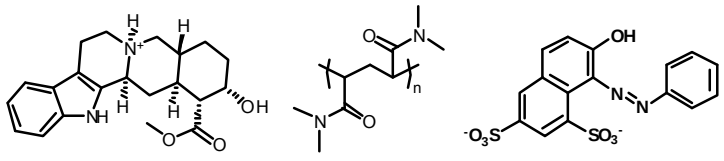

Figure 48 Structures of yohimbine, PDMA and orange G

In addition to the change in model system, we also instituted the use of the polymer sieving matrix PDMA[102] (poly(*N*-*N*-dimethylacrylamide)) to provide separation based on size (similar in concept to the EMSA assays we had previously performed), hypothesizing that the f-IRE RNA would assume a different conformation in the presence of yohimbine than it would free in solution; permitting its separation. Figure 49 shows a representative set of electropherograms. The chromophore Orange G was run as a reference standard to calibrate the migration times. To evaluate binding, samples consisting of Orange G, Orange G with f-IRE RNA, and Orange G with f-IRE RNA and yohimbine were run in triplicate (only one run from each is shown in Figure 49 for clarity). In Figure 49, although it appears that there is a measurable difference in the migration time, this is misleading because the run to run variability in the migration time is greater than the difference between the migration time of the f-IRE and the f-IRE:yohimbine complex.

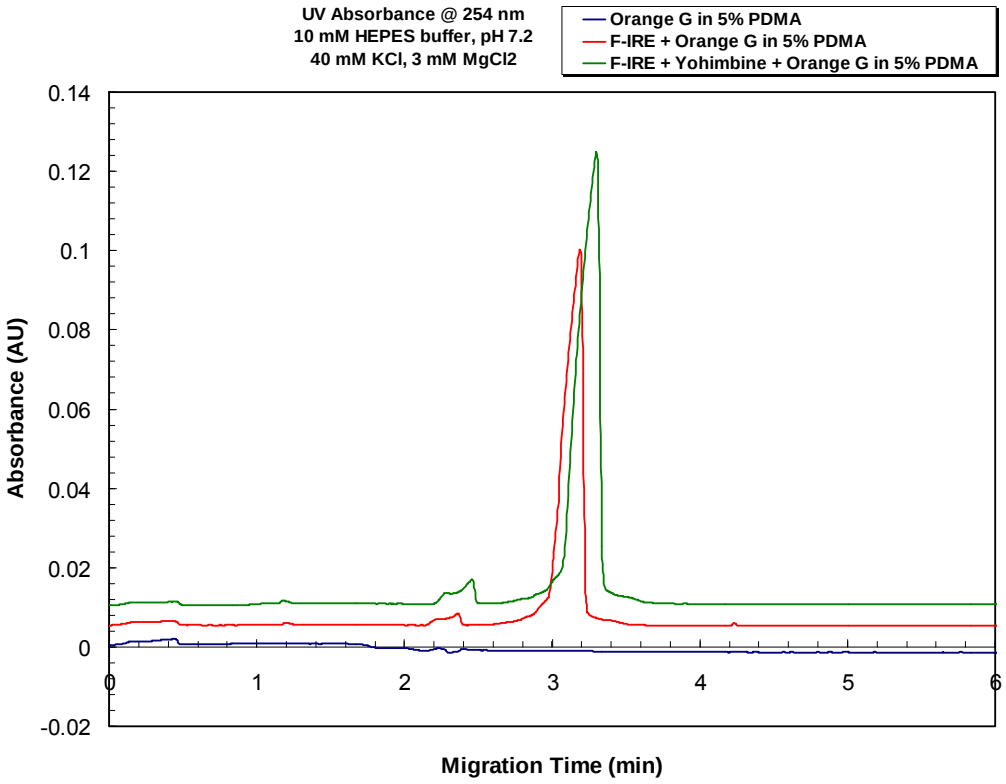

Figure 49 Representative electropherograms

After considering other methods, we concluded that although it may be possible to eventually find conditions to provide sufficient resolution to determine kinetic data, these conditions would be specific to each system studied. Since the goal was to develop a general method to study RNA-small molecule interactions, this approach was put on hold, to hopefully be picked up by another researcher or in collaboration with a research group that specializes in capillary electrophoresis.

4.0 CONCLUSIONS: A NEW PARADIGM FOR RNA SENSORS

Through the convergence of organic synthesis and combinatorial biology, we have developed a new paradigm for the development of fluorescent chemosensors for RNA (Figure 50). By following a rational approach toward sensor design, we have demonstrated that it is possible to synthesize new PET sensors merely by combining existing fluorophores with quenchers possessing appropriate HOMO energy levels, a process that is amenable to building combinatorial chemical libraries of PET sensors. After fluorescent and conformational analysis, candidate sensors were chosen and RNA aptamers isolated for the quencher units of the selected sensors. Once aptamers are isolated, it is possible to morph the sequence into remotely related sequences by further *in vitro* selection using biased libraries.

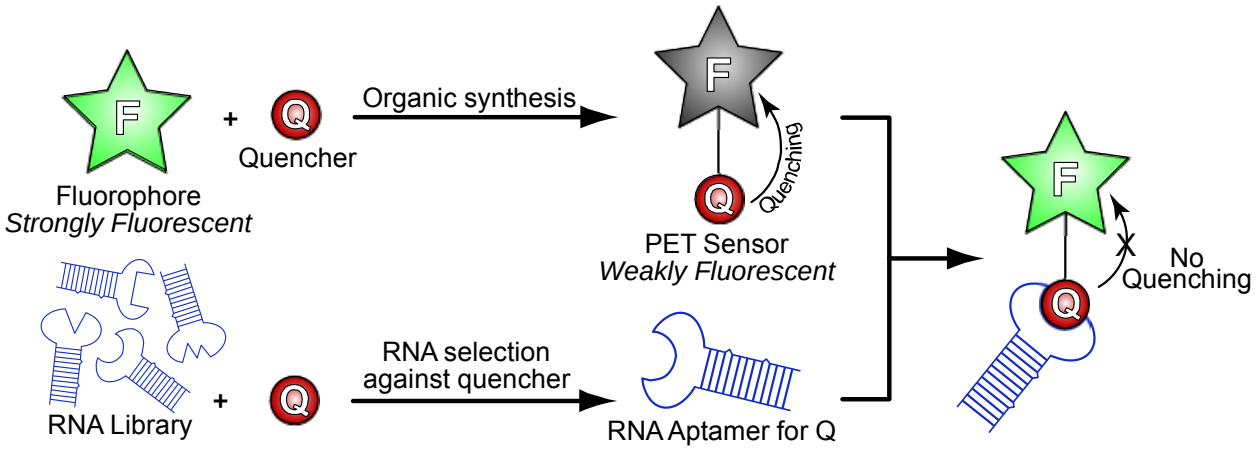

Figure 50 The new paradigm that emerged from this study

Although we have not presented an example here, the independent nature of the fluorophore and quencher make it possible to optimize the sensor system by changing the fluorophore to fit the particular experiment. Once a satisfactory RNA-sensor system is found, the RNA can then be used as a reporter RNA to study gene expression or used to tag endogenous RNAs by forming chimeras with the target RNA. This reporter RNA would function in much the same way as the protein reporters, with the insertion of the artificial RNA sequence downstream of the regulatory domain (similar in concept to Figure 1A). When the gene is activated, the reporter RNA is produced and if the appropriate RNA sensor is present, the RNA will bind to and enhance its fluorescence. In addition to having low background (the sensor is only fluorescent when bound to RNA), such a system has the advantage of being widely applicable, as the same reporter RNA-RNA chemosensor pair can be used to monitor the expression of virtually any gene. The use of an artificial RNA sequence also has the advantage of being less likely to bind to endogenous proteins. The RNA chemosensor DCF-2MPP, the aptamers found to enhance its fluorescence, and most importantly the new paradigm they represent are significant milestones toward a small molecule-based RNA expression assay.

5.0 EXPERIMENTAL

General techniques. Acetonitrile was dried over 3Å molecular sieves. Yields refer to chromatographically and spectroscopically (^{1}H NMR) homogenous materials, unless otherwise stated. All reactions were monitored by thin-layer chromatography (TLC) carried out on 0.25-mm E. Merck silica gel plates (60F-254) using UV-light (254 and 384 nm), 2.4% phosphomolybdic acid/1.4% phosphoric acid/5% sulfuric acid in water, anisaldehyde in ethanol, or 0.2% ninhydrin in ethanol and heat as developing agents. TSI silica gel (230-400 mesh) was used for flash column chromatography. NMR spectra were recorded on AM300 or AM500 (Bruker) instruments and calibrated using a solvent peak or tetramethylsilane as an internal reference. The following abbreviations are used to indicate the multiplicities: s, singlet; d, doublet; t, triplet; q, quartet; m, multiplet; br, broad. High-resolution mass spectra were obtained by using EBE geometry.

Compound 1: To neomycin B (1.03g, 1.10 mmol) in 10:2:1 DMSO:H_2O:triethylamine (26 mL total volume) was added 7 equiv $(Boc)_2O$ (1.68 g, 7.70 mmol). The resulting mixture was heated to 60 °C for 6 h. The crude product was extracted twice with 2:1 ethyl acetate:H_2O and washed over brine. Silica gel flash chromatography in 4.3% MeOH in CH_2Cl_2 yielded a pale white solid in 53% yield. Attempts to verify this structure by NMR and FAB-MS were inconclusive.

Compound 2: Compound **1** (200 mg, 0.164 mmol) was added to 2,4,6-triisopropylbenzenesulfonyl chloride (1.13 g, 3.73 mmol) and placed under a nitrogen atmosphere. Pyridine (4 mL) was added and the mixture was stirred at 24 °C for 8 days. The reaction was then extracted with ethyl acetate:H_2O and neutralized with HCl (1.7 mL). The product was purified via silica gel flash chromatography in 2-5% MeOH in CH_2Cl_2. Although attempts to verify the structure of this compound by NMR and FAB-MS were inconclusive, the mass was able to be verified via ES+MS, calcd MNa_2 2+ , 763.5, found 763.5

Compound 3: Compound **2** (10 mg, 6.75 nmol) was added to aminofluorescein (2.3 mg, 6.75 nmol) and placed under a nitrogen atmosphere. To this mixture was added *N*,*N*-dimethylformamide (100 μL) and triethylamine (2.8 μL). The reaction was stirred for 3 h at rt. Although spots presumed to be from product were observed via TLC, (10% MeOH in CH_2Cl_2) the product was unable to be purified by silica gel chromatography.

Compound 4 A solution of *N*-phenylpiperazine (1.82 g, 11.2 mmol) and paraformaldehyde (2.40 g, 79.3 mmol) in MeCN (10 mL) were refluxed for 30 min. Subsequently, 2',7'-dichlorofluorescein (1.50 g, 3.74 mmol) in H_2O/MeCN (80 mL, 1:1) was added to the resulting solution and the mixture was refluxed for 21 h in the dark. The organic solvent was then removed from the cooled reaction *in vacuo*. The resulting solution was extracted with CH_2Cl_2 (2 × 200 mL), dried over Na_2SO_4 and the solvents were evaporated. Silica gel flash chromatography of the residue (2.5→5% MeOH in CH_2Cl_2) was followed by recrystallization in CH_2Cl_2-hexanes to afford compound **1** as a pink solid (2.37 g, 85%). R_f =

0.46 (silica, 5% MeOH in CH_2Cl_2); IR (KBr pellet): ν_{max} = 3431 (br, O-H), 2925, 2814, 1761 (C=O), 1628, 1596, 1495, 1463, 1396, 1284, 1208, 1090, 997, 922, 893, 757, 697 cm^{-1}; ^1H NMR (300 MHz, DMSO-d_6, 20 °C): δ = 8.05 (br d, *J* = 7.2 Hz, 1H), 7.84 (br dd, *J* = 7.2, 7.2 Hz, 1H), 7.76 (br dd, *J* = 7.2, 7.2 Hz, 1H), 7.40 (d, *J* = 7.2 Hz, 1H), 7.20 (br dd, *J* = 7.2, 7.2 Hz, 4H), 6.93 (br d, *J* = 7.2 Hz, 4H), 6.78 (t, *J* = 7.2 Hz, 2H), 6.64 (s, 2H), 4.16 (s, 4H), 3.22 (br s, 4H), 3.13 (m, 4H), 2.89 (br s, 4H), 2.59 (m, 4H); ^{13}C NMR (125 MHz, DMSO-d_6, 20 °C): δ = 151.1, 150.6, 126.5, 124.0, 119.3, 118.8, 115.8, 15.4, 109.1, 21.9, 51, 48.1 (21 expected signals); ES HRMS calcd for $C_{43}H_{43}N_4O_4Cl_2$ $(M+H)^+$: 749.2661; found: 749.2679.

Compound 5 A solution of 1-(2-pyridinyl)piperazine (1.82 g, 11.2 mmol) and paraformaldehyde (2.40 g, 79.3 mmol) in MeCN (10 mL) were refluxed for 30 min. Subsequently, 2',7'-dichlorofluorescein (1.50 g, 3.74 mmol) in H_2O/MeCN (80 mL, 1:1) was added to the resulting solution and the mixture was refluxed for 21 h in the dark. The organic solvent was then removed from the cooled reaction *in vacuo*. The resulting solution was extracted with CH_2Cl_2 (2 × 200 mL), dried over Na_2SO_4 and the solvents were evaporated. Silica gel flash chromatography of the residue (2.5→5% MeOH in CH_2Cl_2) was followed by recrystallization in CH_2Cl_2-hexanes to afford compound **4** in 77% yield as a pink solid. R_f 0.41 (silica, 5% MeOH in CH_2Cl_2); IR (KBr pellet): ν_{max} = 3435 (br, O-H), 1764 (C=O), 1594, 1479, 1437, 1400, 1288, 1212, 1094 cm^{-1}; ^1H NMR (300 MHz, CD_2Cl_2, 20 °C): δ = 8.15 (dd, *J* = 3.6, 1.2 Hz, 2H), 8.00 (d, *J* = 7.4 Hz, 1H), 7.76 (ddd, *J* = 7.4, 7.4, 1.2 Hz, 1H), 7.68 (ddd, *J* = 7.4, 7.4, 1.2 Hz, 1H) 7.49 (ddd, *J* = 8.5, 6.9, 1.2 Hz, 2H), 7.21 (br d, *J* = 7.4 Hz, 1H), 6.69–6.62 (m, 6H), 4.12 (d, *J* = 14.9 Hz, 2H), 4.06 (d, *J* = 14.9 Hz, 2H), 3.64 (br s, 8H), 2.81 (br s, 8H); Several ^{13}C

NMR experiments resulted in no signals; ES HRMS calcd for $C_{40}H_{37}Cl_2N_6O_5$ $(M+H)^+$: 751.2202; found: 751.2233.

Compound 6 A solution of 4-hydroxy-4-phenylpiperazine (132 mg, 0.747 mmol) and paraformaldehyde (25 mg, 0.798 mmol) in MeCN (10 mL) were refluxed for 30 min. Subsequently, 2',7'-dichlorofluorescein (98.2 mg, 0.25 mmol) in H_2O/MeCN (80 mL, 1:1) was added to the resulting solution and the mixture was refluxed for 21 h in the dark. The organic solvent was then removed from the cooled reaction *in vacuo.* The resulting solution was extracted with CH_2Cl_2 (2 × 200 mL), dried over Na_2SO_4 and the solvents were evaporated. Silica gel flash chromatography of the residue (2.5→5% MeOH in CH_2Cl_2) was followed by recrystallization in CH_2Cl_2-hexanes to afford compound **2** in 75% yield as a pink solid. R_f = 0.22 (silica, 10% MeOH in CH_2Cl_2); IR (KBr pellet): ν_{max} = 3406 (br, O-H), 1760 (C=O), 1571, 1472, 1370, 1285 cm^{-1}; ^1H NMR (300 MHz, DMSO-d_6, 20 °C): δ = 8.03 (d, J = 7.5 Hz, 1H), 7.8–7.7 (m, 2H), 7.49 (br d, J = 7.5 Hz, 4H), 7.35–7.30 (m, 5H), 7.26 (t, J = 7.5 Hz, 2H), 6.70 (s, 2H), ~ 3.4 (obscured by the solvent), 2.15 (br m, 8H); Several ^{13}C NMR experiments resulted in no signals; ES HRMS calcd for $C_{44}H_{41}Cl_2N_2O_7$ $(M+H)^+$: 779.2291; found: 779.2334.

Compound 9 (DCF-2MPP) A solution of 1-(4-methoxyphenyl)piperazine (MPP, 1.984 g, 7.48 mmol) and paraformaldehyde (0.747 g, 24.9 mmol) in MeCN (10 mL) were refluxed for 30 min. Subsequently, 2',7'-dichlorofluorescein (1.50 g, 3.74 mmol) in H_2O/MeCN (80 mL, 1:1) was added to the resulting solution and the mixture was refluxed for 21 h in the dark. The organic solvent was then removed from the cooled reaction *in vacuo.* The resulting solution was extracted with CH_2Cl_2 (2 × 200 mL), dried over Na_2SO_4 and the solvents were evaporated. Silica gel flash chromatography of the residue (2.5→5% MeOH in CH_2Cl_2) was followed by

recrystallization in CH_2Cl_2-hexanes to afford compound **3** in 75% yield as a pink solid. R_f 0.22 (silica, 5% MeOH in CH_2Cl_2); IR (KBr pellet): ν_{max} = 3434 (br, O-H), 1765 (C=O), 1512, 1465, 1285, 1248 cm^{-1}; ^1H NMR (300 MHz, DMSO-d_6, 20 °C): δ = 8.07 (d, J = 7.5 Hz, 1H), 7.85 (dd, J = 7.5, 7.5 Hz, 1H), 7.77 (dd, J = 7.5, 7.5, 1H), 7.41 (d, J = 7.5 Hz, 1H), 6.99-6.76 (br m, 8H) 6.66 (br s, 2H), 4.18 (br s, 4H), 3.68 (s, 6H), 3.11 (br s, 8H), 2.94 (br s, 8H); Several ^{13}C NMR experiments resulted in no signals; ES HRMS calcd for $C_{44}H_{43}Cl_2N_4O_7$ $(M+H)^+$: 809.2509; found: 809.2515.

Compound 11 To Novasyn(™) TG Amino LL Resin (450.7 mg, 0.29 μmol/mg substitution) was added *O*-(7-azabenzotriazol-1-yl)-*N,N,N′,N′*-tetramethyluronium hexafluorophosphate (HATU, 299.6 mg, 6 eq), 5,(&6)carboxy-2',7'-dichlorofluorescein (CDCF, 98.9 mg, 0.225 mmol, 1.7 eq), *n*-diisopropylethylamine (DIPEA, 203.2 mg, 12 eq), and 1-methyl-2-pyrrolidone (NMP, 4.5 mL). The reaction mixture was rotated in the dark at 25 °C for 7 h. The solvents were drained and the resin was incubated with DMF for 30 min followed by washing with CH_2Cl_2 (x5). The resin was then washed with 0.1% HCl in MeOH to remove remaining unbound CDCF, yielding a red resin. FTIR (KBr, cm^{-1}) 3436 (OH), 2922, 2866, 2360, 2342, 1765, 1655, 1627, 1493, 1452, 1350, 1261, 1104, 952, 846, 761, 700. See also included 600 MHz magic spin NMR spectrum

Compound 12 *N*-Phenyl-piperazine (40.1 mg, 0.294 mmol) and paraformaldehyde (61.8 mg, 2.06 mmol) were refluxed for 30 min in H_2O/CH_3CN (0.25 mL, 1:1). Compound **7** resin (33.8 mg, 0.29 μmol/mg substitution) and more H_2O/CH_3CN (1.25 mL, 1:1) were added and the refluxing reaction was placed in a shaker (100 RPM) for 48 h. The resin was then washed with

DMF (x5) and CH_2Cl_2 (x5). FTIR (KBr, cm^{-1}) 3433 (OH), 2961, 2923, 2839, 2360, 2340, 1733, 1632, 1452, 1258, 1106. See also included.600 MHz magic spin NMR spectrum

Compound 13 1-(2-Pyridinyl)-piperazine (43.4 mg, 0.266 mmol) and paraformaldehyde (55.9 mg, 1.86 mmol) were refluxed for 30 min in H_2O/CH_3CN (0.25 mL, 1:1). Compound **7** resin (30.6 mg, 0.29 μmol/mg substitution) and more H_2O/CH_3CN (1.25 mL, 1:1) were added and the refluxing reaction was placed in a shaker (100 RPM) for 48 h. The resin was then washed with DMF (x5) and CH_2Cl_2 (x5). FTIR (KBr, cm^{-1}) 3444 (OH), 3016, 2923, 2859, 2360, 1739, 1649, 1454, 1351, 1252, 1107. See also included 600 MHz magic spin NMR spectrum

Compound 14 1-(4-Methoxyphenyl)-piperazine (461.1 mg, 1.74 mmol), $NaHCO_3$ (292.3 mg, 0.348 mmol) and paraformaldehyde (365.4 mg, 12.18 mmol) were refluxed for 50 min in H_2O/CH_3CN (0.25 mL, 1:1). Compound **7** resin (33.8 mg, 0.29 μmol/mg substitution) and more H_2O/CH_3CN (1.25 mL, 1:1) were added and the reaction was allowed to reflux for 24 h. The resin was then washed with DMF (x5) and CH_2Cl_2 (x5) and dried under high vacuum. FTIR (KBr, cm^{-1}) 3443 (OH), 2982, 2362, 1639, 1451, 1351, 1249, 1104, 951, 702. See also included 600 MHz magic spin NMR spectrum

Compound 15 Novasyn(™) TG Amino LL Resin (300 mg, 0.29 μmol/mg substitution), benzoyl chloride (11.48 mg, 4.35 mmol), and pyridine (0.7mL) were combined in CH_2Cl_2 (3.0 mL) in a sealed container and put on a rotator for 2 h at 24 °C. The resin was then washed with dimethylformamide (DMF, x5) and CH_2Cl_2 (x5). Substitution confirmed by Kaiser Test, product was pale yellow beads.

MPP Resin: To Aminolink™ (Pierce) agarose resin (1200 µL, 1 equiv) was added 1-(4-methoxyphenyl)-piperazine (MPP, 47.4 mg, 10 equiv), NaOAc (150 mg, 50 equiv), and $NaBH_3CN$ (27 mg, 43 equiv) in isopropanol (5.1 mL). The mixture was shaken for 2.5 h at 25 °C then 20 more equiv. of $NaBH_3CN$ was added and shaken for 23 additional hours at the same temperature. The resin was then drained and washed with isopropanol (5 mL), H_2O (10 mL), and incubated with sat. aq. $NaHCO_3$ (10 mL, 30 min). After washing with H_2O (2 x 12 mL), the white resin was stored in 3 volumes isopropanol at 4 °C. Complete reaction was verified by Schiff's test for free aldehydes (present in unreacted resin).

General spectroscopic methods. The cyclodextrins (Aldrich) and 1-(4-methoxyphenyl)piperazine dihydrochloride (Acros Organics) were purchased and used as received. Phosphate buffers (JT Baker) were used after passage through a 22 micron filter.

UV-visible spectroscopy. Absorption spectra were acquired on a Cary 50 or a Perkin Elmer Lambda 19 UV-Visible spectrometer, under the control of Windows-based PC's running the manufacturers' supplied software.

Fluorescence spectroscopy. Fluorescence spectra were acquired in a 1 cm × 1 cm quartz cuvette on a Spex Fluorolog fluorometer under the control of a Windows-based PC running Datamax 32 software. All spectra were corrected for emission intensity using the manufacturer supplied photomultiplier curves.

Solvent dependence measurements. UV-Visible spectra were acquired on a PC2000-UV-VIS spectrometer (Ocean Optics, Inc, Dunedin, FL). Stock solutions (100x) containing 450 μM of the fluorophore to be tested were prepared in DMSO. From these stock solutions, samples in 0.1N NaOH, MeOH, pH 7.4 phosphate buffer, MeCN, dichloromethane (CH_2Cl_2), and $CHCl_3$ were made to a final concentration of 4.5 μM. Fluorescence spectroscopic analyses were performed on a Spex Fluorolog fluorometer using a slit width of 3 nm and photomultiplier voltage of 650 V. Solutions (100x) containing 450 μM of each compound were prepared in DMSO and diluted to a final concentration of 4.5 μM with the appropriate solvent. Corrected emission spectra were taken at 490 nm excitation.

Quantum yield measurements. Quantum yields were determined using fluorescein in 0.1 N NaOH (Φ = 0.95) as a standard. To determine quantum yields relative to fluorescein, stock solutions of the fluorophores were prepared in DMSO (1 mM) and diluted in phosphate buffer (pH 7.0, JT Baker) to OD_{490} = 0.09. The samples were excited at 490 nm and the integrated emission spectra were compared. To calculate the quantum yield, the corrected emission spectra were compared to fluorescein as a quantum yield standard of 0.95 in 0.1 N NaOH.[59] The following equation was used to relate the integrated peak area of fluorescein to each of the unknown compounds.

$$\Phi_{sample} = \Phi_{standard} \times \frac{\int emission_{sample}}{\int emission_{standard}}$$

Fluorescence pH titrations. Phosphate buffers were prepared by adjusting the pH of 4, 7 or 10 with appropriate amounts of HCl or NaOH until 21 different solutions ranging from pH 2.51 to pH 12.49 were prepared. Aliquots of compound 4 or 5 from DMSO stock solutions were

taken and combined with each respective buffer to reach a final fluorophore concentration of 4.5 μM. Corrected emission spectra were acquired from 490 to 660 nm using 490 nm excitation.

UV-Vis pH titration. Solutions of DCF-2MPP (4.5 μM) in quartz cuvettes were prepared from the DMSOP stock solution and titrated with HCl or NaOH from pH 0.12 to pH 11.56. Absorption spectra from 400-600 nm were acquired at each data point using a Perkin Elmer Lambda 19. Spectra were corrected for volume changes during titration

Cyclodextrin titration. Solutions of DCF-2MPP (5 μM) in pH 7.4 phosphate buffer (JT Baker) were prepared containing 0–100 mM α-cyclodextrin (by serial dilution of a 100 mM solution of α-cyclodextrin and DCF-2MPP) or β-cyclodextrin from 0–5.0 mM (from a 10 mM β-cyclodextrin stock solution in H_2O). To test the effect of a competitive inhibitor, MPP (3.75 mmol for a final concentration of 2.5 mM) was added to a 5.0 mM β-cyclodextrin solution containing DCF-2MPP. Samples were excited at 485 nm and integrated emission spectra were compared using Origin Pro software.

Effect of metal ions. Stock solutions (10 mM in pH7 phosphate buffer) of $ZnCl_2$, $FeCl_3$, $CdCl_2$, $MnCl_2$, $CoCl_2$, $MgCl_2$, $CuSO_4$, NaCl were prepared and filtered through a 22 micron filter. Wells of a 96 well plate were loaded with 1 mM of each metal ion solution and DCF, compound **4** or **5** (to a final concentration of 1.0 μM). as well as pH 7.0 phosphate buffer as a control. A second replicate of each well was prepared with a 1 μM concentration of each respective metal ion. Emission spectra were acquired from 490 to 600 nm with excitation at 485nm using a Cary Eclipse Fluorometer equipped with the plate reader attachment. The spectra

were processed using Datamax software and the intensities at the peak emission intensity were compared.

Microscopy and Solid Phase Spectra Acquisition. Confocal images and fluorescence spectra were collected on a Zeiss 510 Meta Confocal Laser Scanning Microscope at 10 nm bin size using a 488 nm argon ion laser light source and the integrated software. The beads were mounted on glass coverslips and imaged at 20X using confocal imaging ensuring an appropriate optical section through the beads.

RNA preparation. DNA templates for the N70 library, biased libraries and oligonucleotides used for primer extension and RT-PCR were prepared by automated DNA synthesis (Keck Biotechnology Resource Laboratory, Yale University). The random region of the N70 library was synthesized with equimolar concentrations of each base in a 0.2 μmol synthesis. The partially randomized portions of the biased library were prepared by varying the molar proportions of each base during synthesis. Oligonucleotides 40 bases or longer were purified by denaturing (8 M urea) PAGE before use. The N70 pool DNA template (1 nmol) was made double-stranded by extension in the presence of 5' PR-N70 primer (5' ATGAATACGACTCACTATAGGAGACAGGACTTCG 3'), introducing the promoter for T7 RNA polymerase. DNA extension reactions were carried out using Superscript II Reverse Transcriptase Polymerase (RT, Gibco BRL) according to manufacturer's instructions.

The double-stranded product was then ethanol precipitated, resuspended in TE buffer and transcribed *in vitro*. Typical transcription reactions (100 μL total volume) included 1 μM template DNA, 40 mM TRIS (pH 7.8), 2.5 mM spermidine, 0.01% triton X, 2.5 mM each

nucleotide triphosphate (ATP, GTP, CTP, UTP), 10 μL T7 polymerase, 10 mM DTT, and 25 mM $MgSO_4$. Each reaction was incubated at 37 °C for 2.5 h. The RNA was then purified via denaturing PAGE, recovered by elution of excised bands in crush-soak buffer (200 mM NaCl, 10 mM Tris-HCl pH 7.5, 1 mM EDTA pH 8.0), and ethanol-precipitated.

Preparation of Affinity Media. The MPP Resin or Aminolink™ (Pierce) agarose resin (120 μL of suspension) was drained of solvent and washed with selection buffer (8 × 100 μL, 300 mM NaCl, 20 mM Tris-Cl pH 7.4, 5 mM $MgCl_2$)

***In vitro* RNA Selection.** In typical selection experiments, pool RNA (approximately 10^{13} molecules, ~900 pmoles) was denatured (100 μL, 300 mM NaCl, 20 mM Tris-Cl pH 7.4, 95 °C, 3 min), allowed to cool to 24 °C, $MgCl_2$ was added (for a final concentration of 5 mM) and the final mixture was added to the MPP resin (50 μL) and incubated at 24 °C for 5 min (unless preceded by a negative selection step, in which case the mixture was first incubated on a 50 μL column of unreacted aminolink resin under identical conditions). The column was then washed with selection buffer (8 x 100 μL) and eluted with elution buffer (8 × 100 μL). Biased library RNA was subjected to a pre-elution step where the column was washed with elution buffer containing 3 μM MPP prior to elution of binding RNA. RNA from the eluted fractions was pooled and ethanol-precipitated with 50 pmol 5'PR-N70 primer and glycogen (0.1 μg) to be resuspended directly into a 50 μL RT reaction. The resulting cDNA was amplified by PCR (15 cycles) with primers 5'PR-N70 and 3'PR-N70 (5' TGGCTCAAGTGCACATGTGC 3') to generate the template for transcription of RNA for the next round of selection. Typical PCR reactions used the following conditions: 1.5 mM $MgCl_2$, 2.5 μM each primer, 200 μM each dNTP

(Roche), 5 units/100 μL reaction Taq polymerase (Promega) with included buffer. PCR was conducted on an Eppendorf MasterCycler *Gradient* thermocycler using the following program: 2 min initial denaturation (92.0 °C) followed by 15 cycles of 1 min denaturation (92.0 °C), 1 min annealing (40.8 °C) and 1 min extension (72.0 °C)

Cloning final round of selection cDNA into pCR®4-TOPO® vector. The cDNA from the final round of selection in each selection experiment was then cloned into the pCR®4-TOPO® vector (Invitrogen) and used to transform the included chemically competent cells following the manufacturer's supplied protocol. Cultures were grown of 24 colonies (2.5 mL LB-AMP media) and the DNA was isolated using an Eppendorf PerfectPrep Plasmid Mini kit according to the manufacturer's supplied protocol. The plasmid DNA was sent directly to the University of Pittsburgh Molecular Medicine Institute DNA Sequencing Core Facility to be sequenced.

Large scale RNA synthesis. RNA for titration experiments was prepared as described above except for *in vitro* transcription. The Promega RiboMAX® high yield transcription kit was instead used to synthesize RNA. A typical reaction (150 μL total volume) was run with 7.5 μg template DNA and was completed according to the manufacturer's included protocol. The RNA was then phenol/chloroform extracted (x3) and ethanol precipitated.

RNA Fluorescence Titrations. RNA aptamers from the selection experiments were tested for their ability to enhance the fluorescence of DCF-2MPP by fluorescence titration in 10 × 1 mm quartz cuvettes on a Spex Fluorolog. Emission spectra for DCF-2MPP were acquired from 500 nm to 670 nm using an excitation wavelength of 490 nm. Samples were prepared

containing 100 μM RNA and 1 μM DCF-2MPP (from a 1 mM DMSO stock solution) in buffer (300 mM NaCl, 20 mM Tris-Cl pH 7.4). The samples were denatured alongside control solutions not containing RNA by heating at 95 °C for 3 min and allowing cool to 24 °C. After the addition of $MgCl_2$ (for a final concentration of 5 mM) the solutions were allowed to incubate at 24 °C for 5 min and the fluorescence emission spectra were obtained. Subsequent data points were obtained by dilution. Specifically, 50% of the solution was removed and replaced with an equal volume of DCF-2MPP (1 μM) in selection buffer (300 mM NaCl, 5 mM $MgCl_2$, 20 mM Tris-Cl pH 7.4) effectively halving the RNA concentration (to a minimum of 812 nM) while keeping the chromophore and buffer concentrations constant. Emission spectra were obtained at each data point and the peak intensities at 525 nm were used to construct the titration plot. It is important to note that the control sample not containing RNA falls in line with the nanomolar titration points.

RNA aptamers from the biased library selection were tested using a similar procedure on a Molecular Devices SpectraMax M2 Microplate reader. Excitation was at 490 nm and emission spectra were acquired from 505 to 600 nm. The experimental procedure was similar to the one described above except that the maximum RNA concentration was 50 μM.

MPP Competition Assay. Samples containing ***Apt01*** RNA (10 μM) and DCF-2MPP (1 μM) in buffer (300 mM NaCl, 20 mM Tris-Cl pH 7.4) were denatured alongside control solutions not containing RNA by heating at 95 °C for 3 min and allowing cool to 25 °C. After the addition of $MgCl_2$ (for a final concentration of 5 mM) the solutions were allowed to incubate at 24 °C for 5 min and fluorescence emission spectra were obtained. To determine the effect of

MPP on ***Apt01*** binding, MPP was added (0.1 μL, neat, to a final concentration of 3.2 mM) to each sample.

Mobility Shift Assays. Mobility shift assays were performed using polyacrylamide gels (5% and 10%) and either standard tris-borate EDTA (TBE) buffer or selection buffer (300 mM NaCl, 5 mM $MgCl_2$, 20 mM Tris-Cl pH 7.4) at various dilutions due to the joule heating caused by the high ionic strength. Despite the buffer and gel composition, the experiments were conducted similarly. Namely, samples containing RNA (25 nM), glycerol (5%; to facilitate gel loading), and either the target small molecule (10 or 100 μM) or control lacking small molecule were prepared. After denaturation at 95° C for 2 min and subsequent cooling to 24 °C, the samples were loaded on the gel and the gel was run at ~100v for ~60 minutes (depending on the gel, gels with higher ionic strength required lower voltages, longer runtimes and buffer circulation). The bands were then stained using Sybr Green II (Molecular probes, Eugene OR) and imaged using transillumination at 254 nm with a Stratagene Eagle-Eye camera.

Capillary Electrophoresis of Aptamer and RRE RNA: Typical optimized experimental conditions for the Biorad Biofocus 3000 Capillary Electrophoresis apparatus using a 50 cm long, coated 50 μm diameter capillary (Zero-Flow; MicroSolv Technologies, Eatontown, NJ). Run voltage was -20 kV for up to 120 mins, 5 second x PSI injection, 20 °C Capillary temp, UV Detection at 260 nm. Fresh buffer was used for each run and flushed through the capillary for 10 min between runs. Aptamer RNA was run with selection buffer (300 mM NaCl, 5 mM $MgCl_2$, 20 mM Tris-Cl pH 7.4) and neomycin:RRE RNA assays were run using the buffer described in Werstuck, *et al.*[70] (10 mM Tris, pH 7.6, 10 mM $MgCl_2$, 50 mM NH_4Cl).

RNA samples were prepared with a final concentration of 21 μM and contained a 80 μM Neomycin where applicable. Each sample was denatured at 80 °C for 2 min and allowed to cool to 24 °C before injection into the capillary.

Capillary Electrophoresis of F-IRE:yohimbine: All f-IRE experiments were conducted on a Beckman P/ACE MDQ Capillary Electrophoresis apparatus in the lab of Jim Schneider in the Chemical Engineering Department at Carnegie Mellon University. The instrument was equipped with a photodiode array detector and 20 cm Zero-Flow coated capillary. Although the electropherograms used for comparison purposes are from a constant wavelength of 254 nm, the initial post-run analysis included a scan from 200-400 nm at each time point to monitor potential contamination from protein. Samples of Orange G (used as a reference marker, 1:40 final dilution of 0.1% solution), Orange G with f-IRE RNA (60 μM), and Orange G with RNA and yohimbine (50 μM) were prepared. Each sample was denatured at 80 °C for 2 min and allowed to cool to 24 °C before injection into the capillary. Each run was conducted in triplicate and the results were analyzed using the manufacturer's supplied software.

6.0 INFRARED AND NMR SPECTRA

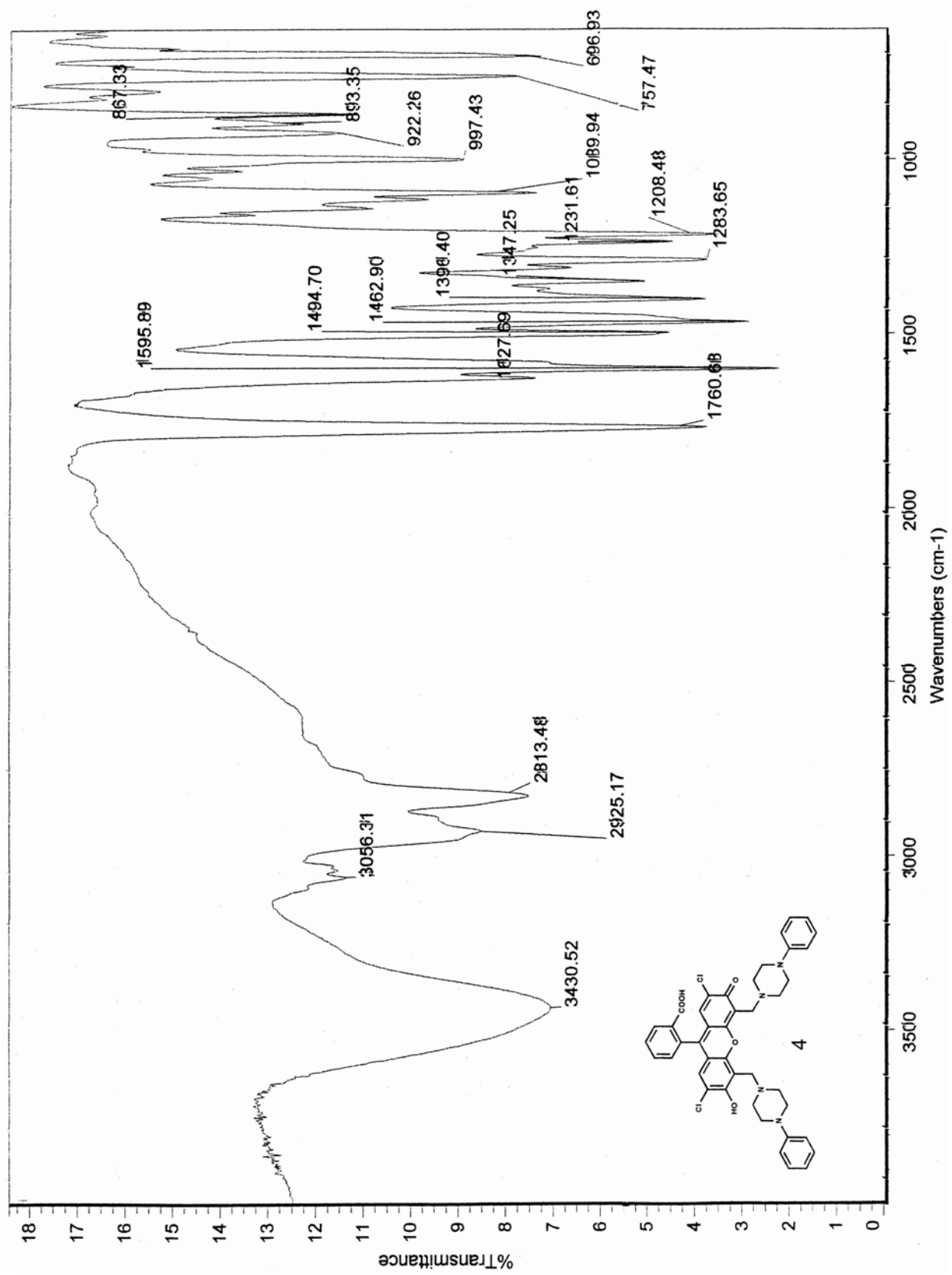

Figure 51 IR spectrum of compound 4 (KBr pellet)

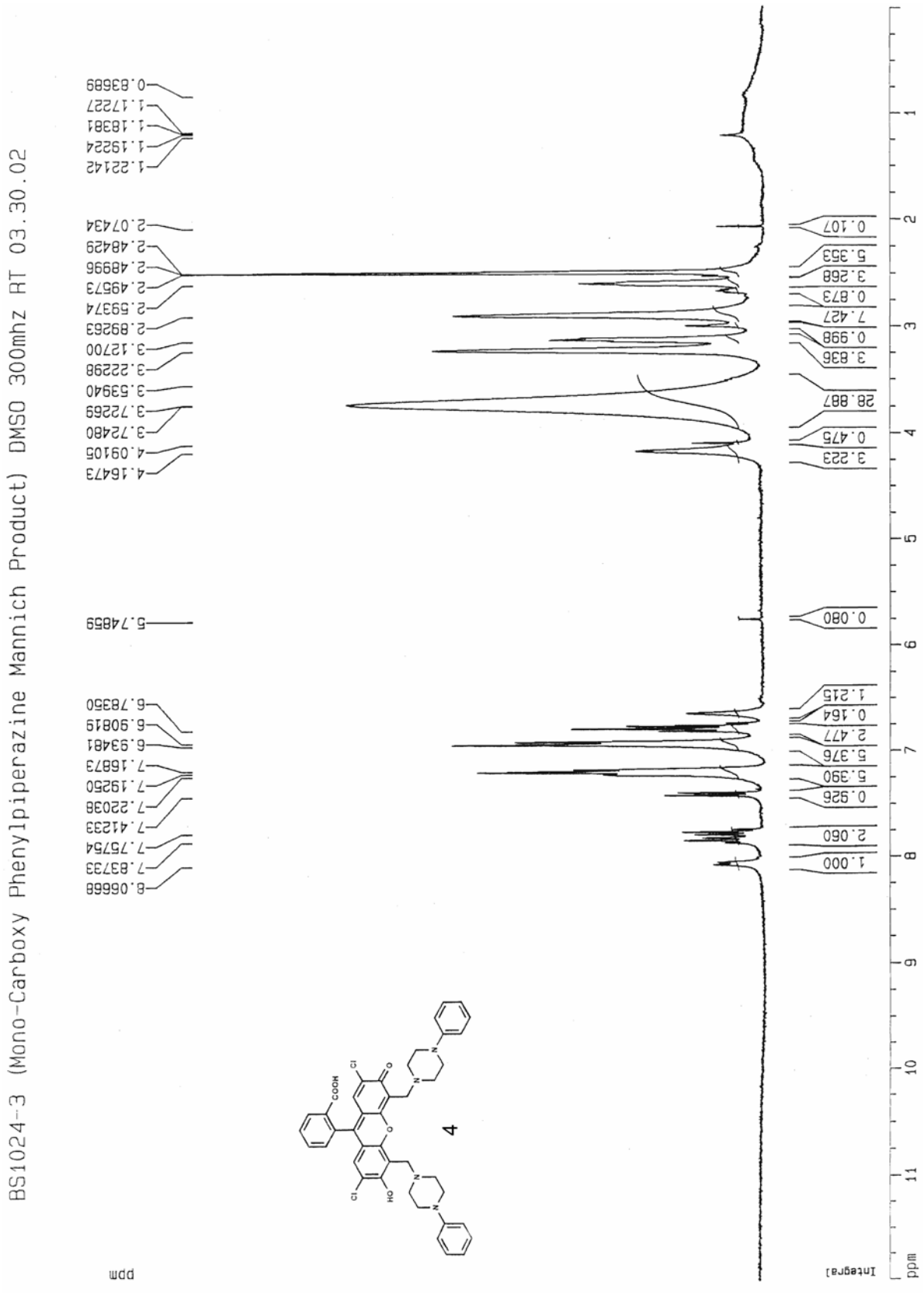

Figure 52 ^{1}H NMR spectrum of compound 4 in DMSO-d_6 (300 MHz)

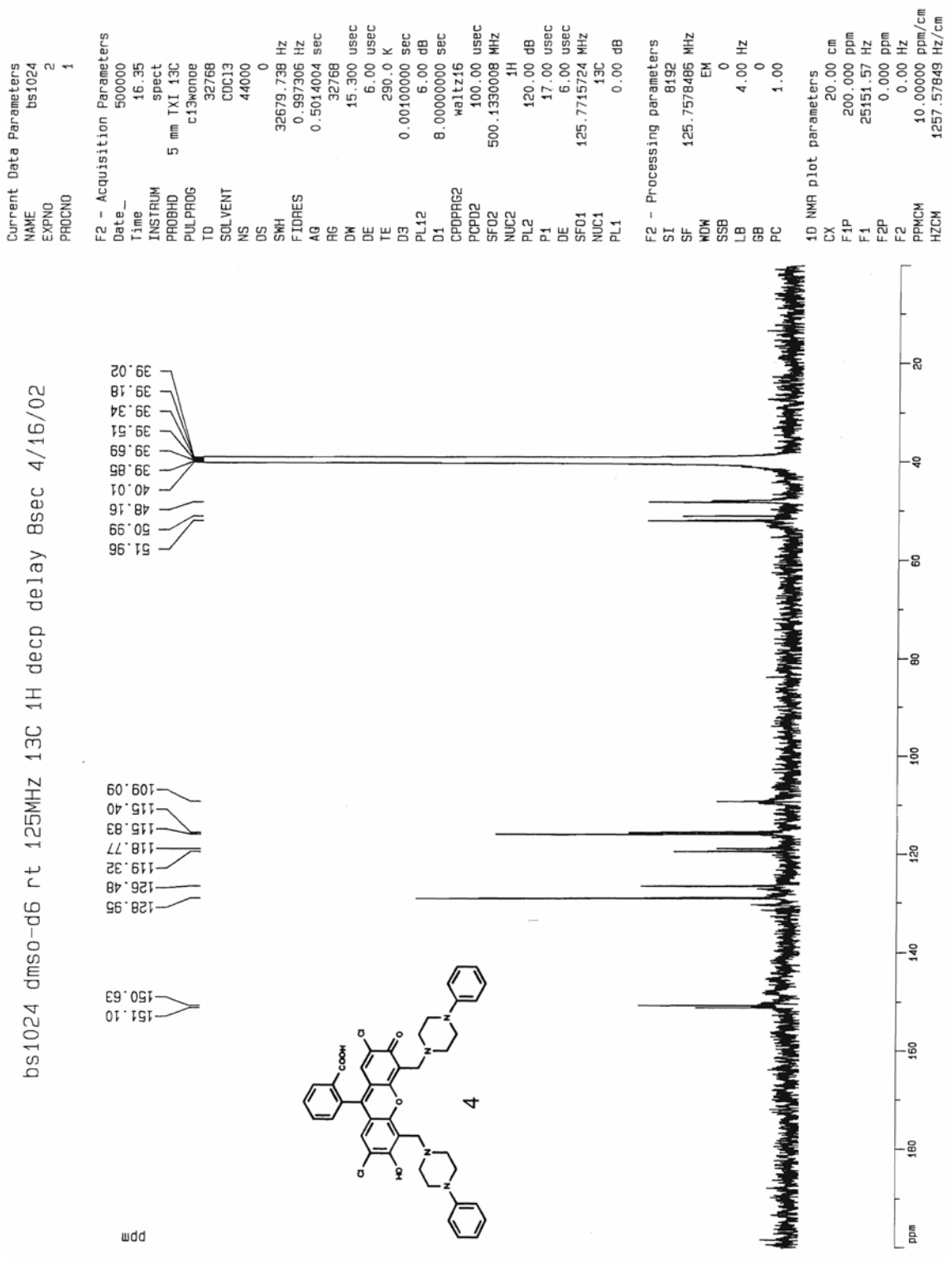

Figure 53 ^{13}C NMR spectrum of compound 4 in DMSO-d_6 (75 MHz)

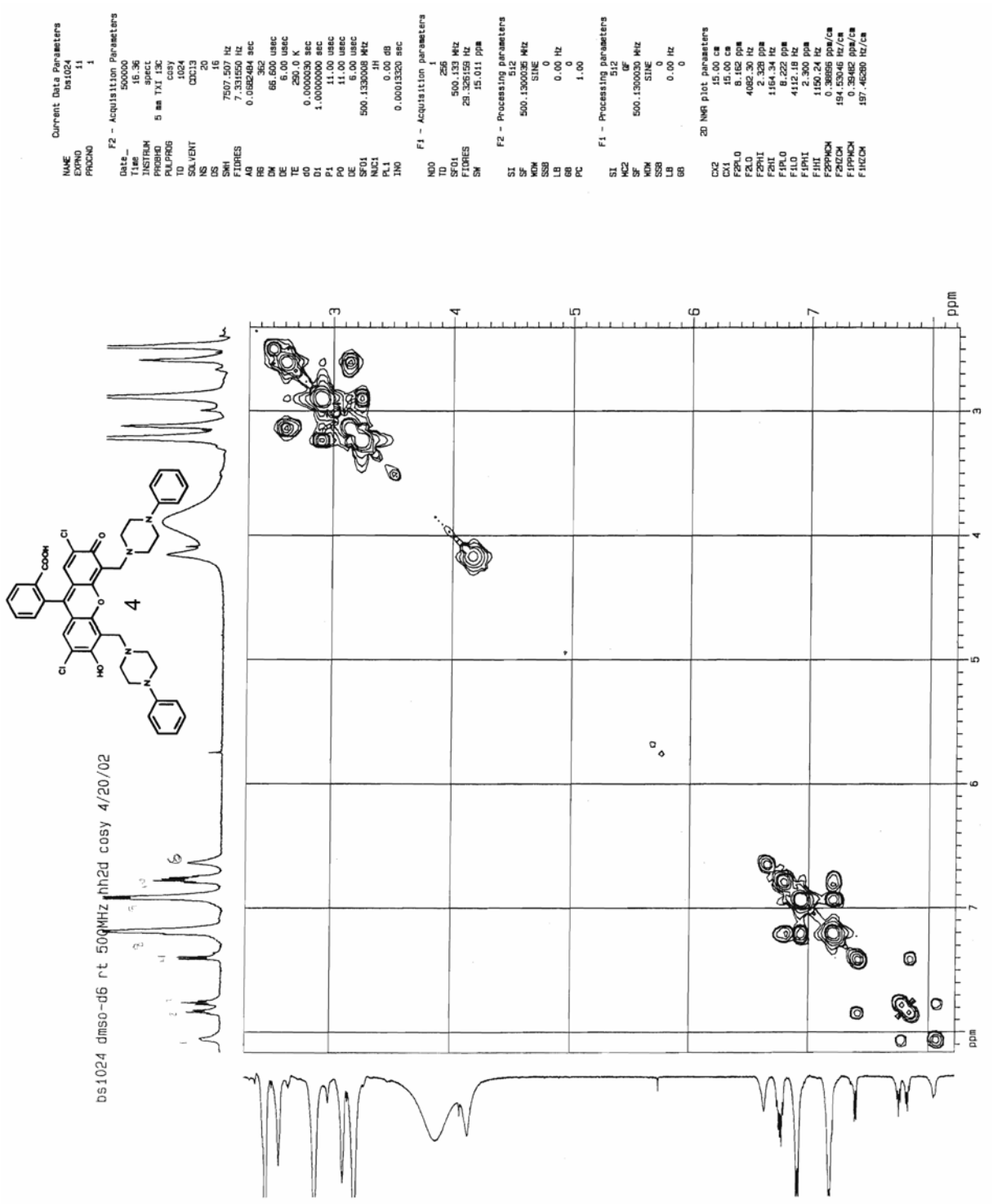

Figure 54 2D COSY NMR spectrum of compound 4 in DMSO-d_6 (500 MHz)

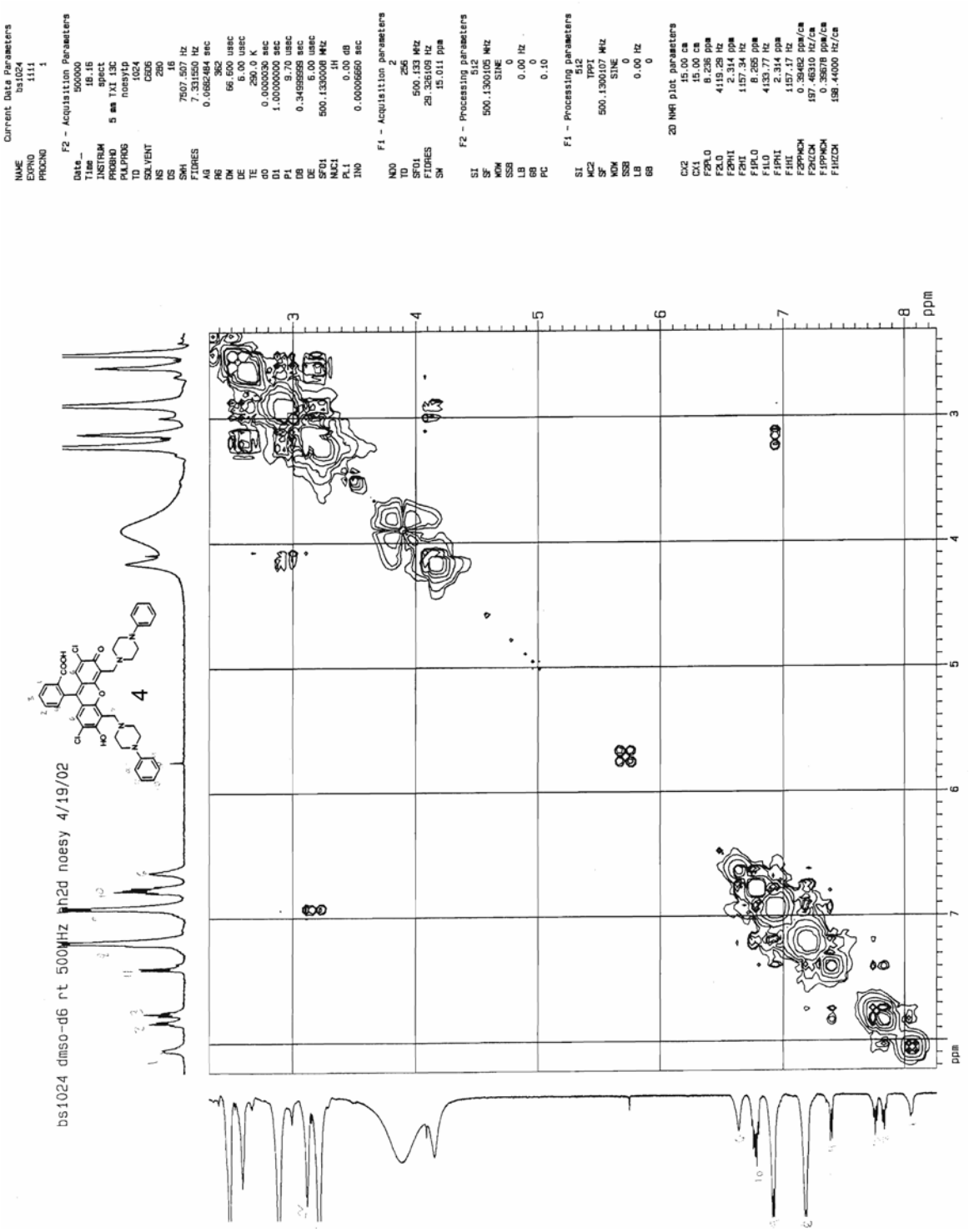

Figure 55 NOESY NMR spectrum of compound 4 in DMSO-d_6 (500 MHz)

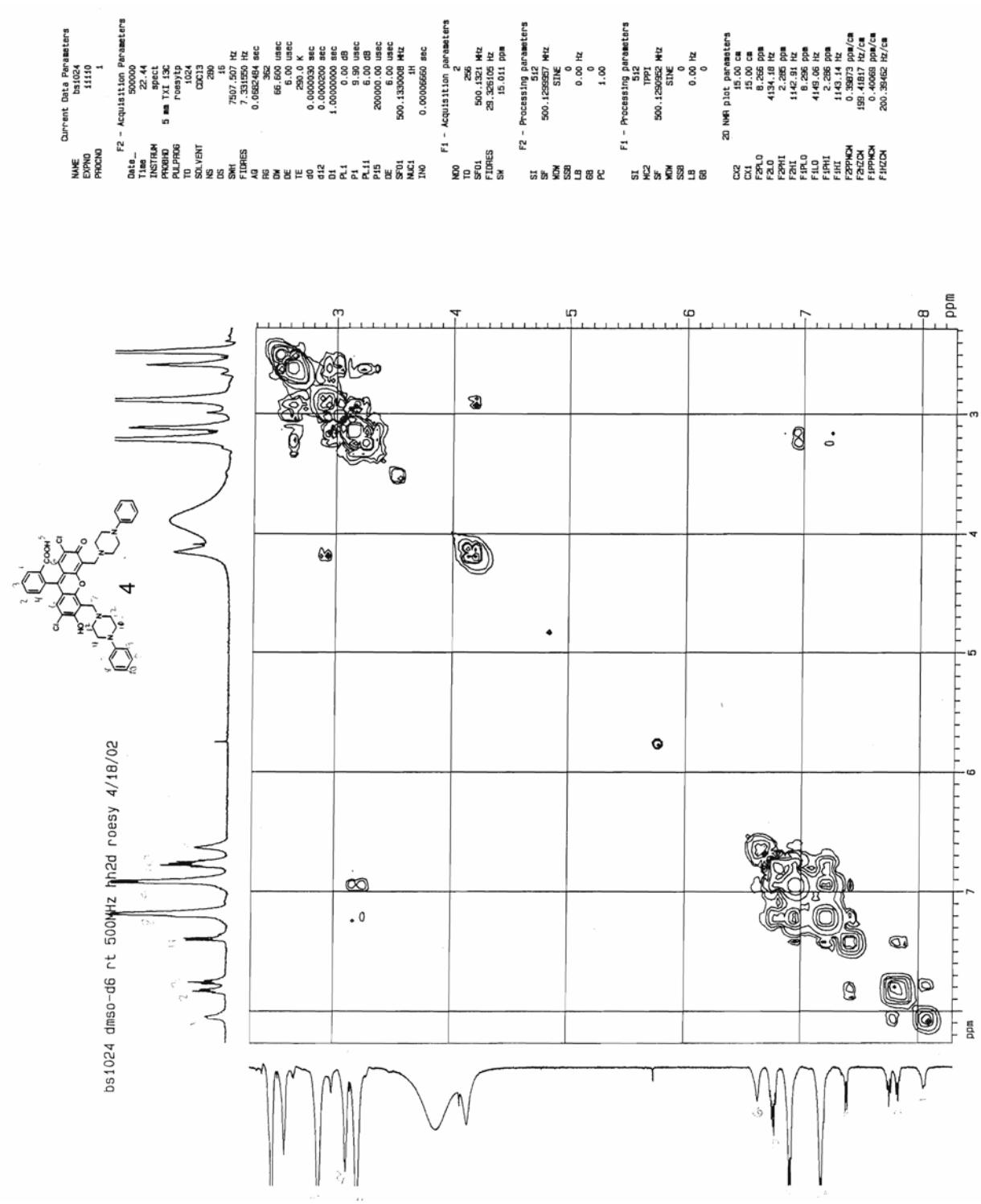

Figure 56 ROESY NMR spectrum of compound 4 in DMSO-d_6 (500 MHz)

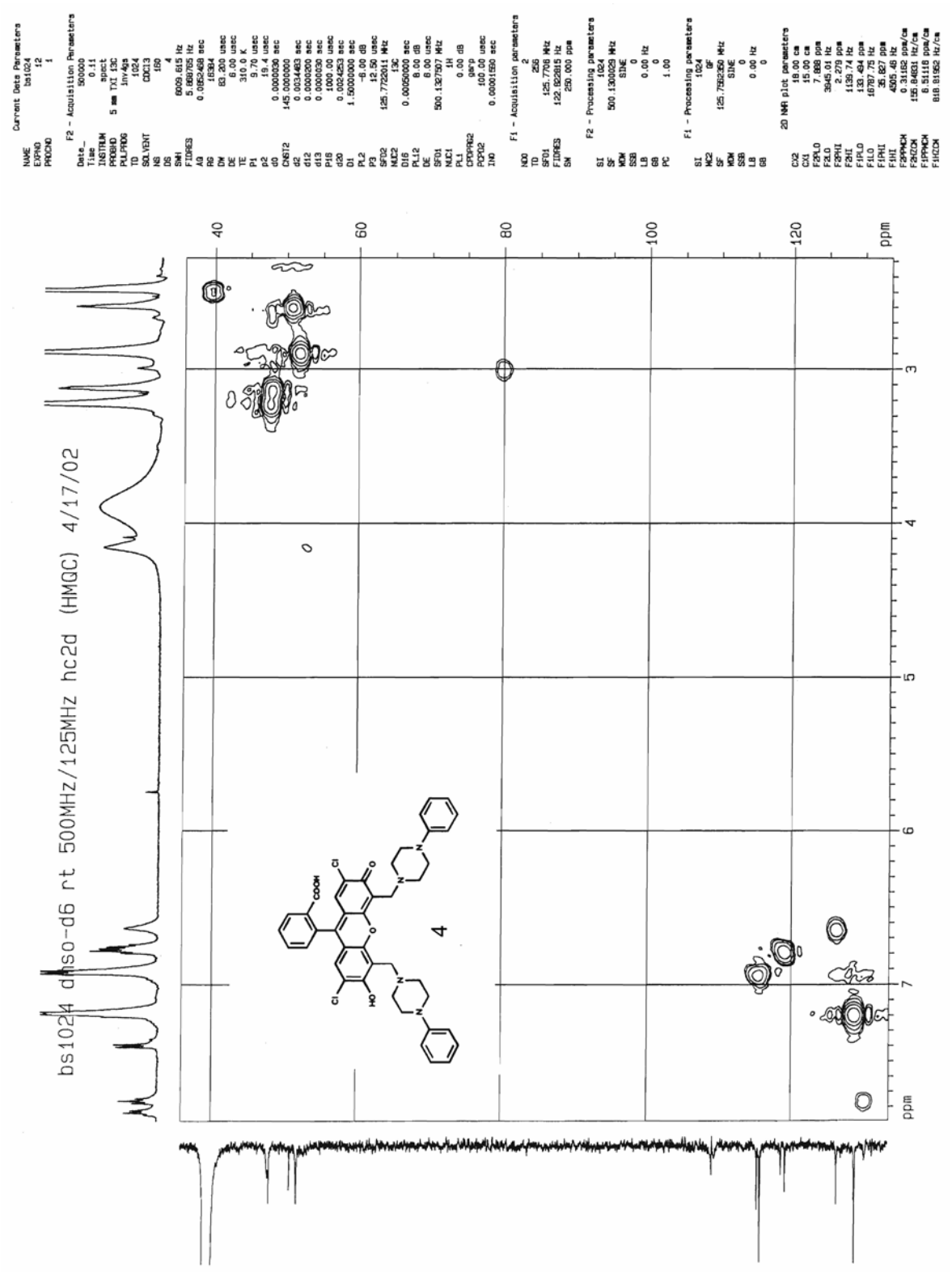

Figure 57 HMQC NMR spectrum of compound 4 in DMSO-d_6 (500 MHz)

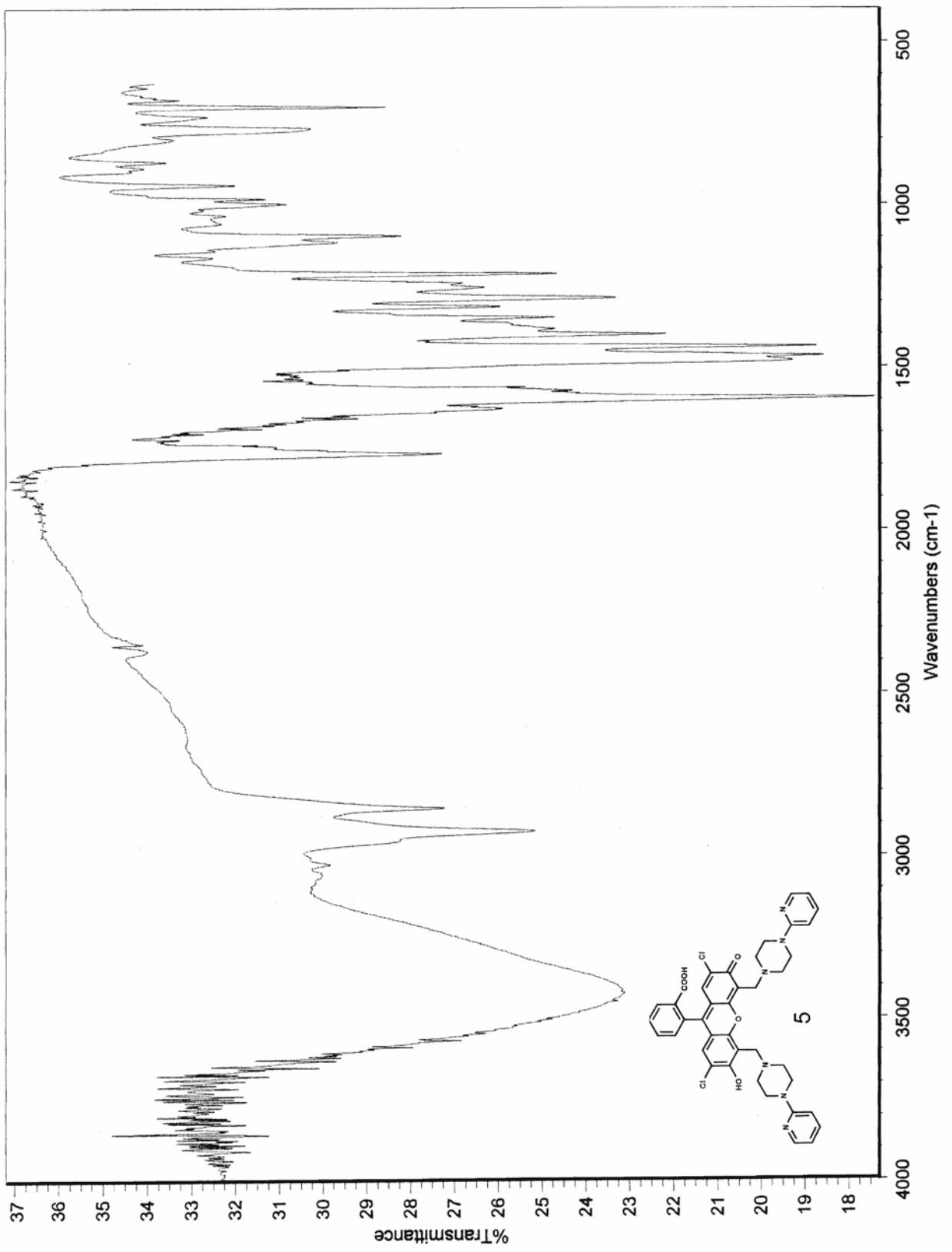

Figure 58 IR spectrum of compound 5 (KBr pellet)

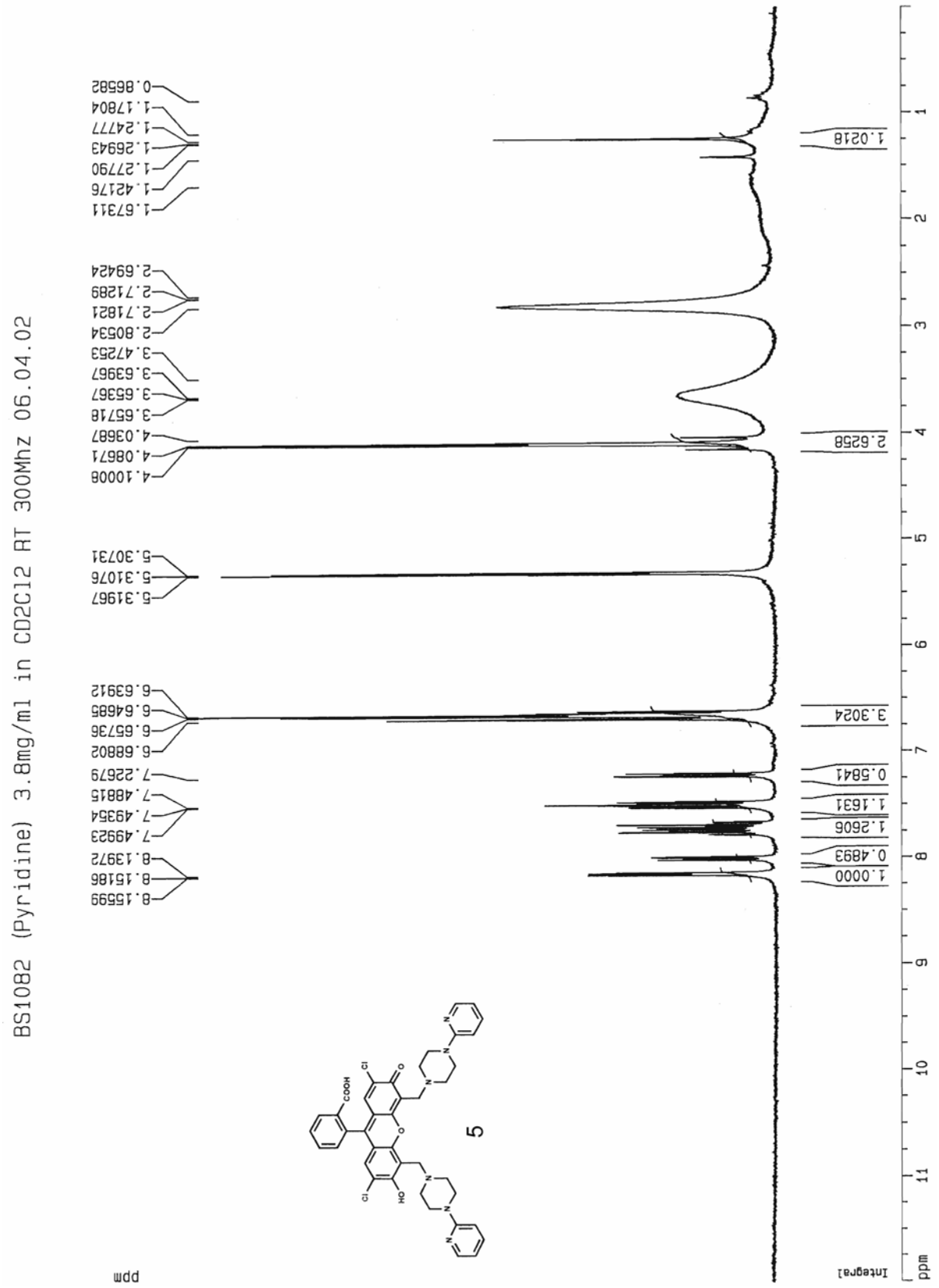

Figure 59 ^{1}H NMR spectrum of compound 5 in DMSO-d_6 (300 MHz)

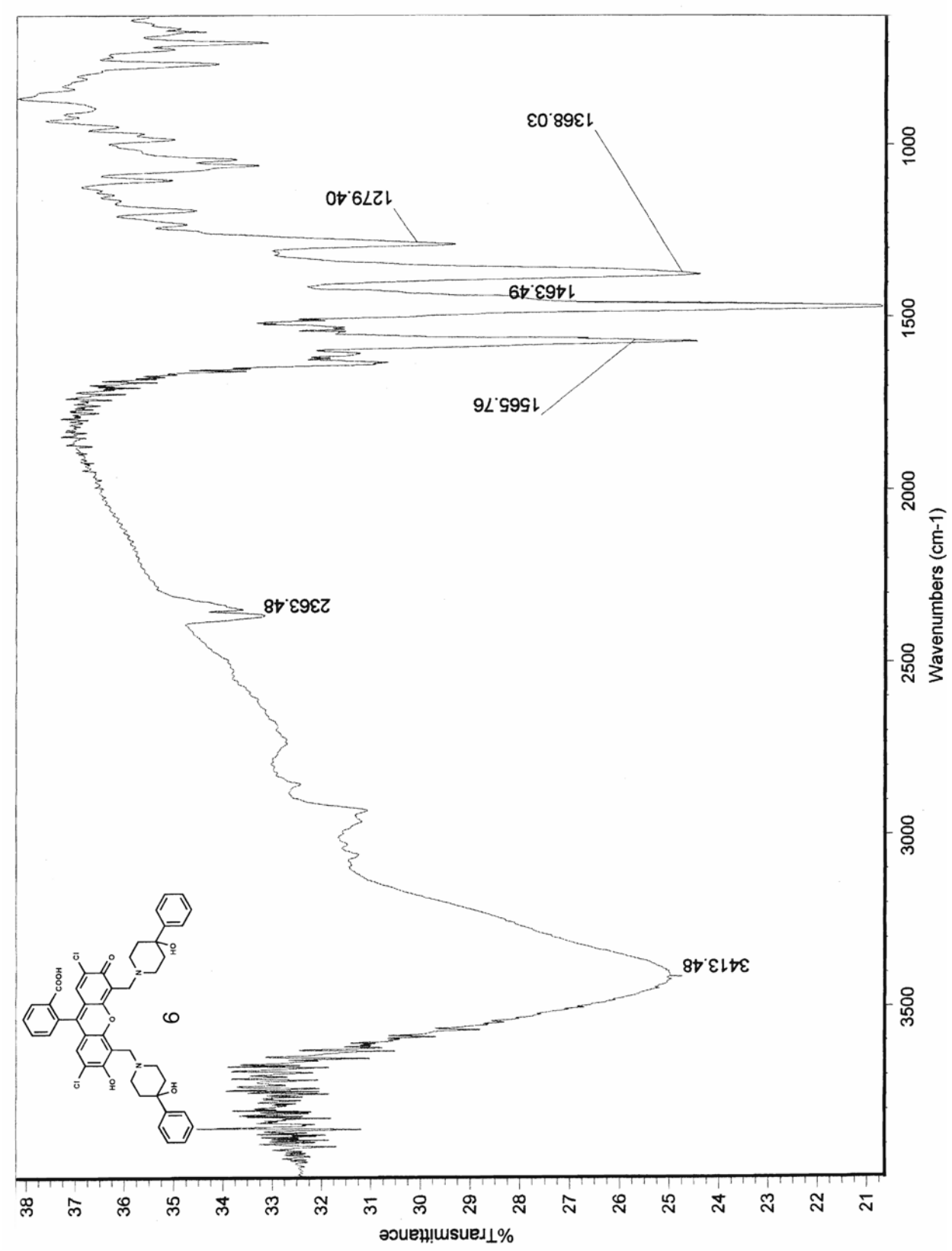

Figure 60 IR spectrum of compound 6 (KBr pellet)

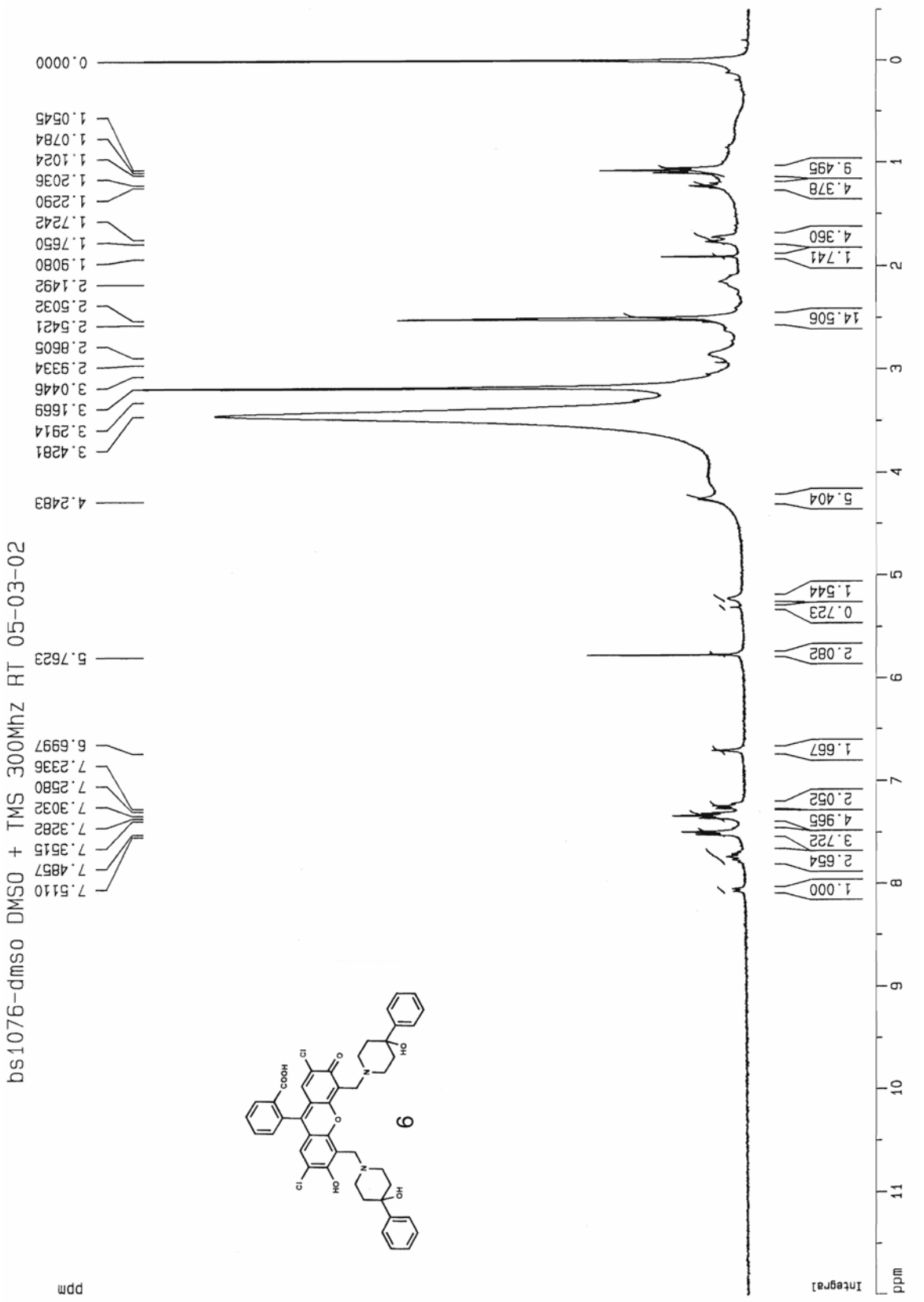

Figure 61 ^{1}H NMR spectrum of compound 6 in DMSO-d_6 (300 MHz)

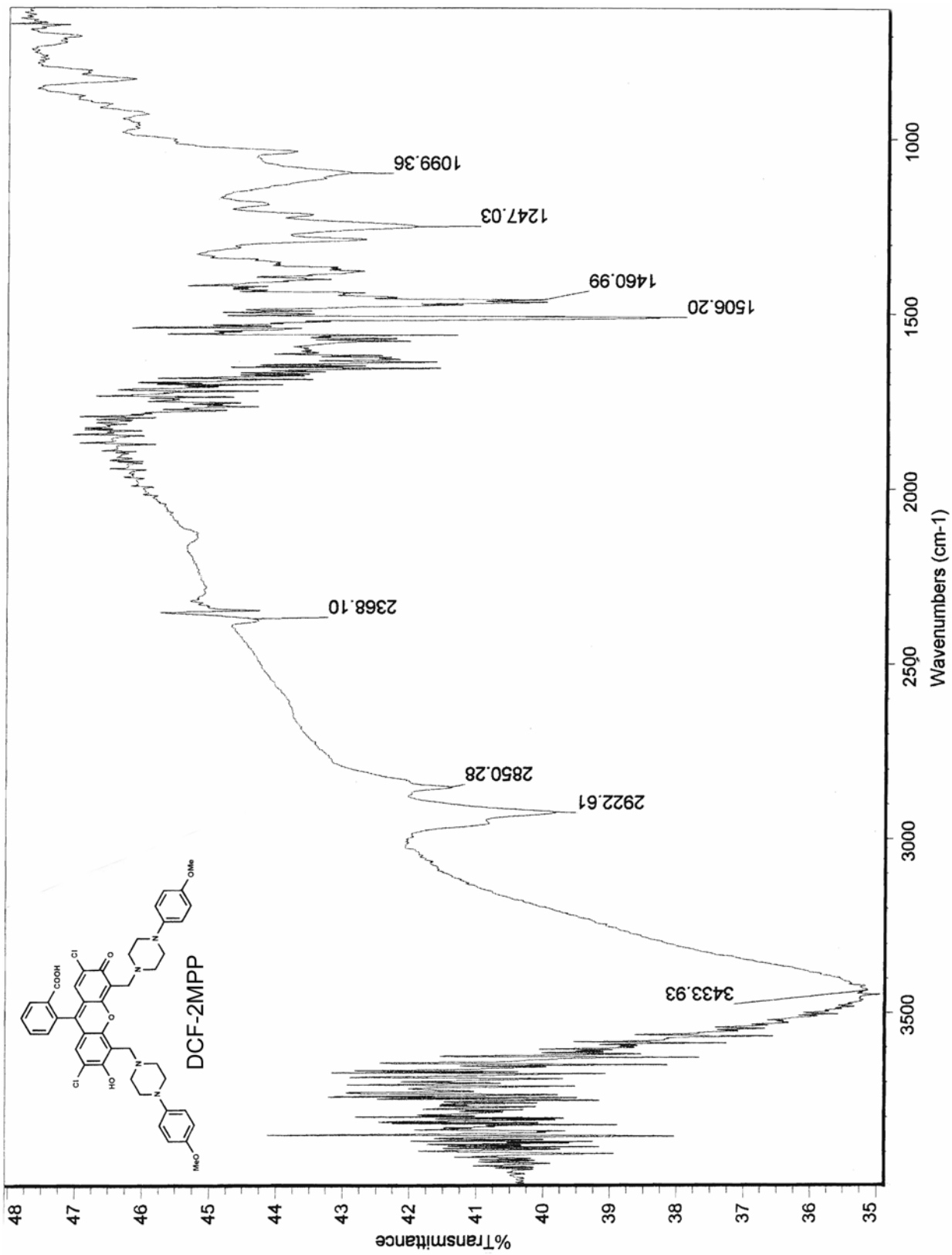

Figure 62 IR spectrum of DCF-2MPP (KBr pellet)

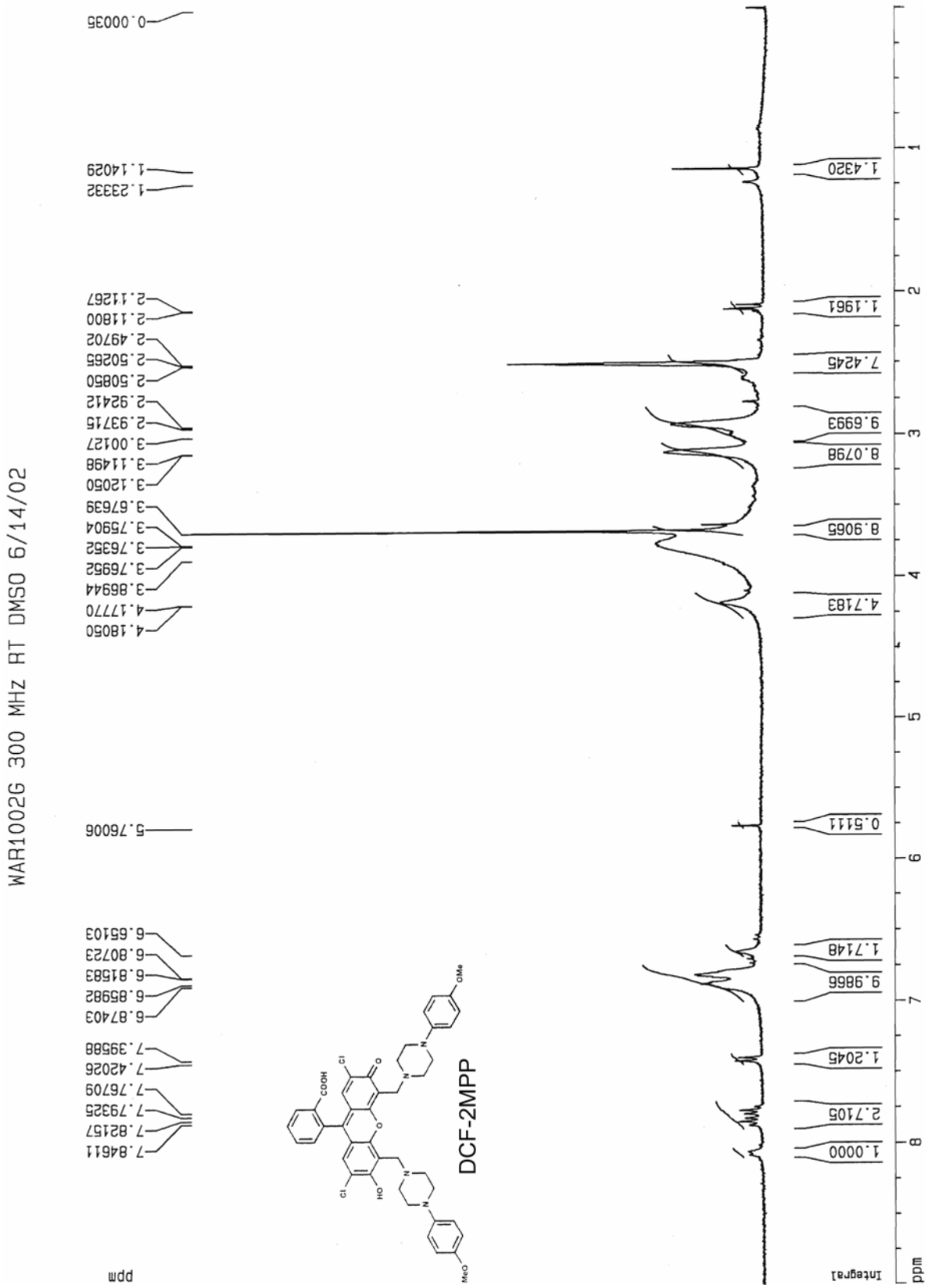

Figure 63 ^{1}H NMR spectrum of DCF-2MPP in DMSO-d_6 (300 MHz)

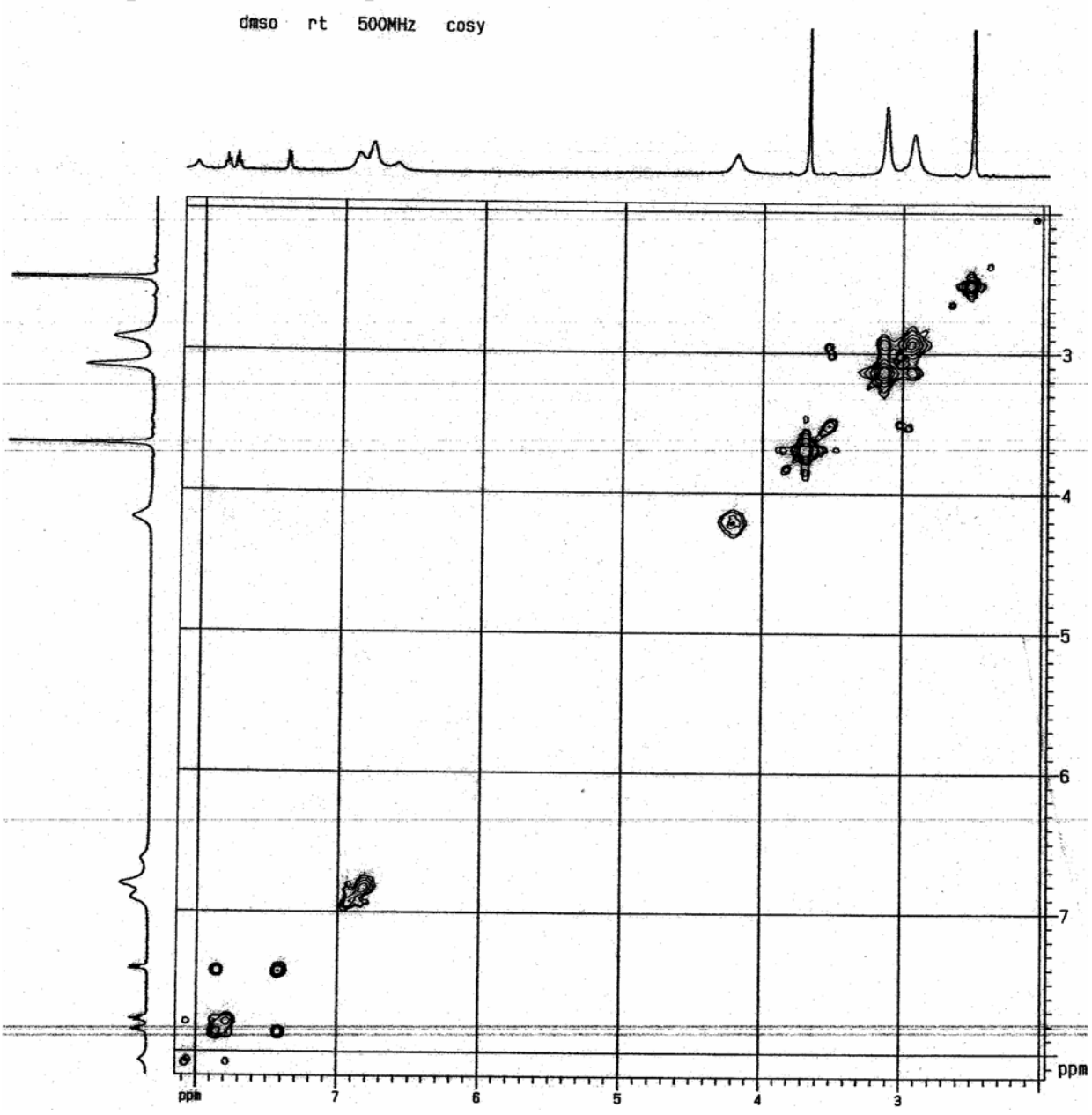

Figure 64 2D COSY NMR of DCF-2MPP in DMSO-d_6 (500 MHz)

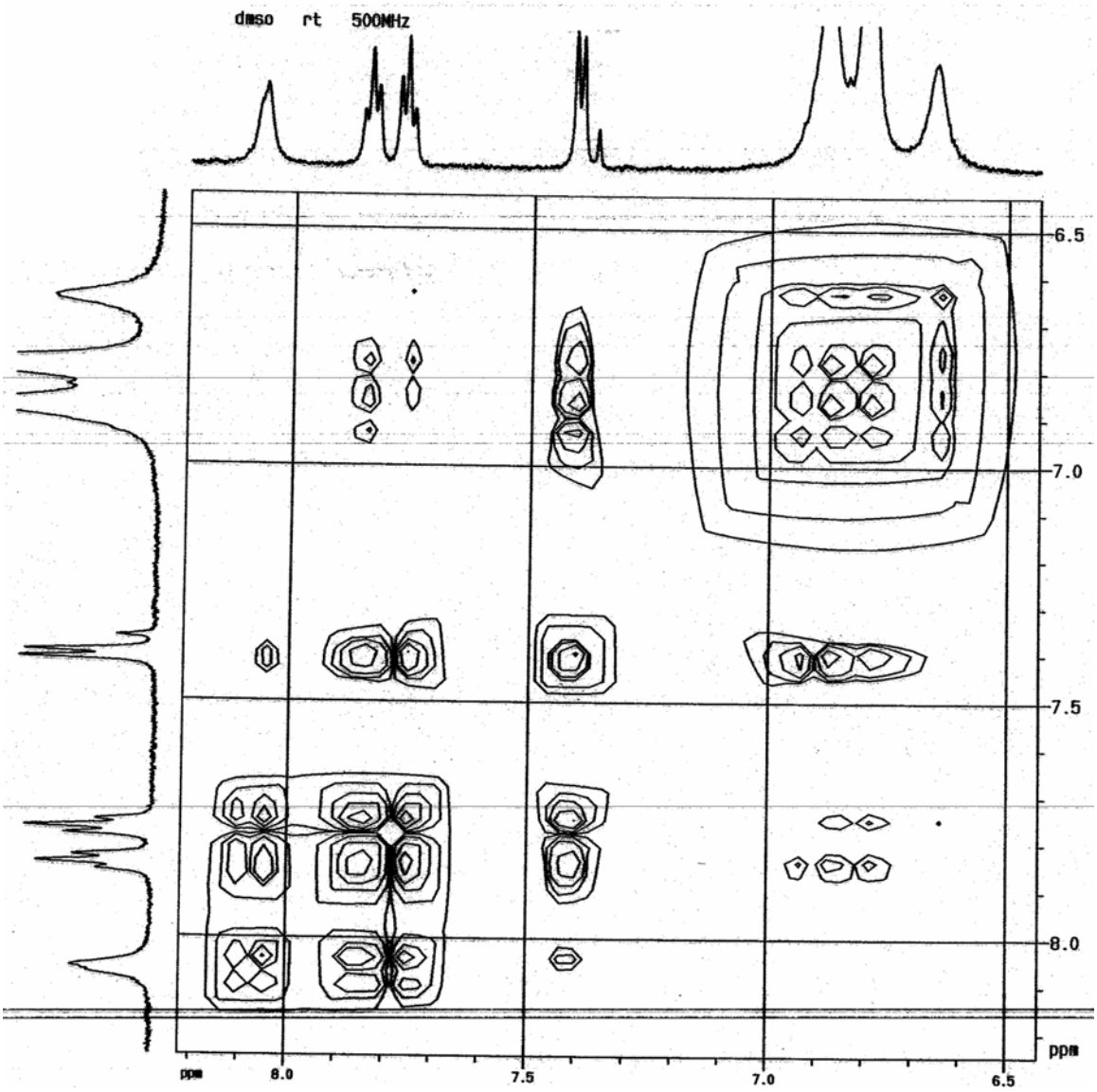

Figure 65 2D NOEOSY NMR of DCF-2MPP in DMSO-d_6 (500 MHz)

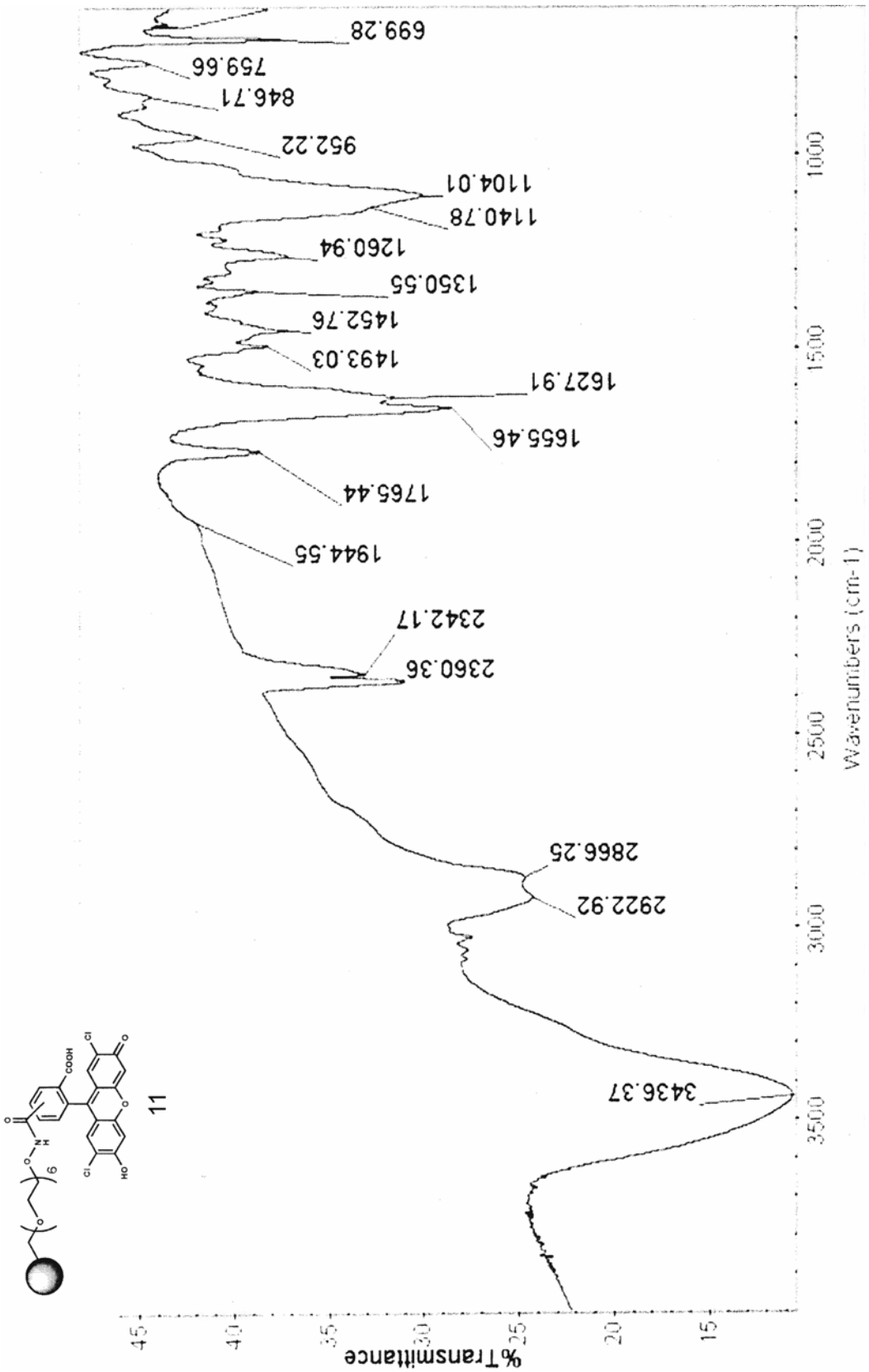

Figure 66 IR spectrum of compound 11 (KBr pellet)

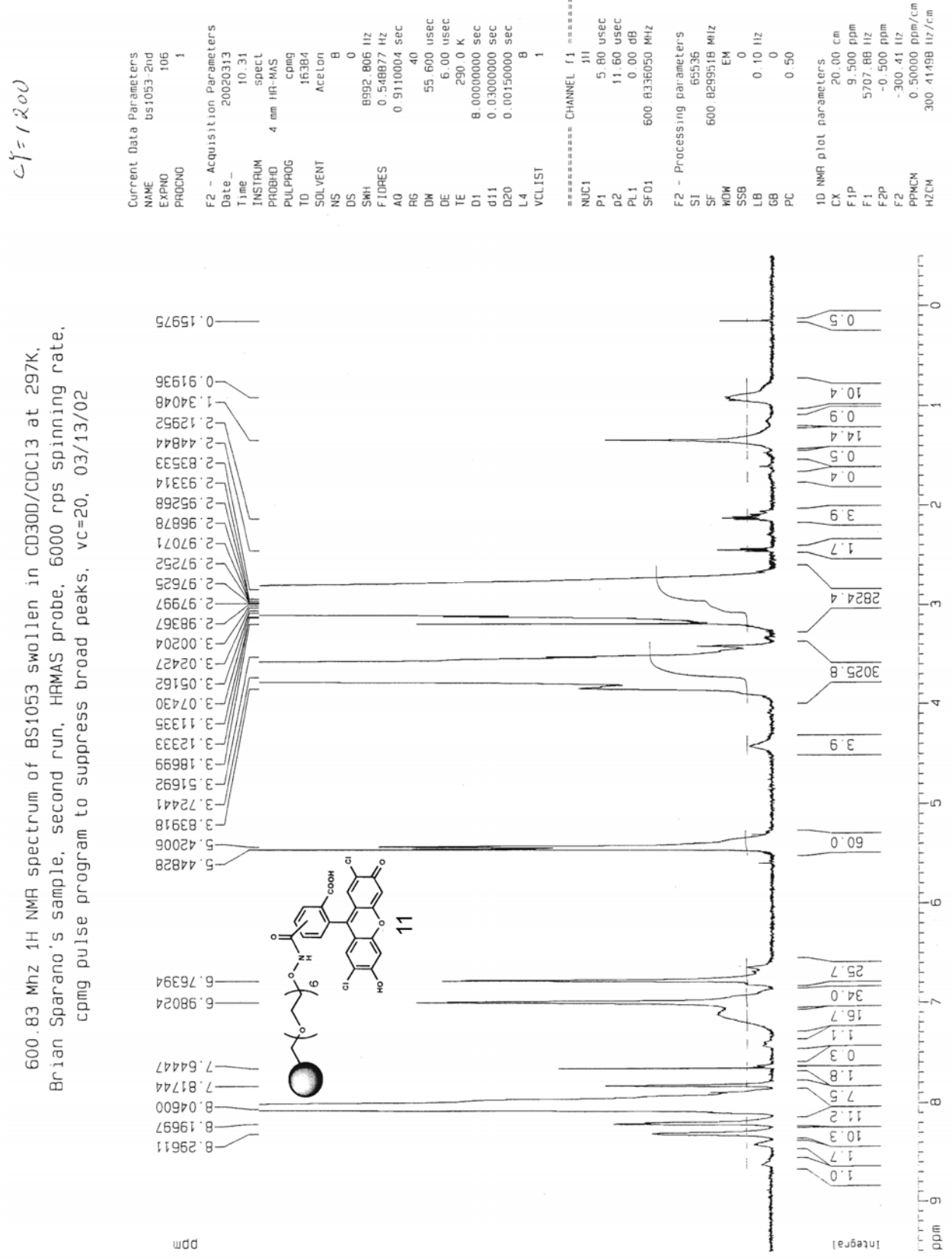

Figure 67 Magic Angle ^{1}H NMR of compound 11 DMSO-d_6 (600 MHz)

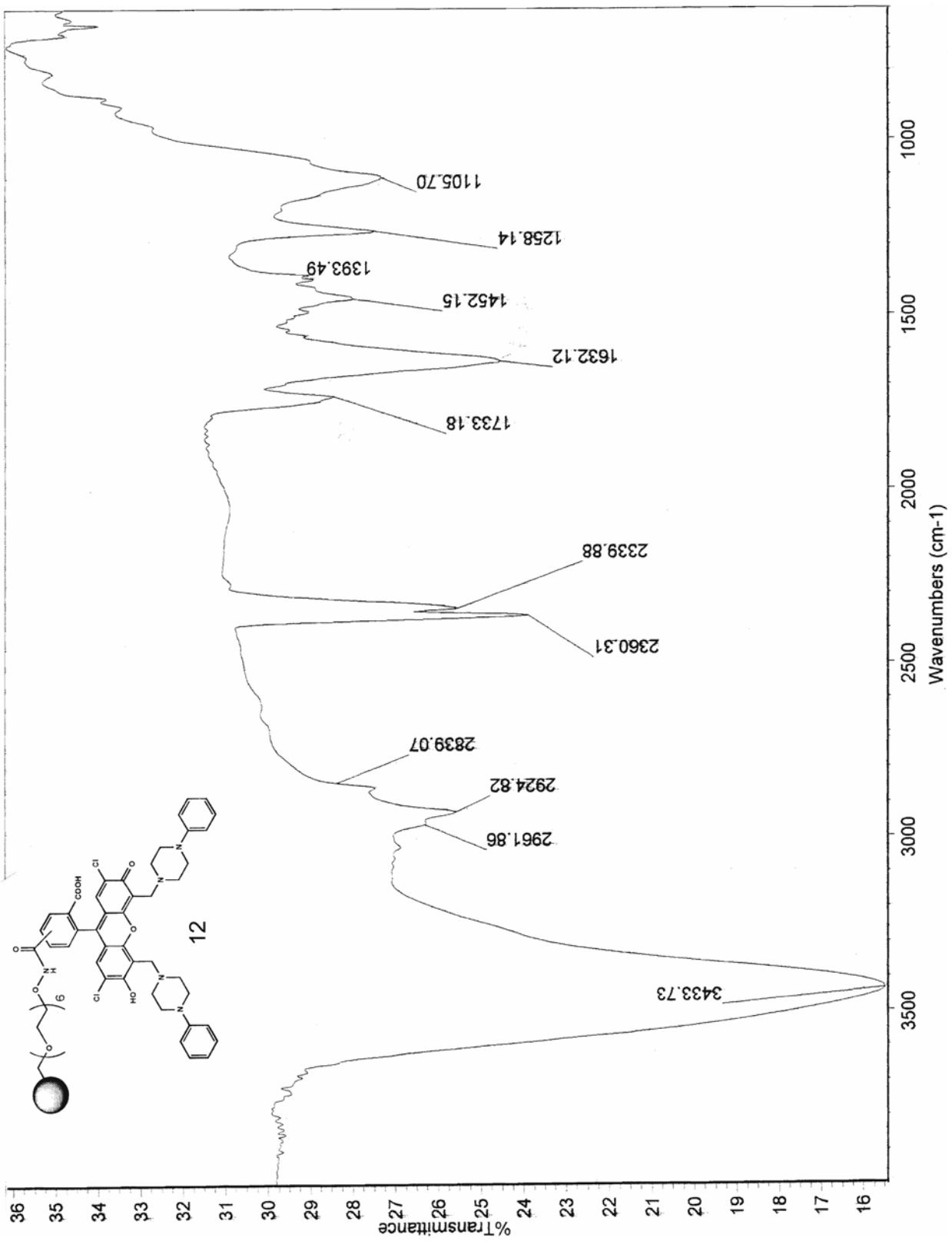

Figure 68 IR spectrum of compound 12 (KBr pellet)

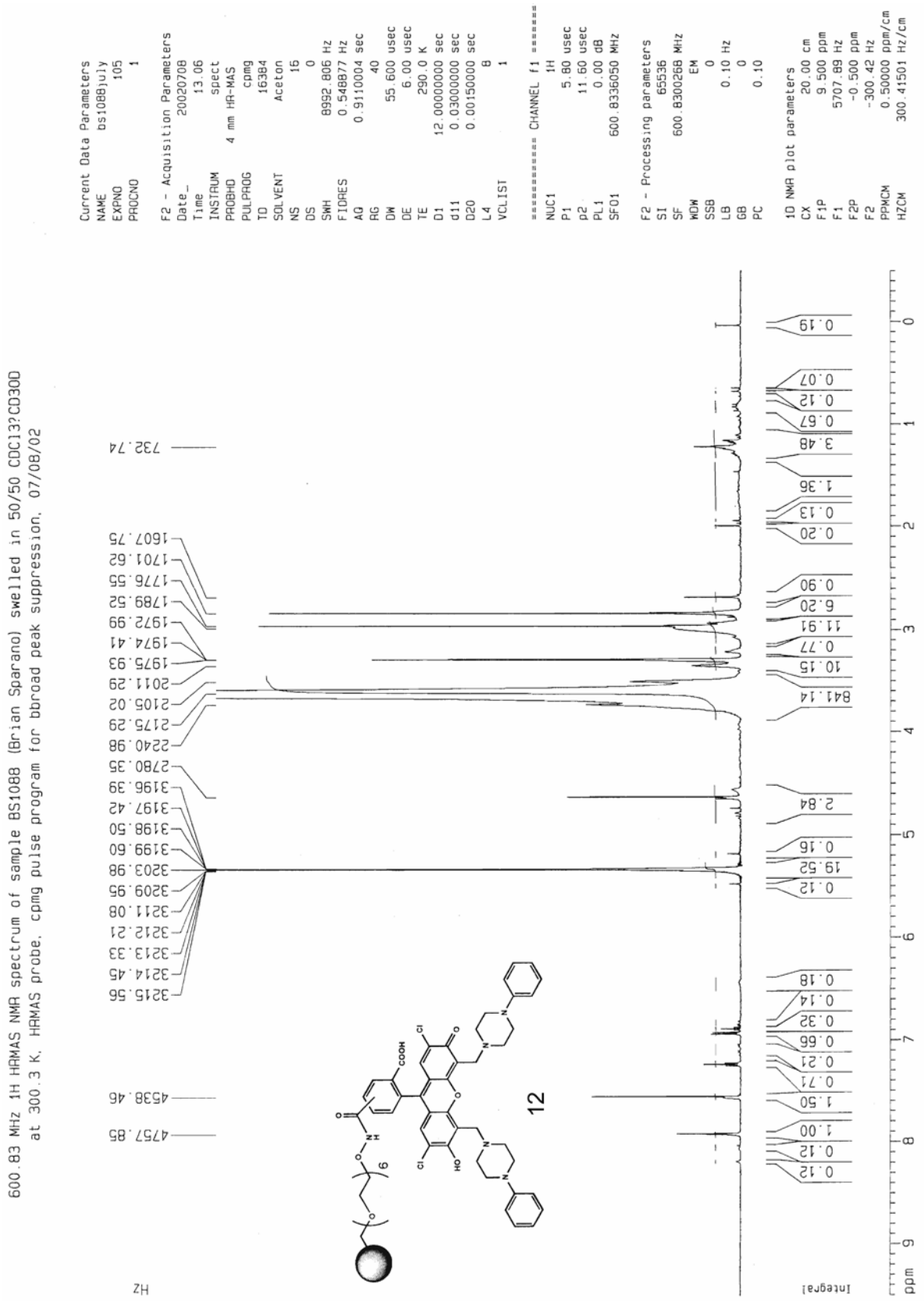

Figure 69 Magic Angle ^{1}H NMR of compound 12 DMSO-d_6 (600 MHz)

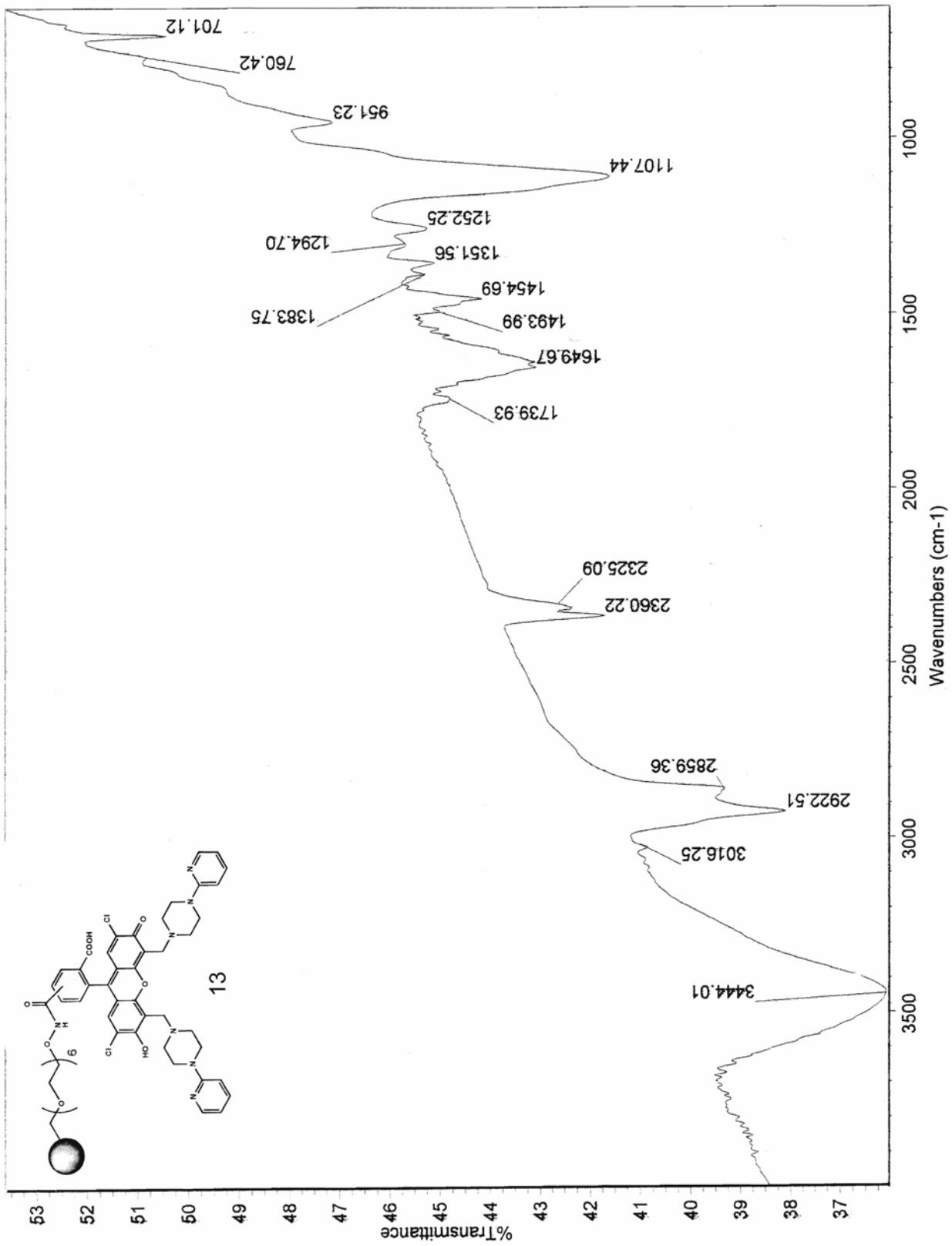

Figure 70 IR spectrum of compound 13 (KBr pellet)

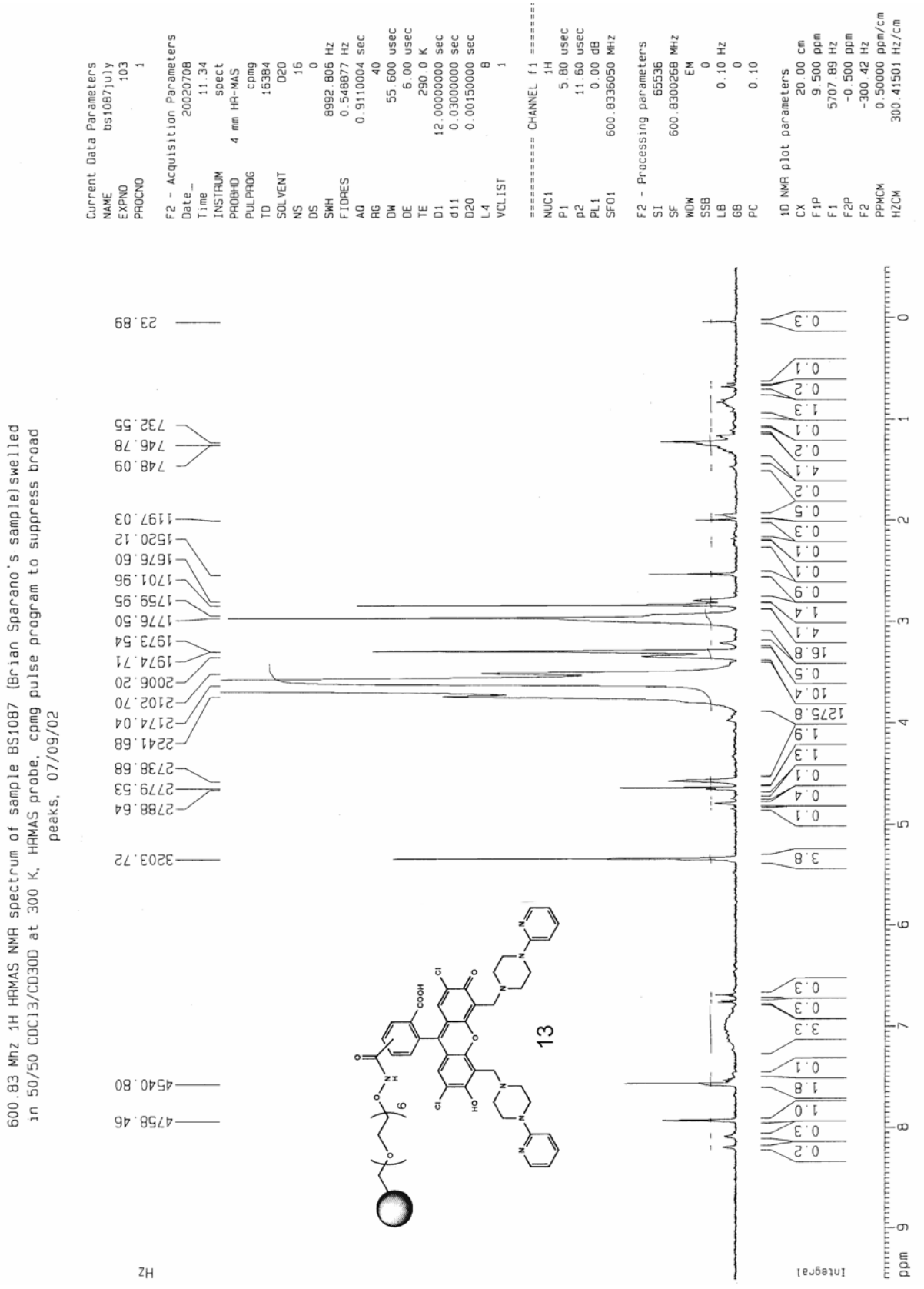

Figure 71 Magic Angle ^{1}H NMR of compound 13 DMSO-d_6 (600 MHz)

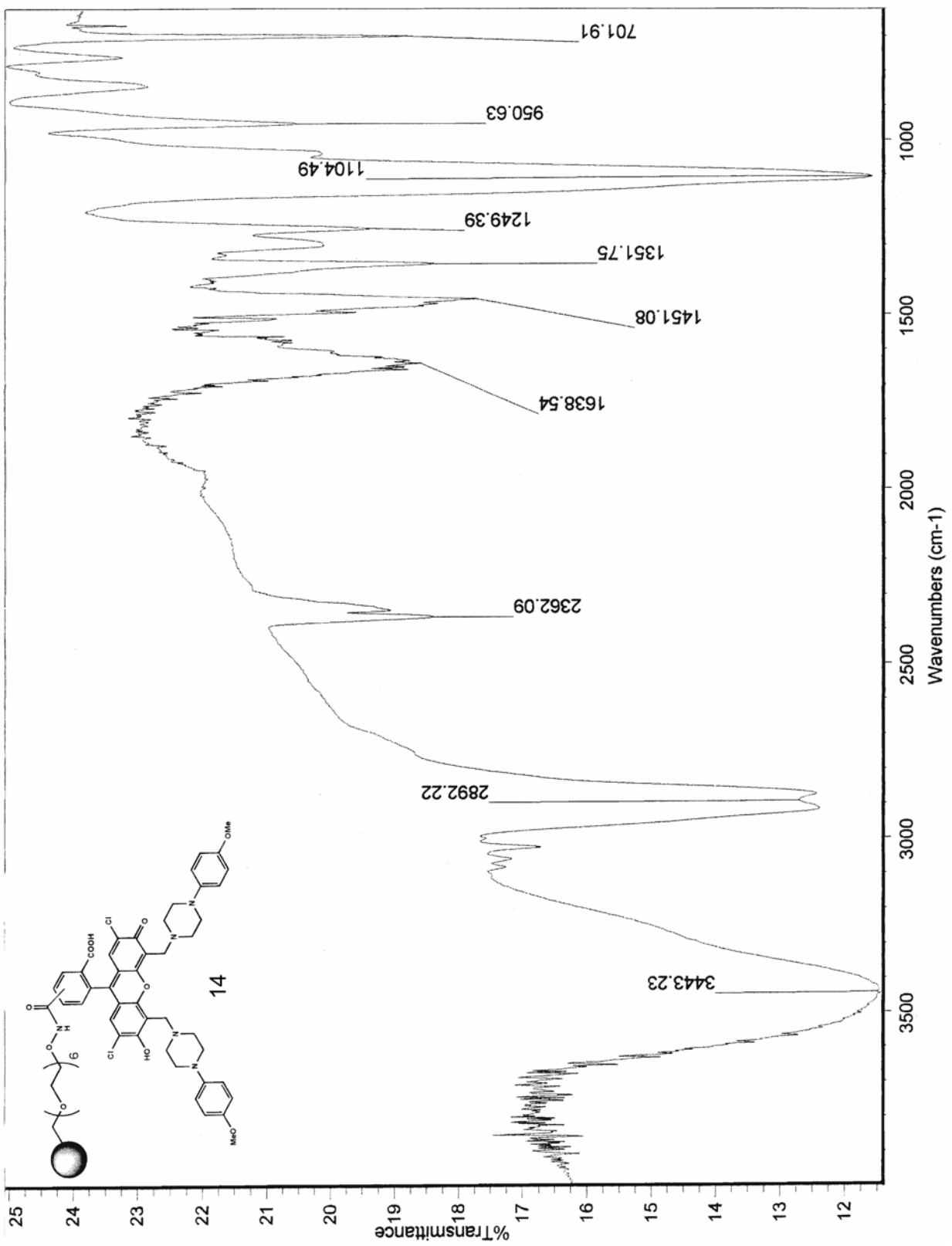

Figure 72 IR spectrum of compound 14 (KBr pellet)

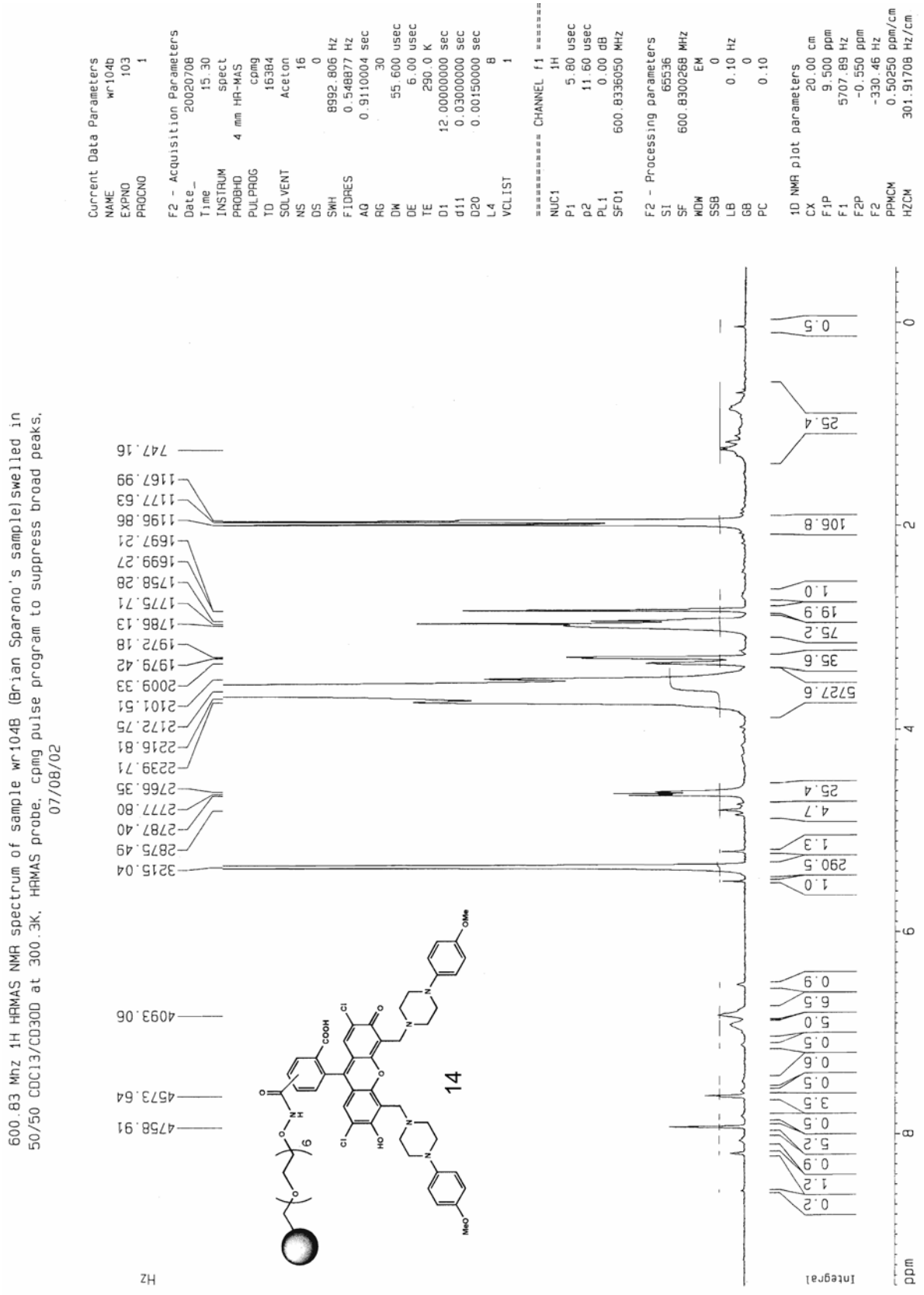

Figure 73 Magic Angle ^{1}H NMR of compound 14 DMSO-d_6 (600 MHz)

BIBLIOGRAPHY

(1) Adams, M. D.; Celniker, S. E.; Holt, R. A.; Evans, C. A.; Gocayne, J. D.; Amanatides, P. G.; Scherer, S. E.; Li, P. W.; Hoskins, R. A.; Galle, R. F.; George, R. A.; Lewis, S. E.; Richards, S.; Ashburner, M.; Henderson, S. N.; Sutton, G. G.; Wortman, J. R.; Yandell, M. D.; Zhang, Q.; Chen, L. X.; Brandon, R. C.; Rogers, Y. H.; Blazej, R. G.; Champe, M.; Pfeiffer, B. D.; Wan, K. H.; Doyle, C.; Baxter, E. G.; Helt, G.; Nelson, C. R.; Gabor, G. L.; Abril, J. F.; Agbayani, A.; An, H. J.; Andrews-Pfannkoch, C.; Baldwin, D.; Ballew, R. M.; Basu, A.; Baxendale, J.; Bayraktaroglu, L.; Beasley, E. M.; Beeson, K. Y.; Benos, P. V.; Berman, B. P.; Bhandari, D.; Bolshakov, S.; Borkova, D.; Botchan, M. R.; Bouck, J.; Brokstein, P.; Brottier, P.; Burtis, K. C.; Busam, D. A.; Butler, H.; Cadieu, E.; Center, A.; Chandra, I.; Cherry, J. M.; Cawley, S.; Dahlke, C.; Davenport, L. B.; Davies, P.; de Pablos, B.; Delcher, A.; Deng, Z.; Mays, A. D.; Dew, I.; Dietz, S. M.; Dodson, K.; Doup, L. E.; Downes, M.; Dugan-Rocha, S.; Dunkov, B. C.; Dunn, P.; Durbin, K. J.; Evangelista, C. C.; Ferraz, C.; Ferriera, S.; Fleischmann, W.; Fosler, C.; Gabrielian, A. E.; Garg, N. S.; Gelbart, W. M.; Glasser, K.; Glodek, A.; Gong, F.; Gorrell, J. H.; Gu, Z.; Guan, P.; Harris, M.; Harris, N. L.; Harvey, D.; Heiman, T. J.; Hernandez, J. R.; Houck, J.; Hostin, D.; Houston, K. A.; Howland, T. J.; Wei, M. H.; Ibegwam, C. *Science* **2000**, *287*, 2185-95.

(2) Hodgkin, J.; Plasterk, R. H.; Waterston, R. H. *Science* **1995**, *270*, 410-4.

(3) McPherson, J. D.; Marra, M.; Hillier, L.; Waterston, R. H.; Chinwalla, A.; Wallis, J.; Sekhon, M.; Wylie, K.; Mardis, E. R.; Wilson, R. K.; Fulton, R.; Kucaba, T. A.; Wagner-McPherson, C.; Barbazuk, W. B.; Gregory, S. G.; Humphray, S. J.; French, L.; Evans, R. S.; Bethel, G.; Whittaker, A.; Holden, J. L.; McCann, O. T.; Dunham, A.; Soderlund, C.; Scott, C. E.; Bentley, D. R.; Schuler, G.; Chen, H. C.; Jang, W.; Green, E. D.; Idol, J. R.; Maduro, V. V.; Montgomery, K. T.; Lee, E.; Miller, A.; Emerling, S.; Kucherlapati; Gibbs, R.; Scherer, S.; Gorrell, J. H.; Sodergren, E.; Clerc-Blankenburg, K.; Tabor, P.; Naylor, S.; Garcia, D.; de Jong, P. J.; Catanese, J. J.; Nowak, N.; Osoegawa, K.; Qin, S.; Rowen, L.; Madan, A.; Dors, M.; Hood, L.; Trask, B.; Friedman, C.; Massa, H.; Cheung, V. G.; Kirsch, I. R.; Reid, T.; Yonescu, R.; Weissenbach, J.; Bruls, T.; Heilig, R.; Branscomb, E.; Olsen, A.; Doggett, N.; Cheng, J. F.; Hawkins, T.; Myers, R. M.; Shang, J.; Ramirez, L.; Schmutz, J.; Velasquez, O.; Dixon, K.; Stone, N. E.; Cox, D. R.; Haussler, D.; Kent, W. J.; Furey, T.; Rogic, S.; Kennedy, S.; Jones, S.; Rosenthal, A.; Wen, G.; Schilhabel, M.; Gloeckner, G.; Nyakatura, G.; Siebert, R.; Schlegelberger, B.;

Korenberg, J.; Chen, X. N.; Fujiyama, A.; Hattori, M.; Toyoda, A.; Yada, T.; Park, H. S.; Sakaki, Y.; Shimizu, N.; Asakawa, S. *Nature* **2001**, *409*, 934-41.

(4) Gygi, S. P.; Rochon, Y.; Franza, B. R.; Aebersold, R. *Mol. Cell Biol.* **1999**, *19*, 1720–1730.

(5) Raj, A.; Peskin, C. S.; Tranchina, D.; Vargas, D. Y.; Tyagi, S. *PLoS Biology* **2006**, *4*, e309.

(6) Mattick, J. S. *Nat. Rev. Genet.* **2004**, *5*, 316-323.

(7) Slavâik, J. *Fluorescent probes in cellular and molecular biology*; CRC Press: Boca Raton, 1994.

(8) Rautenstrauss, B. W.; Liehr, T. *FISH technology*; Springer: Berlin ; New York, 2002.

(9) Egger, D.; Bolten, R.; Rahner, C.; Bienz, K. *Histochem. Cell. Biol.* **1999**, *111*, 319-24.

(10) Sheppard, C.; Shotton, D. *Confocal laser scanning microscopy*; BIOS Scientific Publishers in association with the Royal Microscopical Society: Oxford, England, 1997.

(11) Chudakov, D. M.; Lukyanov, S.; Lukyanov, K. A. *Trends in Biotechnol.* **2005**, *23*, 605–613.

(12) Giepmans, B. N. G.; Adams, S. R.; Ellisman, M. H.; Tsien, R. Y. *Science* **2006**, *312*, 217-224.

(13) Chudakov, D. M.; Lukyanov, S.; Lukyanov, K. A. *Trends Biotechnol.* **2005**, *23*, 605-613.

(14) Giepmans, B. N. G.; Adams, S. R.; Ellisman, M. H.; Tsien, R. Y. *Science* **2006**, *312*, 217–224.

(15) Griffin, B. A.; Adams, S. R.; Tsien, R. Y. *Science* **1998**, *281*, 269–272.

(16) Li, X.; Zhao, X.; Fang, Y.; Jiang, X.; Duong, T.; Fan, C.; Huang, C.-C.; Kain, S. R. *J. Biol. Chem.* **1998**, *273*, 34970–34975.

(17) Dirks, R. W.; Molenaar, C.; Tanke, H. J. *Histochem. Cell. Biol.* **2001**, *115*, 3-11.

(18) Overbergh, L.; Valckx, D.; Waer, M.; Mathieu, C. *Cytokine* **1999**, *11*, 305-12.

(19) Naito, N.; Kawai, A.; Ouchida, M.; Dan'ura, T.; Morimoto, Y.; Ozaki, T.; Shimizu, K.; Inoue, H. *Cancer* **2000**, *89*, 1992-8.

(20) Hurteau, G.; Spivack, S. *Anal. Biochem.* **2002**, *307*, 304.

(21) Wansink, D. G.; Schul, W.; van der Kraan, I.; van Steensel, B.; van Driel, R.; de Jong, L. *J. Cell. Biol.* **1993**, *122*, 283-93.

(22) LaMorte, V. J.; Dyck, J. A.; Ochs, R. L.; Evans, R. M. *PNAS* **1998**, *95*, 4991-4996.

(23) Maniatis, T.; Fritsch, E. F.; Sambrook, J. *Molecular cloning : a laboratory manual*; 2nd ed.; Cold Spring Harbor Laboratory: Cold Spring Harbor, N.Y., 1989.

(24) Dirks, R. W. *Histochem. Cell. Biol.* **1996**, *106*, 151-66.

(25) Dirks, R.; Daniel, K.; Raap, A. *J. Cell. Sci.* **1995**, *108*, 2565-2572.

(26) Dirks, R. W.; Molenaar, C.; Tanke, H. J. *Histochem. Cell. Biol.* **2001**, *115*, 3-11.

(27) Lee, G.; Delohery, T. M.; Ronai, Z.; Brandtrauf, P. W.; Pincus, M. R.; Murphy, R. B.; Weinstein, I. B. *Cytometry* **1993**, *14*, 265-270.

(28) Dowty, M. E.; Williams, P.; Zhang, G. F.; Hagstrom, J. E.; Wolff, J. A. *PNAS.* **1995**, *92*, 4572-4576.

(29) Tyagi, S.; Kramer, F. R. *Nat. Biotechnol.* **1996**, *14*, 303-308.

(30) Tsuji, A.; Koshimoto, H.; Sato, Y.; Hirano, M.; Sei-Iida, Y.; Kondo, S.; Ishibashi, K. *Biophys. J.* **2000**, *78*, 3260-74.

(31) Sei-Iida, Y.; Koshimoto, H.; Kondo, S.; Tsuji, A. *Nucl. Acids. Res.* **2000**, *28*, e59-.

(32) Wang, J.; Cao, L.; Wang, Y.; Pederson, T. *PNAS* **1991**, *88*, 7391-7395.

(33) Jacobson, M. R.; Pederson, T. *PNAS* **1998**, *95*, 7981-7986.

(34) Bertrand, E.; Chartrand, P.; Schaefer, M.; Shenoy, S. M.; Singer, R. H.; Long, R. M. *Mol. Cell* **1998**, *2*, 437–445.

(35) Fusco, D.; Accornero, N.; Lavoie, B.; Shenoy, S. M.; Blanchard, J. M.; Singer, R. H.; Bertrand, E. *Curr. Biol* **2003**, *13*, 161–167.

(36) Le, T. T.; Harlepp, S.; Guet, C. C.; Dittmar, K.; Emonet, T.; Pan, T.; Cluzel, P. *PNAS* **2005**, *102*, 9160-9164.

(37) Beach, D. L.; Salmon, E. D.; Bloom, K. *Curr. Biol.* **1999**, *9*, 569-578.

(38) Kloc, M.; Zearfoss, N. R.; Etkin, L. D. *Cell* **2002**, *108*, 533-44.

(39) Singer, R. H. *Curr. Biol.* **2003**, *13*.

(40) Forrest, K. M.; Gavis, E. R. *Curr. Biol.* **2003**, *13*, 1159–1168.

(41) Shav-Tal, Y.; Darzacq, X.; Shenoy, S. M.; Fusco, D.; Janicki, S. M.; Spector, D. L.; Singer, R. H. *Science* **2004**, *304*, 1797-1800.

(42) Janicki, S. M.; Tsukamoto, T.; Salghetti, S. E.; Tansey, W. P.; Sachidanandam, R.; Prasanth, K. V.; Ried, T.; Shav-Tal, Y.; Bertrand, E.; Singer, R. H. *Cell* **2004**, *116*, 683-98.

(43) Golding, I.; Paulsson, J.; Zawilski, S. M.; Cox, E. C. *Cell* **2005**, *123*, 1025-1036.

(44) Tanaka, K.; Miura, T.; Umezawa, N.; Urano, Y.; Kikuchi, K.; Higuchi, T.; Nagano, T. *J. Am. Chem. Soc.* **2001**, *123*, 2530–2536.

(45) Onoda, M.; Uchiyama, S.; Santa, T.; Imai, K. *Anal. Chem.* **2002**, *74*, 4089–4096.

(46) Hirano, T.; Kikuchi, K.; Urano, Y.; Nagano, T. *J. Am. Chem. Soc.* **2002**, *124*, 6555–6562.

(47) Shults, M. D.; Pearce, D. A.; Imperiali, B. *J. Am. Chem. Soc.* **2003**, *125*, 10591–10597.

(48) Pearce, D. A.; Jotterand, N.; Carrico, I. S.; Imperiali, B. *J. Am. Chem. Soc.* **2001**, *123*, 5160–5161.

(49) Walkup, G. K.; Burdette, S. C.; Lippard, S. J.; Tsien, R. Y. *J. Am. Chem. Soc.* **2000**, *122*, 5644–5645.

(50) Zeng, L.; Miller, E. W.; Pralle, A.; Isacoff, E. Y.; Chang, C. J. *J. Am. Chem. Soc.* **2006**, *128*, 10–11.

(51) Farruggia, G.; Iotti, S.; Prodi, L.; Montalti, M.; Zaccheroni, N.; Savage, P. B.; Trapani, V.; Sale, P.; Wolf, F. I. *J. Am. Chem. Soc.* **2006**, *128*, 344–350.

(52) Lakowicz, J. R. *Principles of fluorescence spectroscopy*; 2 ed.; Kluwer Academic/Plenum Publishers: New York, 1999.

(53) Rehm, D.; Weller, A. *Isr. J. Chem.* **1970**, *8*, 259–271.

(54) Munkholm, C.; Parkinson, D.-R.; Walt, D. R. *J. Am. Chem. Soc.* **1990**, *112*, 2608–2612.

(55) Grynkiewicz, G.; Poenie, M.; Tsien, R. *J. Biol. Chem.* **1985**, *260*, 3440-3450.

(56) Lee, S. K.; Lee, J. Y.; Lee, M. Y.; Chung, S. M.; Chung, J. H. *Anal. Biochem.* **1999**, *273*, 186-191.

(57) Hirano, T.; Kikuchi, K.; Urano, Y.; Nagano, T. *J. Am. Chem. Soc.* **2002**, *124*, 6555-6562.

(58) Burdette, S. C.; Frederickson, C. J.; Bu, W.; Lippard, S. J. *J. Am. Chem. Soc.* **2003**, *125*, 1778-1787.

(59) Burdette, S. C.; Walkup, G. K.; Spingler, B.; Tsien, R. Y.; Lippard, S. J. *J. Am. Chem. Soc.* **2001**, *123*, 7831-41.

(60) Torrado, A.; Imperiali, B. *J. Org. Chem.* **1996**, *61*, 8940–8948.

(61) Sparano, B. A.; Shahi, S. P.; Koide, K. *Org. Lett.* **2004**, *6*, 1947–1949.

(62) Ellington, A. D.; Szostak, J. W. *Nature* **1990**, *346*, 818-22.

(63) Robertson, D. L.; Joyce, G. F. *Nature* **1990**, *344*, 467-8.

(64) Tuerk, C.; Gold, L. *Science* **1990**, *249*, 505-10.

(65) Osborne, S. E.; Ellington, A. D. *Chem. Rev.* **1997**, *97*, 349-370.

(66) Bartel, D. P.; Zapp, M. L.; Green, M. R.; Szostak, J. W. *Cell* **1991**, *67*, 529-536.

(67) Cho, J.; Rando, R. R. *Biochemistry* **1999**, *38*, 8548-8554.

(68) Lacourciere, K. A.; Stivers, J. T.; Marino, J. P. *Biochemistry* **2000**, *39*, 5630-5641.

(69) Tok, J. B. H.; Cho, J.; Rando, R. R. *Tetrahedron* **1999**, *55*, 5741-5758.

(70) Werstuck, G.; Zapp, M. L.; Green, M. R. *Chemistry & Biology* **1996**, *3*, 129-37.

(71) Zapp, M. L.; Stern, S.; Green, M. R. *Cell* **1993**, *74*, 969-978.

(72) Zapp, M. L.; Young, D. W.; Kumar, A.; Singh, R.; Boykin, D. W.; Wilson, W. D.; Green, M. R. *Bioorg. Med. Chem.* **1997**, *5*, 1149-1155.

(73) Kirk, S. R.; Luedtke, N. W.; Tor, Y. *J. Am. Chem. Soc.* **2000**, *122*, 980-981.

(74) McHedlov-Petrossyan, N. O.; Rubtsov, M. I.; Kukatskaya, L. L. *Dyes and pigments* **1992**, *18*, 179-198.

(75) Martin, M. M.; Lindqvist, L. *J. Lumin.* **1975**, *10*, 381–390.

(76) Wang, Y.; Rando, R. R. *Chemistry & Biology* **1995**, *2*, 281-290.

(77) It is important to note that although the synthesis of all six compounds is shown in Scheme 2, the actual synthesis of compounds 6-9 was not attempted until after the characterization and spectroscopy of model compound 4 and 5. This minor break in linearity is necessary for organization and is the explanation behind the lack of extra data on compounds 6 and 9.

(78) Although 2d spectra were also taken of compound 5, the resolution was insufficient for such a thorough examination

(79) Compound 4 was not sufficiently soluble in D2O for two-dimensional NMR studies. The quantum yield relationships in DMSO show the same trends as in pH 7 phosphate buffer.

(80) Gazit, E. *FASEB J.* **2002**, *16*, 77-83.

(81) Semi-Empirical PM3 calculations were made with PC Spartan Pro release 6.0.4 on a Pentium III based computer. Although various starting conformations of 1 were used, none of the optimized geometries were close to the experimentally determined conformation. It is hypothesized that this method's inability to account for solvent effects prevented it from arriving at the correct conformation of this solvatochromic molecule.

(82) Rekharsky, M. V.; Goldberg, R. N.; Schwarz, F. P.; Tewari, Y. B.; Ross, P. D.; Yamashoji, Y.; Inoue, Y. *J. Am. Chem. Soc.* **1995**, *117*, 8830-8840.

(83) Rekharsky, M. V.; Inoue, Y. *Chem. Rev.* **1998**, *98*, 1875-1918.

(84) The [β-CD] could not be increased further due to its low solubility.

(85) Flamigni, L. *J. Phys. Chem.* **1993**, *97*, 9566-9572.

(86) Bartel, D. P.; Szostak, J. W. *Science* **1993**, *261*, 1411-1418.

(87) Holeman, L. A.; Robinson, S. L.; Szostak, J. W.; Wilson, C. *Folding & Design* **1998**, *3*, 423-431.

(88) Sassanfar, M.; Szostak, J. W. *Nature* **1993**, *364*, 550-553.

(89) Wilson, C.; Szostak, J. W. *Nature* **1995**, *374*, 777-782.

(90) Ellington, A. D.; Szostak, J. W. *Nature* **1990**, *346*, 818–822.

(91) Robertson, D. L.; Joyce, G. F. *Nature* **1990**, *344*, 467–468.

(92) Tuerk, C.; Gold, L. *Science* **1990**, *249*, 505–510.

(93) Zuker, M. *Nucleic Acids Res.* **2003**, *31*, 3406–3415.

(94) Breaker, R. R.; Joyce, G. F. *Trends Biotechnol.* **1994**, *12*, 268–275.

(95) 63

(96) Although not statistically significant, the choice to test only 3 aptamers was purely an economic one: the expensive process of producing sufficient RNA for evaluating fluorescent enhancement ability restricted us to testing only those aptamers that were well represented in the sequenced hits and lowing the maximum concentration from 100 μM to 50 μM.

(97) Knemeyer, J. P.; Marme, N.; Sauer, M. *Anal. Chem.* **2000**, *72*, 3717-3724.

(98) Rupcich, N.; Chiuman, W.; Nutiu, R.; Mei, S.; Flora, K. K.; Li, Y.; Brennan, J. D. *J. Am. Chem. Soc.* **2006**, *128*, 780-790.

(99) Fried, M.; Crothers, D. M. *Nucleic Acids Res.* **1981**, *9*, 6505-6525.

(100) Garner, M. M.; Revzin, A. *Nucleic Acids Res.* **1981**, *9*, 3047-3060.

(101) Tibodeau, J. D.; Fox, P. M.; Ropp, P. A.; Theil, E. C.; Thorp, H. H. *PNAS* 2006; Vol. 103, p 253.

(102) Albarghouthi, M. N.; Barron, A. E. *Electrophoresis* **2000**, *21*, 4096-4111.